# Chapter 4

Ferroelastic Behavior

To say that the study of ferroelasticity is an important aspect of this research program might be an underestimate. Indeed, the observation of ferroelasticity in crystals of 2,10-undecanedione has inspired many additional studies and insights into ferroelastic behavior. This chapter and the next will describe what is currently understood about this important and very complex phenomenon as it applies to urea inclusion compounds.

## 4.1 Ferroelastic and Ferroelectric Materials Have Many Similarities

### 4.1.1 Introduction

In many discussions of crystals and crystal growth, it is assumed that crystals are homogeneous with respect to unit cell orientation. For ferroic crystals, this simplification is not ordinarily accurate. Indeed, the possibility of multiple orientation states between which ferroelastic switching may occur means that these crystals can grow as twinned crystals unless preventive steps are taken.[1] The interconversion of orientation states as a response to the application of a uniaxial stress or electric field defines a working ferroelastic or ferroelectric material. These orientation states are structurally similar and are related by simple symmetry transformations.[2] However, the existence of multiple orientation states is not guaranteed, and many potentially ferroic materials may not actually exhibit such behavior.

In order for switching between ferroelastic orientation states to occur, there must be some reasonable mechanism for one orientation state to be transformed into another. The pathway linking orientation states can have an appreciable influence on the

energetics of ferroelastic domain switching. This notion is reflected in studies of solid state photoreactions; in cases where the shape or volume of intermediates or products is different than that of the starting materials, the mechanical properties and connectivity of the crystal can exert an appreciable influence on the progress or outcome of the reaction.[3-7] For instance, for crystals of diundecanoyl peroxide undergoing photolysis, the creation of $CO_2$ molecules within the crystal forces the undecyl radicals apart in a screw-type motion along their chain axes.[3,4] Although it involves large molecular reorientations locally, this motion is apparently favored over those that compress layers of closely packed alkyl chains. Thus, the distribution of strain along one crystal axis is favored over other distributions of strain because this axis provides the least resistance to compression.[5,6] Interestingly, the stress generated in this sort of process exerts an influence on molecular vibrations that can be probed with methods such as infrared spectroscopy.[4,5,8]

In the study of ferroelastics and ferroelectrics, lines of thought similar to those applied to photochemical reactions of the solid state can be useful in understanding the "mechanism" of domain switching. Intuitively, a ferroelastic process that involves an exaggerated energetic penalty should be less likely to occur than alternative, low energy, transformations. Alternative pathways might include large molecular or atomic movements[9] or other situations in which the macroscopic destruction of the material precedes the desired switching event (for instance, when the applied force surpasses the elastic limit of the crystal). In ferroelastic UICs such as 2,10-undecanedione/urea, guest rotation and translation along the channel provide a means by which the crystal can respond to an applied stress. Unlike the photochemical processes discussed above, this

process does not appear to violate the topochemical postulate,[10,11] which poses that least-motion molecular rearrangements are favored over alternative pathways. A plausible mechanism for ferroelastic switching in helical UICs is discussed below.

### 4.1.2 The Similarities Between Ferroelastics and Ferroelectrics

In her book on ferroelectric materials,[12] Helen Megaw described the properties characteristic of ferroelectrics; a review of these is relevant to the comparison of ferroelectricity and ferroelasticity.

According to Megaw, a ferroelectric material will:

1) "Possess a dielectric hysteresis loop, indicating reversible spontaneous polarization"
2) "Show disappearance of hysteresis at a certain temperature, the Curie point"
3) "Have a transition at the Curie point to a form of higher symmetry"
4) "Have a domain structure, which may be visible in polarized light"
5) "Possess a pseudosymmetric structure"
6) Have a macroscopic dipole (be polar)

According to Megaw, conditions 1, 5 and 6 are necessary for indicating the presence of ferroelectricity, while the others may or may not be observable. Conditions 2 and 3 can describe the transition to Aizu's prototype phase (Chapter 3) and therefore remain important indicators of ferroelectric behavior. Conditions 4 and 6 are consequences of the decreased symmetry exhibited in ferroelectric materials (embodied in condition 5). In considering the items in Megaw's list, it becomes evident that with the

substitution of the concept of "strain" for that of "polarity," these qualities characterize ferroelasticity. Thus, a ferroelastic material will exhibit strain hysteresis upon the application of a uniaxial force. By *hysteresis*, it is meant that the reorientation of the crystal's macroscopic strain follows the applied stress, and that upon stress release, the initial strain is recovered only once the stress is lowered to some value lower than that required to induce the ferroelastic response. For such a system, a plot of strain vs. stress will appear as a loop. Here, some critical value of applied stress must be reached before a ferroelastic response is observed. (Such behavior is commonly observed in ferroelastic materials.[13]) At low stresses, the response will grow slowly (or not at all), only to increase dramatically once the stress surpasses some threshold.[13]

The similarity in hysteretic behavior and the large degree of overlap between the symmetries of ferroelectric and ferroelastic materials suggest that these classes of materials have many properties in common. In fact, several well-known ferroelectrics are also ferroelastic; these include the perovskite $BaTiO_3$[14] and Rochelle salt.[15] It is in this spirit that the studies reported herein on the ferroelastic behavior of urea inclusion compounds may provide insight into the properties and behavior of ferroelectric materials.

## 4.2 Ferroelasticity in Urea Inclusion Compounds

### 4.2.1 General Features

Crystals of 2,10-undecanedione/urea are ferroelastic.[16] When adequate stress is applied to {110} faces, these crystals undergo ferroelastic domain switching. This phenomenon involves several features:

1) As adequate stress is applied to {110} faces, a second orientation state appears; its size increases as the stress is increased.
2) The second orientation state arises from the ferroelastic reorientation, or *switching*, of the original domain.
3) Reoriented regions are called *daughters*; the initial orientation state from which the daughter grows is called the *mother*, or *parent*.
4) Within the daughter, strain has rotated by approximately 60° so that it is perpendicular to the applied stress.
5) The boundary between daughter and mother is called the *domain wall*. The reorientation of domains coincides with the motion of a domain wall.
6) The daughter and mother are nominally degenerate twins; they are two ferroelastic orientation states.
7) When daughters do not spontaneously revert to the mother following the removal of stress, they are said to be *plastic*; those that spontaneously revert are said to be *pseudoelastic*.
8) Plastic daughters can be caused to revert when stress is applied to *their* {110} faces.

This chapter will discuss the basics of ferroelastic behavior as it applies to urea inclusion compounds and describe studies aimed at testing hypotheses on the nature of this process.

### 4.2.2 Spontaneous Strain and Domain Reorientation

The crystal structure of 2,10-undecanedione/urea was described in Section 1.1.2. Briefly, in this crystal, the guest molecules are confined within [001] channels and are arranged antiferroelectrically along [100]. Guest ketone carbonyls form hydrogen bonds

with the every third urea on {100} faces of the channel. The network of hosts and guests held together by hydrogen bonding offers a degree of stabilization that leads to a commensurate structure that is stable to over 100 °C, which is more than 50 °C above the melting point of 2,10-undecanedione. Because the ketones are directed toward channel *faces* instead of *vertices*, the channel becomes stretched from the shape of a regular hexagon. For a cell with no distortion, $b = a\sqrt{3}$; when distortion occurs, spontaneous strain is quantified as:

$$\frac{\left|a\sqrt{3} - b\right|}{b}. \qquad (1)$$

At room temperature, 2,10-undecanedione/urea exhibits[16] approximately 3.7% strain along [100] (Section 1.1.2). For this crystal, the optical anisotropy induced by the guest orientation and strain leads to linear birefringence so that the direction of largest refractive index perpendicular to the channel is parallel to [100]. As outlined above, the application of force to {110} induces ferroelastic domain switching. The slow axis of the daughter is oriented approximately 60° to the mother and 90° to the applied stress; this difference in orientation facilitates observation of ferroelasticity under a polarizing microscope (Figures 1.4 and 4.1). Because they are simply rotational twins, the daughter and mother are ideally degenerate. As will be described, this is not necessarily the case for ferroelastic UICs.

During ferroelastic reorientation, several processes must occur. The reorientation of the optical slow axis indicates a rotation of the guest and ferroelastic strain. However, simple rotation does not allow the formation of new hydrogen bonds between host and guest because the channel is helical, and the ureas along adjacent channel walls are not

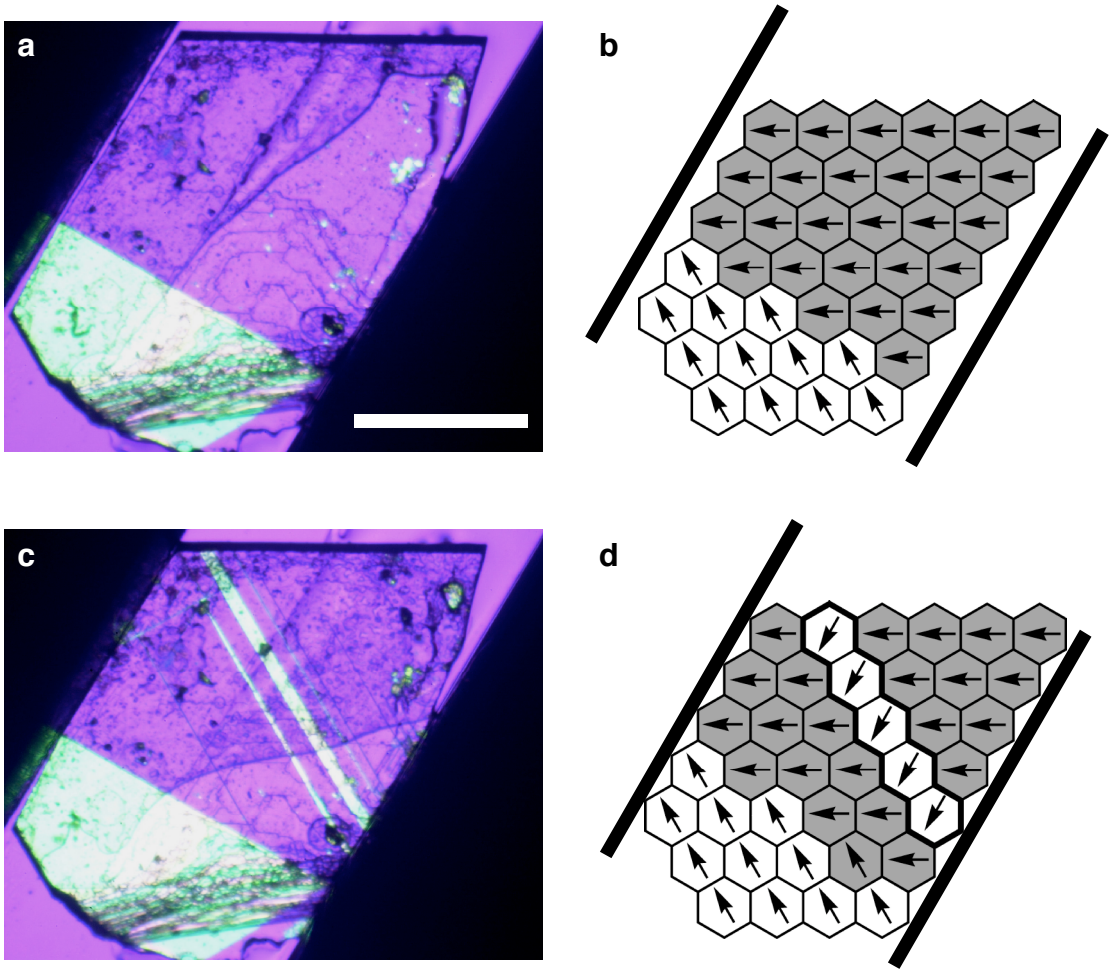



**Figure 4.1** Ferroelastic domain switching in a UIC crystal containing a 83:17 mixture of 2,10-undecanedione and 2-undecanone. **(a)** Photomicrograph of the crystal taken before the application of stress, between crossed polars and with λ plate. In this crystal, the upper rotational twin is in the extinguishing position so it appears dark between crossed polars. Scale bar = 0.50 mm (Nikon 1.3x). **(b)** A schematic representation of the crystal in **a**. Here, the black bars represent the stress bars in **a**. For both rotational twins, the spontaneous distortion is oriented ~30° to the stress bars. **(c)** The crystal, compressed by 1.05% of its original width (1.05% strain). The application of force along [310] has caused some of the extinguished sector to reorient so that the strain (and slow axis) has become aligned perpendicular to the applied stress. **(d)** A schematic representation of the crystal in **c**. This drawing shows that the daughter is not in the extinguishing position and will transmit light when between crossed polars. Note the epitaxially-matched {110}{110} domain boundary (in bold) between mother and daughter. This strain epitaxy makes this boundary energetically preferable to alternatives in which strain epitaxy does not occur. Strain epitaxy between neighboring domains, therefore, can dictate the location and orientation of crystal regions that undergo ferroelastic reorientation. The pair of daughter domains formed in this experiment were analyzed for their reversion kinetics, as described in Section 4.4.1 and in Figures 4.22 and 4.23.

located at the same longitudinal position. The nearest urea is located 1.83 Å up (or down) the channel. In order to produce a degenerate domain structure, the guest must couple its ~60° rotation with a 1.83 Å translation along the channel. For stress applied along a particular direction, the helical nature of the urea helix ensures that this rotation-translation will occur preferentially in one direction along the channel. (Although the guest could rotate and translate in either of two directions, the application of uniaxial stress favors one option over the other. The disfavored alternative includes the rotation of strain so that it would at some point be in opposition to the applied stress.)

In order for the guest to reorient, it must break its hydrogen bonds with ureas at its initial position. Once translation and rotation have occurred, the ureas in the correct positions to hydrogen bond with the relocated guest will rotate about their C=O axes to expose their syn-N-H groups into the channel for hydrogen bonding. (The "initial" urea donors must undergo the opposite operation and will be reoriented along the channel wall, where they can reform hydrogen bonds with other ureas.) Because guests are packed end-to-end in linear tunnels, the translation of one guest requires a similar operation for guests along the entire channel. Thus, ferroelasticity is a very cooperative process in 2,10-undecanedione/urea.

The above mechanism provides a means of visualizing the domain switching process on the molecular level. It must be emphasized that the *sequential order* of these events is unclear. However, it is not unrealistic to assume that the high degree of cooperativity required of this process makes many of these events at least somewhat concurrent. One fact is evident: ferroelastic domain switching is completed very quickly. As discussed below, the domain wall can travel across millimeters of crystal in

a few hundredths or thousandths of a second. The events that must occur on the molecular scale are therefore thought to be highly concomitant.

### 4.2.3 Cooperativity in the Domain Reorientation Event

For 2,10-undecanedione/urea, cooperativity along the channel is complimented by connectivity between channels. The hydrogen bond network that connects hosts and guests throughout the crystal imparts a large degree of association between channels in the domain switching process. Each channel shares faces (and ureas) with adjoining channels, so that reorganization of one channel may bias a similar response in its neighbors. Hydrogen bond donor ureas provide "tethers" between guests in neighboring channels and increase the degree of long-range connectivity within the crystal (Figure 4.2).

When a guest is reoriented by the ~60°/1.83 Å rotation-translation, the urea donor loses one of its hydrogen bond acceptors; at such time, it may be more favorable for that urea to break its contact with the guest in the neighboring channel and recede into the channel wall where it can form hydrogen bonds with other ureas. (NMR studies[17,18] of alkane UICs indicate facile rotation of ureas about their carbonyl axis. It is therefore more appropriate to speak of urea orientations in terms of equilibrium positions instead of fixed positions.) For the guest in the adjacent channel, the loss (or reduction in equilibrium population) of a hydrogen bond donor leads to destabilization so that its reorientation is facilitated. This process continues over many channels to the extent that the breaking of guest-host-guest hydrogen bonds in one channel can trigger large-scale domain reorientation.

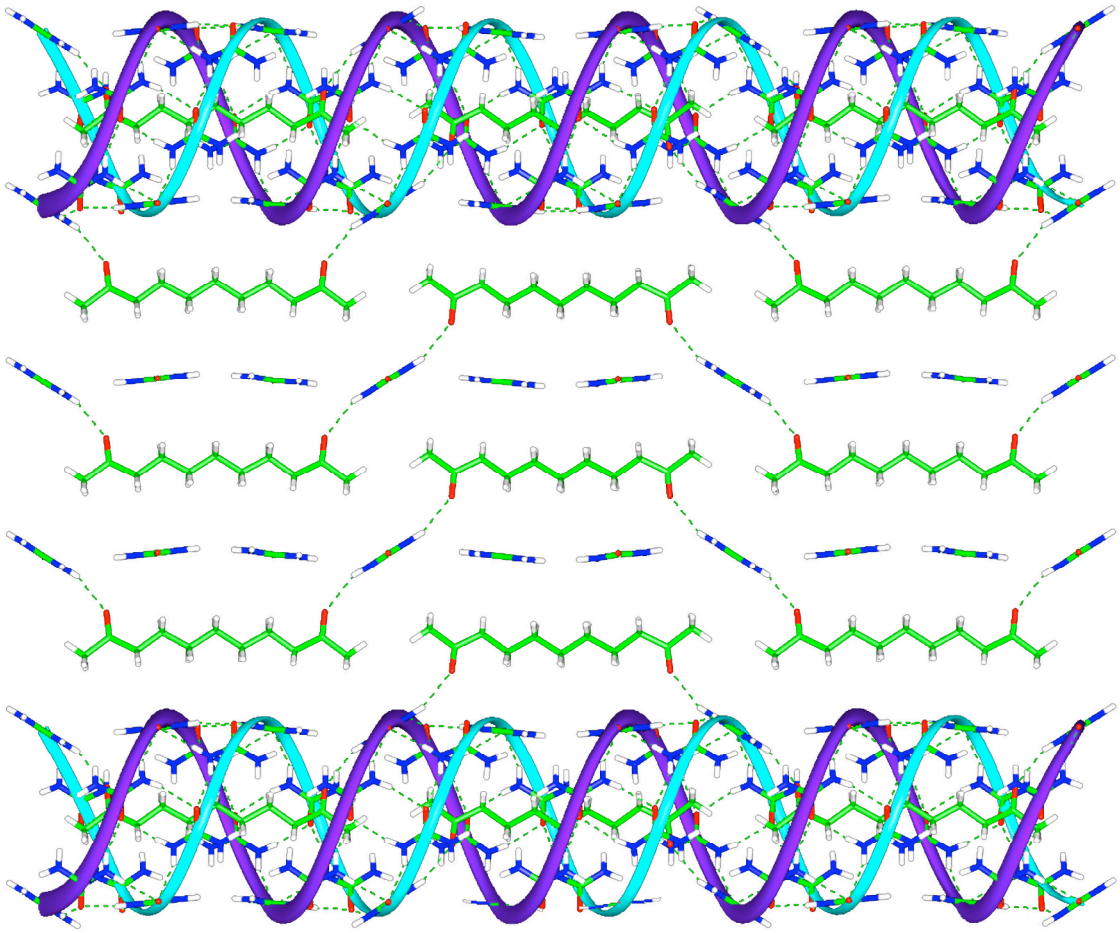


**Figure 4.2** A cutaway view of 2,10-undecanedione/urea, viewed along [010]. (See also Figure 1.3.) The urea host forms helical channels that surround the diketone guest. The helical backbone is emphasized in the top and bottom channels. For the channels in the center, some of the host ureas have been removed to expose the guests they enclose. Here, guests exhibit antiferroelectric ordering and form hydrogen bonds with every third urea along the {100} walls. These ureas donate syn-hydrogens to guests on both sides of the channel wall to form an interchannel host-guest hydrogen bonded network. This network is thought to influence the ferroelastic properties of the crystal. Figure adapted from Brown and Hollingsworth, *Nature (London)*, **376**, 323, (1995).

The coincidence of molecular motion required within and between channels establishes a high degree of cooperativity in the dynamic properties of 2,10-undecanedione/urea. The collective motion of many guests is presumed to be energetically more difficult than reorganization of host molecules (which do not translate nearly as much), so the degree of cooperation should have an appreciable influence on the energetics of domain switching. Ideally, ferroic reorientation leads to a new orientation state that is degenerate with the first.[19,20] With ferroelastic 2,10-undecanedione/urea, this requires fulfilling several conditions, including the reconstruction of host-guest hydrogen bonds and favorable guest bond angles and torsions within the new domain. When these conditions are not met, the potential energy of the orientation states will differ, and they become, strictly speaking, different structures. As described in the sections that follow, minor differences in energy can have an appreciable effect on the relative stabilities of ferroelastic domains.

### 4.2.4 Domain Walls

In a ferroic crystal, the boundary between two adjacent orientation states is known as a *domain wall*. In UICs, adjacent channels share channel walls (and the ureas that comprise those walls), so the projection of ferroelastic strain onto either side of these boundaries should be equivalent.[21] When this condition is met, the strain is accommodated by neighboring channels and is said to be *epitaxially matched*. The absence of strain epitaxy at the domain wall decreases its stability substantially because the distortion of the channels is not balanced at their intersection.[22-24]

Several types of possible domain walls between hexagonal-shaped channels are outlined in Figure 4.3, which was adapted from the work of Hollingsworth, et al.[21,25] These include the epitaxially matched boundaries that divide the twelve possible rotational twins in crystals of 2,10-undecanedione/urea (Figure 2.6). The {130}{130} boundary has the channel distortion on either side oriented approximately 30º from the wall. These boundaries typically run perpendicular to the growth faces in 2,10-undecanedione/urea. At {110}{110} boundaries, the unit cell distortion (on either side) is aligned approximately 60º from the domain wall. These domain boundaries are normally found roughly 60° to the growth face and in general do not coincide with the corners of a crystal. Several other varieties of domain wall are possible (Figure 4.3c-d), but because they lack strain epitaxy, they are thought to be metastable.

As discussed in Chapter 1, crystals such as 2,10-undecanedione/urea are thought to achieve considerable structural stability through a network of host-guest hydrogen bonds. Within the interior of a crystal domain, the uniformity of guest orientation allows for hydrogen bonding to each guest ketone. However, at the domain boundary, ureas must be shared between domains with different orientations, and it is likely that not all possible host-guest hydrogen bonds are formed. An example where this might occur is the {100}{100} merohedral twinning depicted in Figure 4.3c. For an orthorhombic crystal, merohedric twins are related by a two-fold rotational element.[26,27] For crystals of 2,10-undecanedione/urea, every 60° rotation is accompanied by 1.83 Å translation along the channel so that guests related by 180° are separated by 3× 1.83 Å, or 5.5 Å. (Another variant in which the guests are offset by 16.5 Å is also allowed.) Thus, for these crystals, merohedric twins are differentiated by a two-fold rotation-translation in which

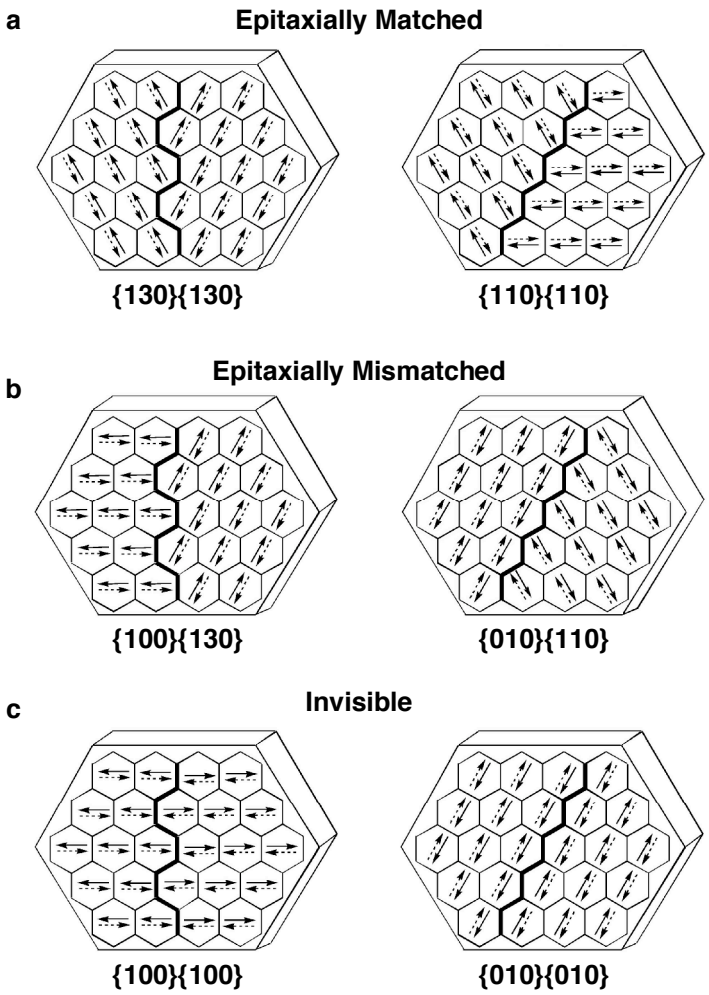



**Figure 4.3** Twin boundaries between distorted hexagonal channels such as those present in 2,10-undecanedione/urea. Although there are several possible ways that neighboring domains may be oriented, only two families are predicted to exhibit strain epitaxy (**a**). In these diagrams, antiferroelectric ordering of guest ketones is depicted by the double arrows. Here, the upper arrow depicts the topmost guest in the channel; a $2_1$ screw relates this guest to the next guest down the channel (dashed arrow). Because the ketones are oriented in the same direction as the distortion from hexagonal symmetry, these arrows also depict the strain for each channel. **(a)** For the {130}{130} type boundary, the strain within each twin is oriented ~30° to the domain wall. For the {110}{110} type boundary, the strain within each twin is oriented ~60° from the domain wall. These types of boundaries are energetically favored because they are epitaxially matched. **(b)** Two examples of unfavorable domain boundaries. In either crystal a 60° domain reorientation of the leftmost twin will result in strain epitaxy at the domain wall. However, should the rightmost twin in either crystal reorient by +60°, distortion within the neighboring twins will possess the same orientation, as depicted in **c**. For these, unit cell distortion and the slow axis (in the *ab* plane) are coincident; such boundaries are invisible to the polarizing microscope. Reoriented twins such as these may be related by either one-half or one and one-half of the urea helical repeat along [001] so that guests at the same channel height are directly opposed. For these twins the unit cells are related by merohedry. Figure adapted from Hollingsworth, et al., *Cryst. Growth Des.*, **5**, 2100-2116 (2005).

adjacent guests are related by 180° rotation and 5.5 Å (or 16.5 Å) translation along the channel. Thus, the domain boundary that joins merohedric twins can be epitaxially matched because the strain orientation on either side of the boundary is equivalent. However, across the domain boundary there is a 5.5 Å or 16.5 Å shift in the longitudinal position of the guests. Along this boundary, ureas cannot donate hydrogen bonds to guests on either side; the host-guest hydrogen bonding network is therefore interrupted, and the domain boundary is destabilized accordingly.

Studies into the characteristics of domain walls and their effect on ferroelastic switching have been most instructive. One striking example of how epitaxy can influence crystal twinning was observed by Brown and Hollingsworth. Their findings, abstracted from the publication[21] of Hollingsworth et al., are presented in Figure 4.4. Here, a crystal of 2,10-undecanedione/urea was grown on a microscope slide by evaporation of the methanol solvent, and the event was recorded on video. In the video, sequential frames are related by 1/30 second. Immediately following frame 434, the collision of a moving crystallite with the growing crystal (see arrow) leads to a marked change in crystal growth. This collision precedes twinning within the yellow sector on the opposite side of the crystal, which leads to a change in the orientation of the domain boundary between this domain and its extinguished neighbor. Following this event, additional growth within that same opposite sector exhibits strain that is reoriented by 60°. (See blue region in subsequent frames). In order to preserve strain epitaxy between the newly formed blue channels and their magenta neighbors, the {110}{110} boundary that previously divided the yellow and magenta domains becomes redirected to a {130}{130} boundary.

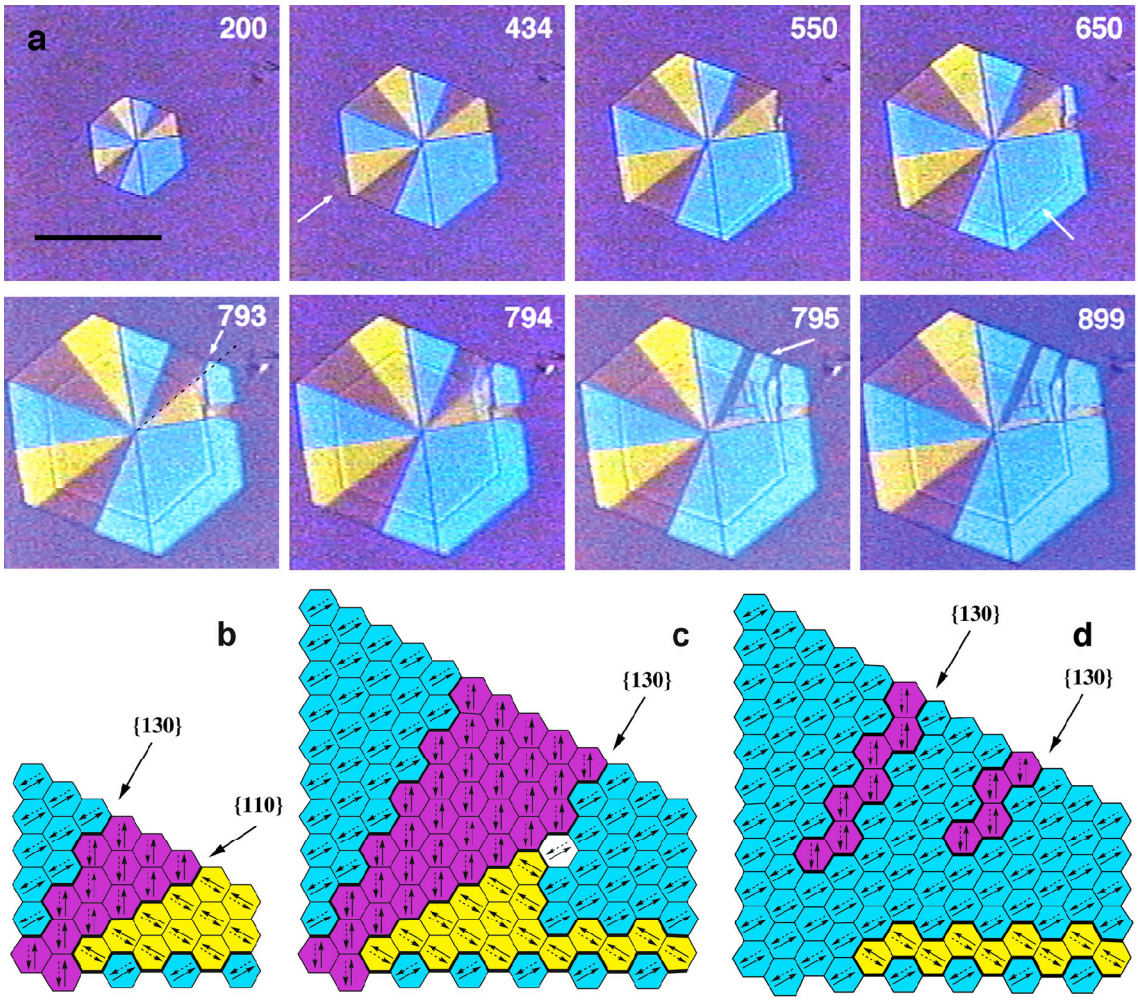



**Figure 4.4** Collision-induced twinning during growth of 2,10-undecanedione/urea from methanol. **(a)** Selected video frames recorded during crystal growth (taken between crossed polars and with λ plate). The frames are numbered in sequence with each integer separated by 1/30 sec. Scale bar = 100 μm. The arrow in frame 434 points to the crystallite that has just struck the growing crystal and has generated a disturbance around the periphery of the crystal at the moment of impact (see arrow in frame 650). Note the redirection of the twin boundary (arrow and dashed line) in frame 793. **(b-d)** Schematic of domain orientations and interference colors. **(b)** Before the twinning event. Arrows within the channels represent the orientation of the ferroelastic distortion for each (as Figure 4.3). The {130} and {110} twin boundaries are epitaxially matched because, on either side of the boundary, the projection of the strain onto the domain wall has the same magnitude. **(c)** After collision-induced twinning, the {110} boundary can no longer be sustained because the outer blue domain has become epitaxially mismatched with its magenta neighbor. This twin boundary therefore reorients so that the blue and magenta domains are separated by an epitaxially matched {130} boundary. The white hexagon at the trisection between the magenta, yellow and blue domains indicates the high energy, mismatched region that becomes the epicenter of the subsequent domain switching event, which relieves this local stress. **(d)** Here, the blue domain has overtaken the yellow and magenta sectors to leave behind epitaxially matched boundaries. Figure and caption adapted from Hollingsworth, et al., *Cryst. Growth Des.*, **5**, 2100-2116, (2005).

Although the interfaces between blue, yellow and magenta domains are each epitaxially matched, the trisection of these three domains is not. (See the white region in the video frames and in Figure 4.4c.) Here, a {110}{110} boundary (between yellow and blue domains) and a {130}{130} boundary (between blue and magenta) domains intersect in what appears to be an epitaxially mismatched boundary. Continued growth of the blue domain requires the repair of this high-energy site. This is accomplished by the ferroelastic reorientation of much of the yellow and magenta domains and the preservation of the {130}{130} boundaries between blue and magenta (and blue and yellow) domains. (See arrow in frame 793 and in c and d).

From the experiment described above, two important observations can be made. First, twinning within the yellow sector led to a change in the orientation of a domain boundary so that strain epitaxy between the new twin and its magenta neighbor could be achieved. Second, for a region in which strain epitaxy could not be established by other means, spontaneous domain reorientation gave rise to its repair. Therefore, energetics of strain epitaxy are significant: destabilization incurred by strain mismatch at a domain boundary is sufficiently large enough for the activation barrier to domain switching to be surmounted. Apparently for this crystal, the driving force for domain reorientation was preferred to destabilization at the mismatched defect site. However, the reorientation of a small number of channels in the immediate vicinity of the defect would not eliminate the strain mismatch; this required reorganization within several domains. The high degree of interchannel connectivity within the crystal "transmits" the ferroelastic reorientation so that a large region was affected. Although difficult to observe, this form of defect annealing may occur often in growing crystals.

When a ferroelastic UIC such as 2,10-undecanedione/urea is observed along [001] under a polarizing microscope at high magnification, the domain walls appear to have a finite thickness. Furthermore, these interfaces do not exhibit obvious slow axis orientations. Instead, domain walls tend to appear extinguished regardless of crystal orientation. This implies that those regions are much less birefringent than the bulk domains or are perhaps even uniaxial, a consequence of reduced average symmetry over the length scales observable with visible light microscopy. Thus, at the domain wall there is probably a shift from orthorhombic (biaxial) symmetry toward higher symmetry, which may arise from reduced guest order and/or strain in these regions. This phenomenon can be investigated using birefringence mapping.

Figure 4.5 depicts the analysis of optical properties across domain boundaries in a UIC crystal grown in a methanol solution containing an 83:17 mixture of 2,10-undecanedione and 2-undecanone and 2.5 M urea.[28] (This crystal was grown as the solution was agitated on a Thermolyne Rotomix.) For this crystal, photomicrographs and the orientation map indicate significant homogeneity in slow axis orientation within the domains and clean, sharp, boundaries between them. A retardation image, calculated from measurements taken at 550, 580 and 600 nm incident wavelength, is provided in Figure 4.5c. In this image, interior regions in each sector appear relatively homogeneous in phase retardation; here, $\delta$ is approximately 2.5 to 3.0 (Sections 2.2.3.2 and 4.4.1.2). For the $25 \times 25$ px$^2$ ($5 \times 5$ $\mu$m$^2$) region outlined in Figure 4.5c, the average $\delta = 2.87$ (3).[29]

However, this homogeneity is lost at and around the domain walls, which reveal dramatic changes in birefringence. Plots of retardation and orientation at these boundaries (Figure 4.6) tell the story. For each region analyzed, as the domain

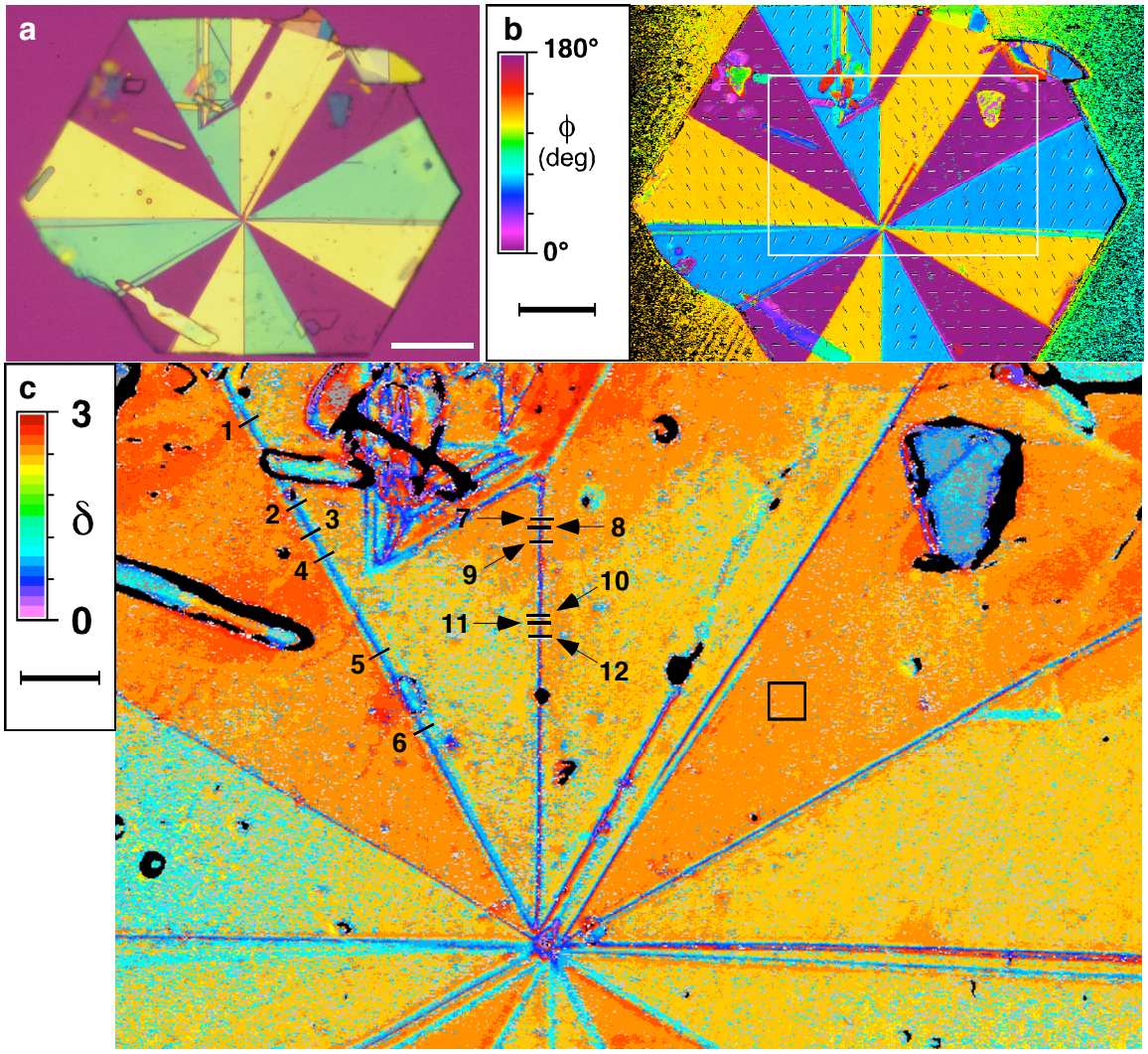



**Figure 4.5** Disorder at ferroelastic domain boundaries is observable as changes in birefringence. A UIC grown from a methanolic solution of 83:17 2,10-undecanedione:2-undecanone. This crystal is estimated to be 7.3 (2) μm thick. **(a)** Photomicrograph taken between crossed polars and with λ plate. Scale bar = 50 μm (Nikon 20x). **(b)** Metripol orientation (ϕ) map calculated from measurements at 550, 580 and 600 nm incident wavelength. The box outlines the sample region for **c**. Scale bar = 43.4 μm (Metripol 20x); azimuthal bars span 25 px. **(c)** Metripol phase retardation (δ) map calculated from measurements at 550, 580 and 600 nm incident wavelength and at 40x. (For this calculation, the dispersion factor, R = 1.) Scale bar = 11.6 μm (Metripol 40x). Note the similarities in retardation between sectors and the reduction in retardation at the twin boundaries and near the crystal nucleus. For data from this birefringence map, line profile analysis of δ and orientation was performed across {110}{110} and {130}{130} type domain boundaries. (See Figure 4.6.) The locations analyzed are denoted by the numbers 1-12. (Sections 1-6 are of a {110}{110} boundary while sections 7-12 are of a {130}{130} boundary.) The black box denotes a region for which δ was analyzed (see text). Figure and caption adapted from Hollingsworth, *et al., Cryst. Growth Des.*, **5**, 2100-2116 (2005).

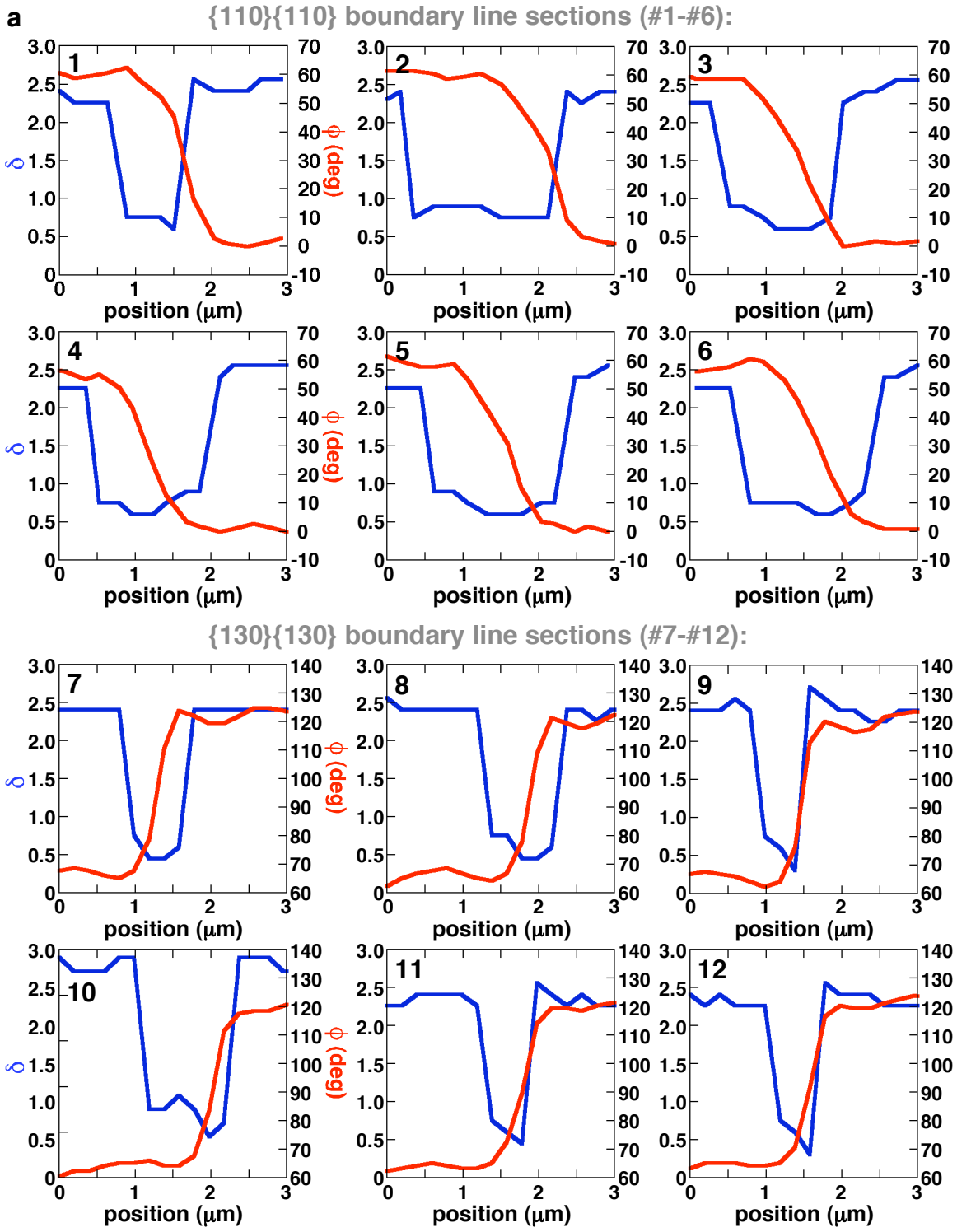



**Figure 4.6** **(a)** Profile plots of sample regions 1–12, as described in Figure 4.5c. For each section the line of analysis spans 3 μm and runs approximately perpendicular to the domain walls. Plotted are phase retardation (δ, in blue) and orientation (ϕ, in red) vs. position (in μm). In each case the retardation decreases substantially toward the center of the domain wall, and the orientation changes smoothly from one endpoint to the other. **(b)** Tabulated data from the plot profiles; these include the minimum observed δ, the width of the boundary (estimated by the full-width at half maximum of the δ curve), and the lateral distance over which ϕ decreases by 75% (from the maximum value).

| Line Section | Type | δ, minimum | δ, FWHM (μm) | ϕ , 75% decrease (μm) |
|---|---|---|---|---|
| 1 | {110}{110} | 0.60 | 0.85 | 0.93 |
| 2 | {110}{110} | 0.75 | 1.99 | 0.88 |
| 3 | {110}{110} | 0.60 | 1.50 | 1.0 |
| 4 | {110}{110} | 0.60 | 1.54 | 0.80 |
| 5 | {110}{110} | 0.60 | 1.78 | 1.0 |
| 6 | {110}{110} | 0.60 | 1.74 | 0.90 |
| | | **average** | **1.6** | **0.92** |
| | | **σ** | **0.4** | **0.07** |
| 7 | {130}{130} | 0.45 | 0.77 | 0.45 |
| 8 | {130}{130} | 0.45 | 0.97 | 0.40 |
| 9 | {130}{130} | 0.30 | 0.69 | 0.35 |
| 10 | {130}{130} | 0.45 | 1.16 | 0.45 |
| 11 | {130}{130} | 0.45 | 0.59 | 0.50 |
| 12 | {130}{130} | 0.30 | 0.62 | 0.40 |
| | | **average** | **0.8** | **0.43** |
| | | **σ** | **0.2** | **0.05** |

orientation changes rather smoothly over the domain boundary, the phase retardation (δ) drops abruptly to a fraction of the value observed in either of the surrounding domains. Although strain epitaxy is achieved (see Figure 4.3) across the domain boundaries, the interfaces exhibit a reduction in the number of guest-host-guest hydrogen bonds because the ureas in this region cannot form hydrogen bonds with all of the available guest acceptors. The same should be true near the crystal nucleus, where multiple rotational twins are joined. (Note the decrease in |sin δ| in the phase retardation image shown in Figure 4.5c.)

Although the disorder arising from the loss of host-guest hydrogen bonding near the domain boundaries gives rise to the lowered phase retardation observed in these regions, the finite values of δ indicate that some ordering may be preserved. Perhaps these regions are composed of many small domains that differ in orientation. If these domains are smaller than the resolution limit of the microscope (discussed in Section 7.5.4) but somewhat larger than the wavelength of light, their combined effect (average phase retardation and orientation) may still be observed in the microscope, and a marked decrease in the phase retardation should result. In any event, the significant decrease in birefringence (to roughly one-fifth the value observed in the crystal bulk) suggests a reduction in interchannel ordering and concomitant ferroelastic strain at the domain boundary.

Crystal disorder at the domain boundaries shown in Figure 4.5 is not confined to an infinitesimally small region. The plots provided show this disorder can span at least 1-2 μm. For each line section it was possible estimate the width of the domain boundary by measuring the width of each "valley" observed in δ. These and other data are tabulated

in Figure 4.6. For the six {110}{110} sections measured,[30] the widths of the boundary at half maximum height (FWHM) spanned 0.85 to 1.99 μm with a mean of 1.6 (4) μm. For six {130}{130} sections, the boundary widths ranged from 0.59 to 1.16 μm with a mean of 0.8 (2) μm. Similar behavior was observed in the orientation images. These were quantified by measuring the distance over which the orientation (ϕ) decreased by 75%; the data are tabulated in the final column. (These values were determined by printing each plot and measuring the linear distance over which ϕ decreased by 75% from its highest value.) Again, the average apparent width of {110}{110} boundaries, 0.92 (7) μm is over twice that of the {130}{130} boundaries, 0.43 (5) μm. Far from being a sharp intersection, domain boundaries within this crystal appear to incorporate an appreciable number of channels. The difference in average widths for the two kinds of boundaries may be artifactual, but the {110{110} boundaries appear to be broader than the {130}{130} boundaries.

To summarize, the domain wall functions as a border between orientation states in a ferroic material. In ferroelastic UICs, epitaxy is achieved when each domain projects an equivalent strain onto the domain wall. In cases where this does not occur, the instability and local stress generated at the mismatched domain boundary can induce spontaneous ferroelastic domain switching. This phenomenon may occur often in growing crystals so that strain mismatch is minimized.

Domain boundaries are microscopic structures of measurable size. Optical studies of these regions indicate decreased phase retardation, which may be a consequence of reduced long-range crystal ordering and strain. Further evidence for disorder at domain boundaries is provided by X-ray dynamical diffraction contrast, an

effect that is observable due to variations in crystal strain.[21] Studies of this nature will be discussed in Section 5.1.2.

## 4.3 Guest Impurities

Crystals of 2,10-undecanedione/urea comprise an intricate network of host-guest hydrogen bonds. Experiments described thus far suggest that the large degree of connectivity provided by this network can influence the ferroelastic properties of UIC crystals. One way of adjusting those properties, then, is to disrupt the hydrogen bond network. This problem has been approached, typically, by growing crystals of 2,10-undecanedione with specific impurities containing fewer hydrogen bond acceptors. For UICs containing 2,10-undecanedione, the impurity most utilized is 2-undecanone.[16,21,31] The incorporation of this guest has been illustrated throughout previous chapters. However, the effect of this impurity (and others) on the ferroelastic properties demands greater exploration.

Chemical intuition and molecular modeling indicate a similar size and shape for 2-undecanone and 2,10-undecanedione. The important structural difference between these guests is the presence of one hydrogen bond acceptor instead of two. Such an alteration in guest functionality can stimulate marked structural changes in urea inclusion compounds. Unlike their diketone counterparts, crystals of 2-undecanone/urea are incommensurate at room temperature.[32] For 2-undecanone/urea, Hollingsworth, et al. measured[32] a 16.27 (7) Å guest length, which is roughly 0.2 Å shorter than that required for a commensurate repeat with the host. In 2,10-undecanedione/urea the unit cell repeat, 33.0 Å, corresponds to the commensurate relationship $2c_g' = 3c_h'$. However, with a

hydrogen bond acceptor at both ends, the diketone guest is capable of matching the necessary length to attain registry with the host. On the other hand, 2-undecanone/urea has no such capability.

The incorporation of 2-undecanone (typically, between 1 and 20%) into a UIC containing mostly 2,10-undecanedione decreases the number of host-guest hydrogen bonds.[16] This reduction should have important structural consequences. The substitution of some fraction of diketone with monoketone impurity should lead to a decrease in the continuity of the hydrogen bond network. In this fashion, interchannel cooperativity should be reduced so that channels (or groups of channels) become more independent of one another, and ferroelastic reorientation becomes more facile. These effects are explored below.

### 4.3.1 Probing Ferroelasticity

Studies probing the ferroelastic behavior of urea inclusion crystals have centered on the stress-strain experiment. In this experiment, a uniaxial force is applied to opposing {110} faces. At this geometry, the force is oriented at approximately 30° to the spontaneous strain so that ferroelastic reorientation of ~60° will produce a domain whose strain is aligned perpendicular to the applied stress (see Figure 1.4). Previous investigations[16,31,33] utilized a stress-strain device that applied force via an analog dynamometer and thumbscrew. Much of the work described herein utilized the device illustrated in Figure 4.7a. This device was designed in-house and constructed by the Electronics Design Laboratory and the Advanced Manufacturing Institute of Kansas State

University. Further description of this device, along with general information on the stress-strain experiments, can be found in Section 7.5.6.

Using a zirconia stress bar, the ultrafast stress-strain device compresses the crystal in increments as small as 20 nm. The zirconia surface is polished and is very flat; it lies quite close to the bottom surface upon which the crystal rests so that crystals of roughly 40 μm thickness can be stressed. The stress bar can be retracted from the crystal at an initial rate of 27 cm $sec^{-1}$ (see Section 7.4 for details), which is faster than the rate of crystal expansion or movement typically observed. In conjunction with high-speed video recording equipment, domain reversion can be measured at rates of up to 10,000 frames per second (fps).

In a ferroelastic stress experiment it is necessary to measure the amount of compression (the strain) applied to a crystal. This quantity is calculated as a percentage change in the initial dimension of the crystal along which the force is applied, i.e.,

$$\text{strain}(\%) = \frac{(L_0 - L)}{(L_0)} \times 100\%. \qquad (2)$$

Here, $L_0$ is defined as the length of the crystal (along the stress axis) *before* stress is applied. This value is measured from photographs taken at first contact between stress bar and crystal and is expressed in μm for these experiments. At any point in the stress experiment, L describes the distance between the stress bars and, therefore, the width of the crystal. This quantity is calculated as the change in position from $L_o$, which is provided by the computer output of the device. Thus, the term ($L_0$ - L) describes the amount of compression of the crystal for some position of the stress bar. By expressing the amount of compression as a percentage of original crystal size it is possible to

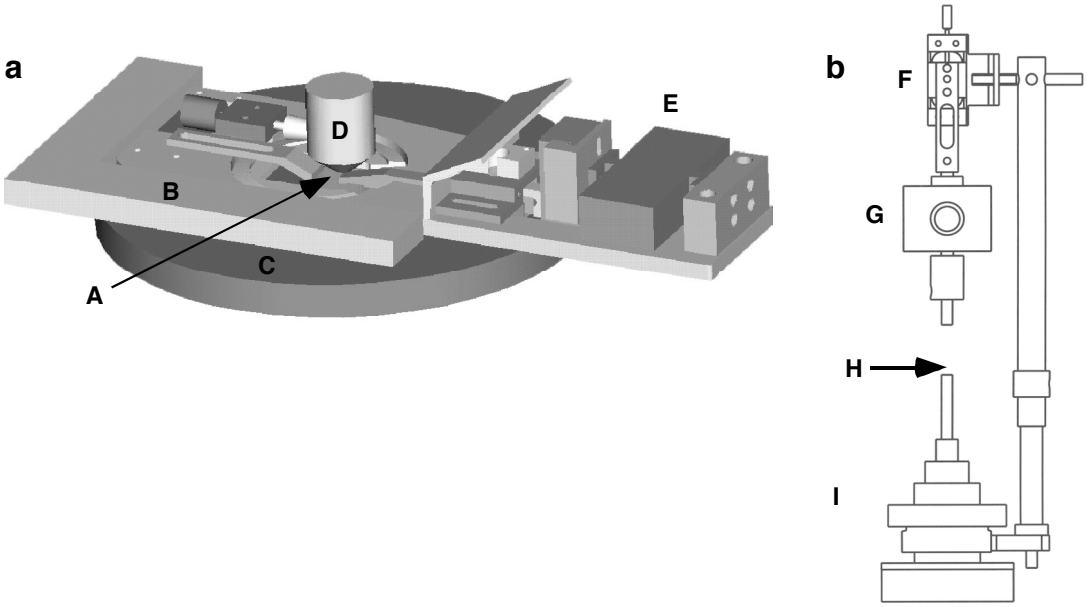



**Figure 4.7** Stress-strain devices utilized. **(a)** Ultrafast stress strain device for use on the polarizing microscope. This computer controlled device is driven by a piezoelectric transducer with a positional accuracy of 20 nm. Experiments measuring the rate of domain reversion included the rapid retraction of the stress bar from the crystal (at a maximum initial rate of 27 cm $sec^{-1}$; see Section 7.6.6 for more information). **(b)** Goniometer-mounted stress strain device for performing *in-situ* stress experiments. (These are discussed in Section 5.2.1.) For this device, stress is applied using a thumbscrew. Both were designed and constructed by Mark D. Hollingsworth and members of the Electronics Design Laboratory and the Advanced Manufacturing Institute at Kansas State University. Legend: **A**, crystal (not present), stressed between a zirconia stress bar and stainless steel "dead" stop; **B**, X-Y stage translator; **C**, microscope stage; **D**, microscope objective; **E**, piezoelectric transducers, load sensor and position sensor; **F**, fine strain adjustment assembly with thumbscrew at top; **G**, load sensor; **H**, crystal (not present), stressed between two hard nylon pins; **I**, eucentric goniometer head. These drawings were created by Nathan Hermesch (**a**) and Clint Linnebur (**b**), of the Advanced Manufacturing Institute at Kansas State University.

compare strain values for crystals of varying sizes. For ferroelastic UICs there is a compliance limit above which most crystals will crack or shear; typically this is about 3% strain. Most crystals studied were on the order of 1 mm across; for these, 1% strain is equivalent to approximately 10 μm compression.

One consideration in the stress experiment lies in the use of crystals whose growth faces are flat and clean of debris. Poor contact with the stress bar or improper alignment of the crystal (from debris or high spots on the crystal face) can lead to shearing or other damage that can alter ferroelastic behavior. For these experiments only crystals with nice, clean growth faces were selected. As crystal history can potentially influence the ferroelastic properties, care was taken in handling of the samples. In some cases (notably, in experiments where an X-ray data set would be collected following the stress experiment) crystal surgery (cutting) was unavoidable (this is pointed out where necessary); for most experiments, however, no surgery was performed prior to the stress experiment.

Following the stress experiment, crystal of sufficient size were typically dissected into their constituent growth sectors and analyzed by HPLC using the instrument described in Sections 2.2.4.2 and 7.5.3. This analysis allowed a reliable determination of the guest content within the sectors of interest. Usually, sectors of about 0.1 mg or greater were large enough to analyze with two or more 25 μL injections with methanol. Smaller sectors were dissolved in less solvent and were analyzed with a single injection; the error in these measurements was estimated using the variation over several injections in the analyzed content of a sample of known ratio of monoketone and diketone.

### 4.3.2 The Incorporation of Guest Impurities Induces a Ferroelastic Memory Effect

Earlier studies[16,34] indicated a critical threshold phenomenon for pseudoelastic ferroelastic domain reversion in UIC crystals containing mixtures of 2,10-undecanedione and 2-undecanone. In most cases, crystals grown from methanol solutions containing more than 16% 2-undecanone formed daughters that were reliably pseudoelastic. However, UICs containing 100% 2,10-undecanedione have also been shown to exhibit pseudoelastic reversion.[34] This behavior is probably dependent on numerous factors including the amount of compression and, as discussed in Chapter 5, the formation of stressed defects that destabilize the daughter domain in a stressed crystal.

Irreversible ferroelastic behavior is demonstrated by a crystal of 2,10-undecanedione/urea in Figure 4.8a-c.[16] For this crystal, the daughter domain formed under stress remains after the removal of the compressive force. This behavior is known as a *plastic* ferroelastic response and is common in ferroelastic materials. For a plastic crystal, the retreat of daughter domain does not accompany the removal of the compressive force (Figure 4.8c). Indeed, the reversal of the strain requires either substituting an expansionary force for the compressive force or application of a uniaxial force along a direction that opposes the ferroelastic distortion of the daughter domain.

Pseudoelastic behavior is demonstrated by a crystal containing 16% monoketone in Figure 4.8e-h. As the crystal is stressed to 2.8% strain (Figure 4.8g), the daughter domain grows to cover about 94% of the stressed sectors.[35] However, the release of stress yields the reversion of the daughter and complete strain recovery; at the resolution attainable with polarized light microscopy, this crystal appears unchanged. A plot of strain vs. stress (measured for this crystal) is provided in Figure 4.8d. Here, the closed

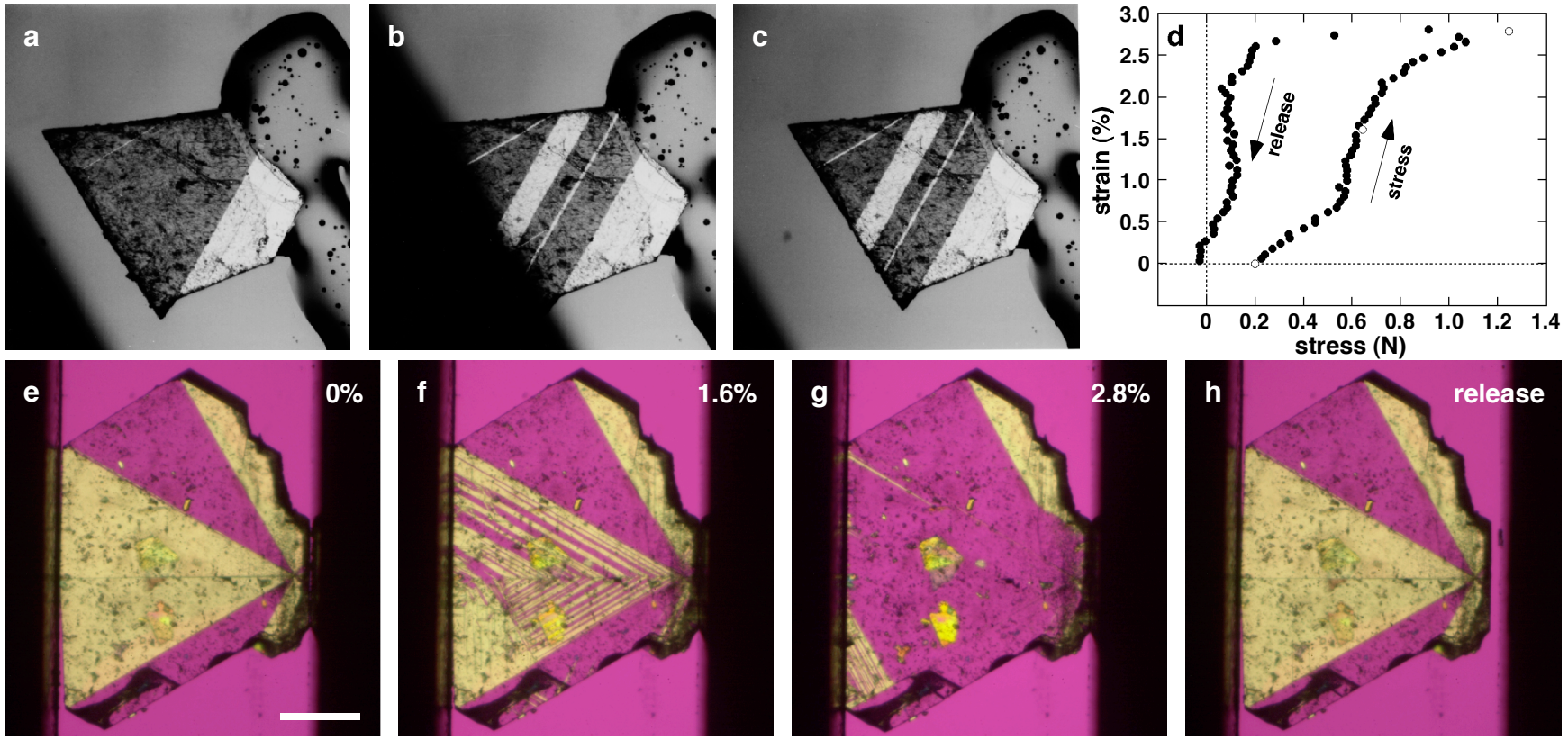



**Figure 4.8** Ferroelastic domain switching in urea inclusion compounds. **(a-c)** A crystal of 2,10-undecanedione/urea exhibiting a plastic ferroelastic response when stressed with a compressive force. Before stressing, the extinguished region of the crystal is composed of a single orientation state (mother). During stress (**b**) daughter domains (light regions) emerge. **(c)** Following stress release, the daughter remains. This domain is said to be *plastic*. For this crystal, the reversion of daughter to mother would require either an expansionary force in the same direction or compression along a direction that opposes the ferroelastic distortion of the daughter. **(e-h)** A UIC containing a 84:16 (±0.8%) mixture of 2,10-undecanedione:2-undecanone (as measured by HPLC). This crystal is stressed to a maximum strain of 2.8% (**g**); here, approximately 94% of the area within the switched sectors has undergone ferroelastic reorientation. Upon release (**h**), the daughter domain retreats completely. This is reflected in the stress-strain curve measured for this crystal (**d**), in which complete strain recovery is achieved without the application of expansionary forces, which would be plotted as negative stresses. In this curve, the open symbols correspond to images **e**, **f** and **g**. Scale bar (in **e**) = 0.50 mm (Nikon 1.3x).

loop occupies only positive values of stress. Such behavior defines pseudoelasticity.[36] As discussed in Chapter 1, this type of pseudoelastic response (known as rubber-like behavior) is simply the spontaneous reversion of a ferroelastic daughter as the stress is removed. For the plastic crystal illustrated in Figure 4.8a-c, negative stresses (i.e., expansionary ones), or stresses that oppose the ferroelastic distortion of the newly switched domains, are required to close the stress-strain loop. This behavior has been reviewed in the book by Salje.[37]

Such observations of spontaneous domain reversion encouraged an investigation of the concentration dependence of this effect. In the study, 90 crystal sectors with 2-undecanone concentrations ranging from 4 to 17% were compressed to strains of up to 3.7%. (These are documented in Figure 7.9b.) For crystals that exhibited pseudoelastic reversion, additional stress experiments were performed, usually until the crystal was shown to be plastic (at reasonable strains), or damaged. Following the stress experiment(s), stressed sectors were cleaved and analyzed for guest content using HPLC. Figure 4.9 presents the results; for these experiments plastic or pseudoelastic behavior is identified for each crystal at a particular strain and monoketone concentration. Here, data for crystals that exhibited complete pseudoelastic reversion are presented as circles, whereas crystals that exhibited incomplete reversion (or did not revert at all) are presented as triangles. For both groups, the shading motif indicates the number of stresses for that sector. First stresses are denoted by filled symbols, second stresses by grey symbols, third (through sixth) stresses by open symbols. (In these experiments there are seven sectors that were stressed more than three times.)

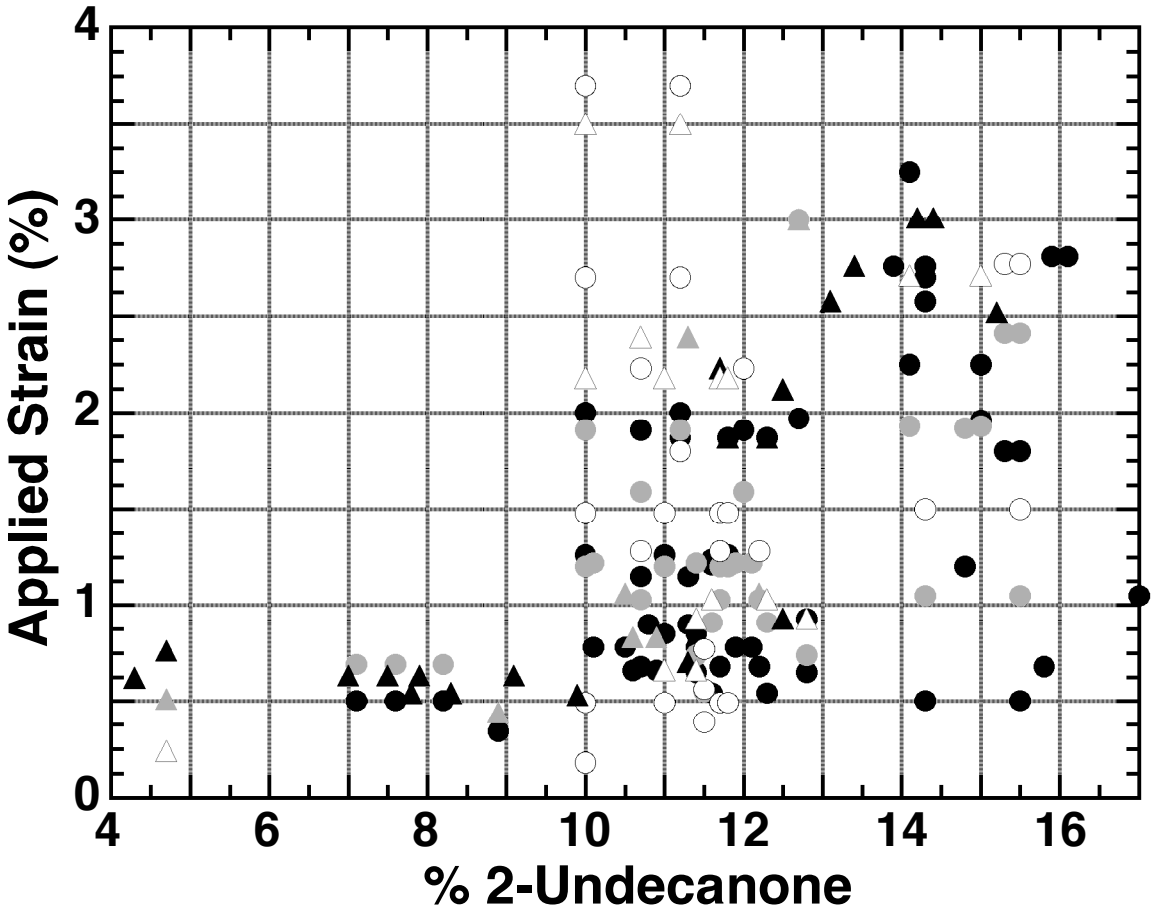



**Figure 4.9** Results of stress-strain experiments for 91 UIC crystals containing mixtures of 2,10-undecanedione and 2-undecanone. Crystals containing between 4 and 17% monoketone were compressed to a strain maximum and then allowed to relax. Monoketone concentrations (as a percentage of the total guest content) was determined for each stressed sector using HPLC. Sectors that exhibited pseudoelastic behavior are represented as ●. Crystals that exhibited incomplete (or no) ferroelastic reversion were deemed plastic; these data are represented as ▲. Crystals exhibiting pseudoelastic behavior were stressed more than once (up to five times total, or until plastic behavior was observed). Filled symbols denote the first stress, grey symbols denote the second stress, and open symbols denote the third, fourth or fifth stress attempts for a given crystal. (In this data there are six crystals that were stressed more than three times.) At approximately 13-14% monoketone concentration, the strain threshold for reliable pseudoelastic domain reversion increases dramatically from approximately 1% to greater than 2.5% strain.

The dependence of pseudoelasticity on monoketone concentration is evident. Two crystals containing less than 5% 2-undecanone exhibited plastic behavior at very low (≤ 0.5%) strains. Between 5 and 10% monoketone, a mixture of plastic and pseudoelastic behavior was observed for different crystals stressed to 0.5-0.7% strain. The strain threshold for plastic behavior increases slightly as the concentration of 2-undecanone reaches 11-12%; all of the crystals tested within this range of concentrations exhibit pseudoelastic reversion for strains up to about 0.65%. (Above 0.65% there is a mixture of pseudoelastic and plastic behavior.) In this series, a striking change in behavior is noted at around 13-14% monoketone. Below this *critical concentration*, many crystals produce irreversible daughter domains from strains of about 1% or less. However, all of the crystals containing greater than 14% 2-undecanone exhibit reliable pseudoelastic domain reversion to roughly 2.5% strain. (Below 13% monoketone, pseudoelasticity at strains of 2.5% or greater was observed in only three sectors, two of which were in the same crystal. These sectors contained 10.0, 11.2 and 12.7% 2-undecanone.) Thus, there is a discontinuous change in pseudoelastic behavior near 13-14% monoketone.

The emergence of spontaneous domain reversion and a critical concentration threshold is remarkable. That crystals revert from daughter to mother indicates an energetic preference for the parent and a surmountable kinetic barrier. Why should this be so? A principal assumption in the study of ferroic behavior is that different orientation states are degenerate in energy.[19,20] For UICs containing mixtures of 2,10-undecanedione and 2-undecanone, this assumption is apparently untrue. Instead, the relative stabilities of mother and daughter, or the kinetic barrier that separates them, become altered as a

function of guest impurity. Precisely how does this occur? What can these observations teach us about the energetics of domain states in ferroelastic crystals? These and other questions will be addressed in the following sections.

### 4.3.3 The Role of Defects in Ferroelastic UICs

The cooperative nature of solid-state reactions makes them subject to the effects of structural defects. Many workers have approached the issue of cooperativity in solid state reactions from various angles, including the work by McBride and coworkers [3-6,8] on the effects of local stress in photochemical reactions and the studies by Luty and Eckhardt[38-40] on compression and strain propagation. A common theme that unites this work is that a crystal can transmit mechanical perturbations over extremely long distances. Therefore, reactions that occur in the solid state are subject to perturbations that originate from regions not necessarily close to the reactive center. These perturbations can change the energetic landscape and therefore exert an influence on the outcome of the reaction. Ultimately, this makes reactions in the solid state subject to factors not present in more familiar fluid-phase reactions.

With regard to materials properties, many workers have devoted appreciable attention to the study of "rubber-like behavior" in martensitic alloys. (Refer to Section 1.2 for a discussion of these materials.) The nature of "rubber-like behavior" has been attributed to a difference between the local (short range) ordering of point defects and long-range order in the bulk.[36,41-46] A mismatch in symmetry between defects and their surroundings can lead to the shape memory effect exhibited by these materials;

interestingly, such defects can be repaired by aging of the stressed alloy so that the memory becomes "erased."

The repair of crystal defects in martensitic alloys is analogous to the process of defect annealing described in Section 4.2.4. In a growing crystal of 2,10-undecanedione/urea, epitaxial mismatch resulting from collision-induced twinning was annealed by the large-scale reorientation of channels residing within adjacent domains. Presumably, this process occurs often during crystal growth. The process of crystal growth normally takes hours or days and provides the parent structure with many opportunities to repair mistakes that may be made during its formation. On the other hand, the daughter is typically formed in a fraction of a second, in a comparatively chaotic process that is ultimately controlled by the experimentalist. During ferroelastic switching there may not be sufficient time for a process of defect annealing to repair mistakes. In cases such as this, the daughter can become filled with stress-induced (*stressed*) defects, one example of which is a site created during the stress experiment at which epitaxial mismatch occurs. Such imperfections are arguably metastable; it follows that their presence contributes to decreased stability within the daughter domain. The domain structure of the daughter is therefore said to be *less perfect* than that of the mother.[21]

The idea of a destabilized daughter domain runs contrary to the traditional view of ferroelasticity, which asserts that daughter and mother domains are degenerate. In an ideal ferroelastic, pseudoelasticity is not observed because there is no driving force for domain reversion. For these, domain switching of the daughter domain is only observed when an appropriate stress is applied. For 2,10-undecanedione/urea, the observation of

pseudoelasticity suggests the mother and daughter domains are not degenerate. Since pseudoelasticity has been observed in crystals well below the critical threshold (Figure 4.9) and in crystals containing no guest impurity,[21] it appears reasonable that the daughter domain is always less stable than mother, regardless of guest content.

One way the daughter can be destabilized (compared to the mother) in a fashion not dependant on guest content is through the formation of stressed defects. (Other possible causes of destabilization are introduced in Chapter 5.) Stressed defects may therefore contribute to spontaneous domain reversion once the stress is released. If stressed defects favor reversion, then why do some crystals exhibit permanent, plastic domain switching? Just as certain defects can *favor* domain reversion, other defects could *resist* domain reversion. Regions that resist domain wall motion may include sites that are not epitaxially matched with regenerated mother domain. These are known as *pinned defects*, and they may give rise to the range of domain reversion rates measured in the experiments described in Section 4.4. However, the story is not yet complete: the critical concentration (of guest impurity) described in Section 4.3.2 suggests that the incorporation of 2-undecanone also plays an important role in the domain reversion process. How might this be so?

An important structural consequence of 2-undecanone incorporation merits consideration. For crystals of 2,10-undecanedione/urea, the parallel ordering of guest carbonyls along [100] expands the unit cell (from hexagonal metric symmetry) along [100] by 3.7%, while a complimentary contraction is observed along [010].[16] However, for crystals containing 2-undecanone, the ferroelastic distortion is reduced.[16] By comparison, a crystal containing 18% 2,10-undecanedione in 2-undecanone/urea exhibits

a strain of 0.01%,[47] while 2-undecanone/urea is metrically hexagonal.[32] For crystals containing mixtures of 2,10-undecanedione and 2-undecanone, a trend connects macroscopic strain and monoketone concentration. The monoketone is anchored to the host with a single ketone at one end of the alkyl chain. Because the other end is not anchored to the channel wall, an appreciable portion of the molecule is free to rotate so that it may not distort the channel. Thus, the macroscopic strain decreases with the incorporation of 2-undecanone impurity.

Because it does not support hydrogen bonding at both ends, 2-undecanone interrupts the host-guest hydrogen bond network that extends throughout the crystal (Section 4.2.2). By doing so, the monoketone impurity reduces interchannel connectivity and therefore increases the capacity for channels (or groups of channels) to reorient independently. As the number of channels that must be reoriented concomitantly is decreased, this reduction in cooperativity should have a substantial effect on the potential energy barrier that separates orientation states. A similar argument was offered by Brown and Hollingsworth.[16]

In an ideal crystal, the reduction in hydrogen bonds between host and guest would lower the barrier to reversion in two possible ways: by decreasing the stability of daughter (and mother), and by increasing the stability of the transition state (relative to daughter and mother). Furthermore, NMR studies of UICs containing mixtures of 2,10-undecanedione-3,3,9,9-$d_4$ and 2-undecanone-3,3,-$d_2$ (conducted[21] by Werner-Zwanziger, Brown and Hollingsworth) demonstrate that 2-undecanone increases the tendency of guests to populate alternative orientations about the channel axis, which may help

facilitate defect annealing. (See Section 4.2.4.) Thus, 2-undecanone is said to be a *relaxive impurity*.[21]

### 4.3.4 Acoustomechanical Relaxation Facilitates Defect Annealing

What is the nature of stressed defects within the daughter? If the observation of defect annealing during crystal growth is any indicator, a mismatch in strain epitaxy between adjacent domains can destabilize the domain boundary. In a fashion not unlike defect annealing observed during crystal growth, it should be possible to repair stressed defects generated within the daughter. Figure 4.10 summarizes an elegant test of this hypothesis performed by Alexis Black and Mark Abel.[21] In this investigation, a UIC crystal containing a 90:10 mixture of 2,10-undecanedione and 2-undecanone was reliably pseudoelastic to a maximum stress of 35 cN for 5.5 minutes (Figure 4.10a-c). (In this experiment, the strain was not reliably measured.) However, when subjected to 31 cN force (for 5.0 minutes) accompanied by vibration parallel to the channel axis from a 4.1 kHz piezoelectric transducer (described in Section 7.5.6), this same crystal yielded incomplete (plastic) domain reversion (Figure 4.10d-e).

This striking change in behavior demonstrates that acoustomechanical vibration altered the ferroelastic behavior of this crystal, which should arise from a change in the energetics of pseudoelastic reversion. It is conceivable that acoustomechanical treatment induced guest reorientations within the urea channels. This effect could influence the energetics of domain reversion in several different ways. First, acoustomechanical vibration may increase the stability of the daughter domain relative to the mother (thermodynamic stability). This might involve the repair of stressed defects that are

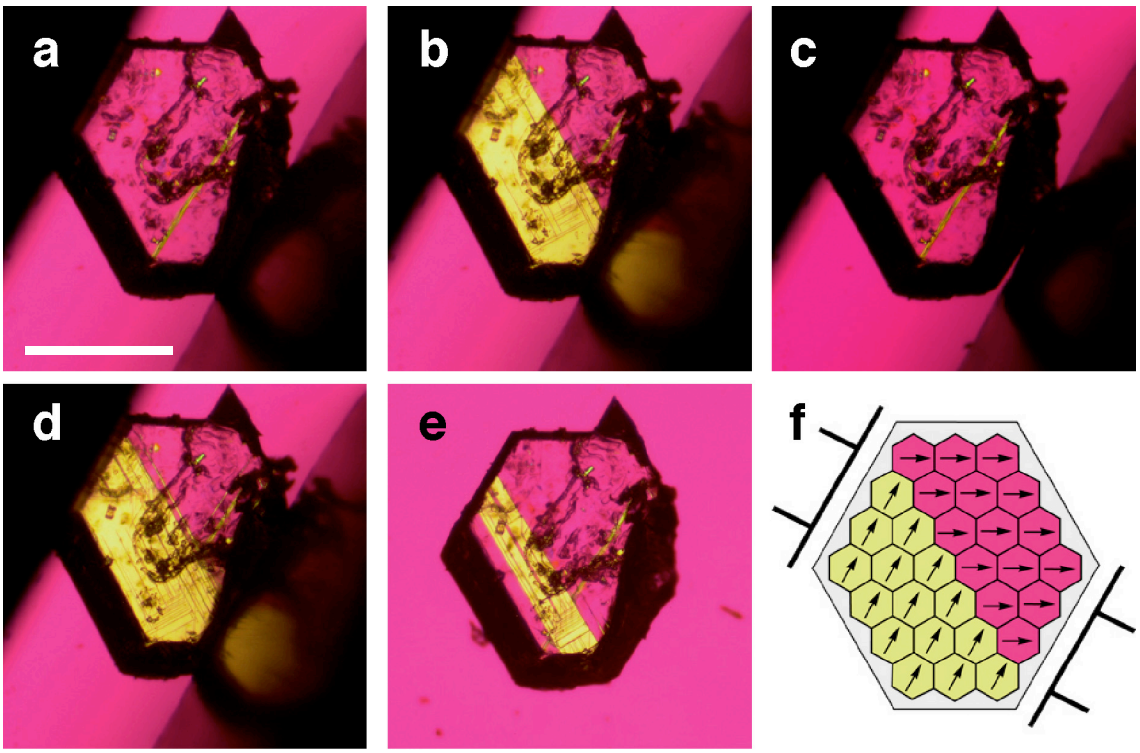



**Figure 4.10** Acoustomechanical relaxation of daughter domains. **(a)** A UIC containing a 90:10 mixture of 2,10-undecanedione:2-undecanone viewed along [001], between crossed polars and with λ plate. In this orientation, [100] runs horizontal so the crystal is in the extinguishing position. Scale bar = 0.50 mm. **(b)** Under 35 cN stress (along {110}), a large daughter domain is visible as a bright band. The slow axis orientations for mother and daughter are provided in **f**. Here, the daughter is rotated by approximately 60° so that [100] is perpendicular to the applied force. The crystal was held in this position for 5.5 minutes. **(c)** Pseudoelastic reversion following stress release. **(d)** A second stress in which 31 cN force produces a slightly smaller daughter domain. This time, the crystal was held at 31 cN for a total of 5.0 minutes, which included 3.0 minutes of acoustomechanical vibration along [001]. The vibration was supplied by a piezoelectric transducer, with a 4.1 kHz fundamental frequency, located 1.5 cm from the crystal (not shown). This transducer is rated at 70 dB (minimum) from 30 cm distance at 12 V potential. (For the current experiment the transducer was operated at 15 V.) **(e)** Plastic behavior following the release of stress after **d**. **(f)** Schematic of domain switching in **b** and **d**. This work was conducted by Alexis Black and Mark Abel and was discussed by Abel, M. J. in *Honors Thesis in Undergraduate Chemistry Research, Oregon State University* (2004). The figure and caption were taken from Hollingsworth, *et al.*, *Cryst. Growth. Design*, **5**, 2100, (2005).

that are thought to destabilize the daughter (Section 4.2.4). Annealing stressed defects may also repair the host-guest hydrogen bond network at those sites. By increasing interchannel connectivity, acoustomechanical relaxation may increase the barrier to pseudoelastic reversion and improve the *kinetic stability* of the daughter domain. Of course, both effects may be operative in this crystal.

A schematic potential energy curve, provided in Figure 4.11, summarizes this line of thought. From the observation of a pseudoelastic memory effect, it is clear that the mother is lower in energy than the daughter. However, the absolute energy is known for neither; therefore, changes in the thermodynamic or kinetic stability of the daughter are difficult to discern. Thus, an increase in the barrier to domain reversion (a measurable property) can arise from a decrease in the (relative) potential energy of the daughter, an increase in the activation energy for domain reversion, or a combination of these.

By disrupting the host-guest hydrogen bond network, monoketone impurity should decrease the absolute stability of both mother and daughter domains. In principle, this effect should be similar for both mother and daughter so that no change in their *relative* energies is observed. However, as discussed in Section 4.3.3, the incorporation of monoketone impurity increases tendency of guests to populate alternative orientations about the channel axis,[21] which is thought to favor defect annealing. Since the daughter domain is thought to possess a greater number of stressed defects, this might actually *lower* its energy relative to the mother. Other things being equal, an increase in the thermodynamic stability of the daughter can be observed as an increase in the barrier to domain reversion. By the same token, facilitated guest reorientation could lower the

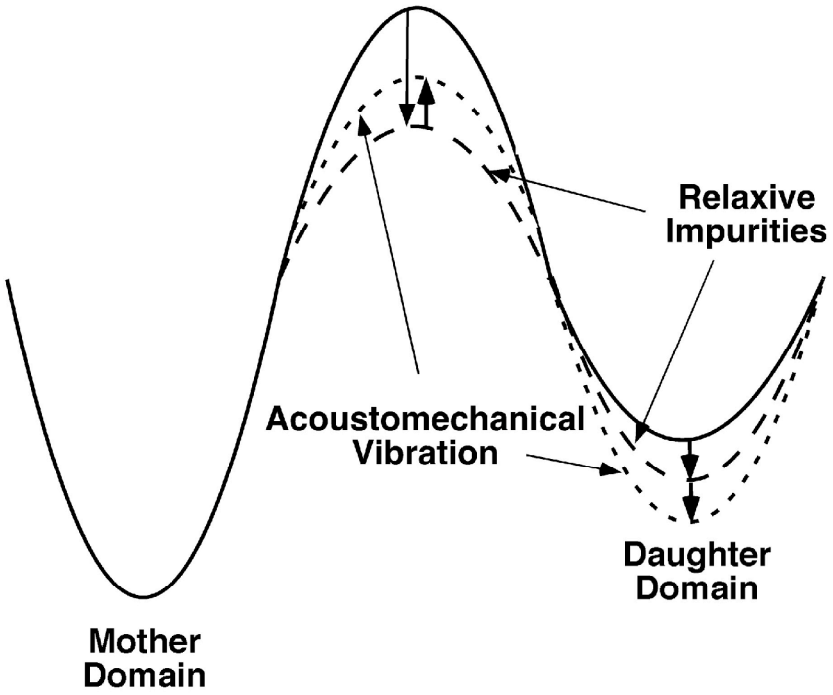



**Figure 4.11** A schematic ferroelastic potential energy surface for ferroelastic UICs such as those containing mixtures of 2,10-undecanedione and 2-undecanone. Although their absolute energies are not known, spontaneous pseudoelastic domain reversion reveals that the daughter is metastable with respect to the mother. The incorporation of 2-undecanone (a relaxive impurity) is thought to raise the energies of both orientation states because of loss of a hydrogen bond acceptor. However, interruption of the hydrogen bond network caused by the relaxive impurity also facilitates defect annealing. The daughter, with more stressed defects, is therefore stabilized by monoketone impurity to a greater extent than the mother. However, because monoketone incorporation facilitates pseudoelastic domain reversion, it must lower the barrier to reversion more than it stabilizes the daughter. The pseudoelastic behavior of crystals may be altered by applying acoustomechanical vibration under stress. This treatment is thought to stabilize the daughter domain kinetically by raising the barrier and/or lowering the energy of the daughter. This may occur through the repair of stressed defects and the reconstruction of hydrogen bonded networks at those sites. Figure taken from Hollingsworth, *et al*., *Cryst. Growth Design,* **5**, 2100, (2005).

barrier to domain reversion and speed up that process. These hypotheses form the basis for studies of reversion kinetics, which are discussed in Section 4.4. As discussed above, acoustomechanical vibration should also affect a crystal's tendency for pseudoelastic reversion, possibly by raising the barrier or by stabilizing the daughter (or both).

In summary, the incorporation of 2-undecanone into UICs containing predominantly 2,10-undecanedione leads to dramatic changes in ferroelastic behavior. Above the critical monoketone concentration, a daughter domain will spontaneously revert to the mother following release of strains approaching 3% (in a few instances, even higher). This implies a *reduced* barrier to domain reversion, which may be a consequence of several features, including decreased interchannel connectivity and facilitated guest motions. At this point it unclear to what extent each of these effects contributes to the overall energetics of domain switching. However, acoustomechanical vibration induces a striking change in the persistence of the daughter domain. Whether this change arises from improved thermodynamic or kinetic stability of the daughter has not been demonstrated. These phenomena will be addressed below.

## 4.4 The Kinetics of Domain Reversion

It has been suggested recently that stressed defects can indefinitely retard the motion of domain walls in ferroelastic UICs.[21] If such stressed defects destabilize the daughter domain with respect to mother domain, then the longevity of daughter domains in stressed crystals of 2,10-undecanedione/urea results not from thermodynamic stability of the daughter but from the kinetic stability afforded by a high barrier to reversion. As stated above, the introduction of relaxive impurity 2-undecanone can induce

pseudoelasticity in UICs containing mostly 2,10-undecanedione. Because spontaneous reversion is a collective phenomenon in which channels do not revert independently, the abrupt change in behavior appears at a critical monoketone concentration. However, this kind of information does not reveal subtle variations in the domain barrier that are thought to result from differences in monoketone concentration. These details can instead be examined by a study of domain reversion kinetics.

The potential energy curve presented in Figure 4.11 was a working hypothesis for many of the studies described in this thesis. Although it does not portray completely the current understanding of the energetics of domain states, it provides an important question for the ferroelastic behavior of UICs, the testing of which has expanded appreciably the knowledge of this phenomenon:

> If monoketone impurity reduces the potential energy barrier to domain reversion, how does the rate of reversion vary with monoketone concentration?

To address this question, ten unstressed and uncut UIC crystals containing mixtures of 2,10-undecanedione and 2-undecanone were stressed and released; the kinetics of domain reversion were quantified for a total of twelve sectors by video analysis of the events. Following the stress experiment, guest stoichiometries were determined with HPLC analysis of the stressed sectors using the same procedure described in Section 2.2.4.2. The crystals studied contained between 4.7 and 17.6% of 2-undecanone impurity. Nine of the sectors were compressed to strains between 0.44 and 1.21%. Three additional sectors were stressed to greater values (up to 2.12%). Once the maximum compression had been attained, the stress anvil was retracted at its maximum

rate, which was faster than the rate of crystal expansion. (Refer to Sections 4.3.1, 7.4 and 7.5.6 for details.) The domain reversion process was captured with ultrafast videomicroscopy (at frame rates of up to 10,000 fps) using either a Kodak MotionCorder SR-Ultra or an X-Stream Vision XS-4 (borrowed from Speed Vision Technologies, Inc.) Ultrafast videos were converted to QuickTime movies, and still frames were extracted using Adobe Premiere 5, X-Stream X-Vision 1.05, or Xcitex MiDAS 2.0 (all for Windows).

The reversion events are summarized in Figures 4.12 through 4.23, and relevant experimental information is provided in Figure 4.26a (below). (In addition, a schematic diagram describing the domain structure of each crystal is provided in Figure 4.26b-l.) The time duration for this series of crystals spanned 1.0 ms to 1.5 s (column 7 of Figure 4.26a). In the figures, the time intervals between successive frames were chosen to represent the entirety of the domain reversion event for each crystal. For instance, in Figure 4.17 (entry 6), fast domain reversion is observed immediately following retraction of the stress bar; for later stages of the event, reversion slows down appreciably. During the first 20.0 ms, still images from the ultrafast video are spaced in 1.0 ms increments; for the last 54.0 ms, still images are spaced by 9.0 ms. A similar scheme is utilized in Figure 4.18 (entry 7). Here, images collected during the first 68 ms (when the changes in luminosity are the most rapid) are presented in 4.0 ms increments (images c-t); for the remainder of the 1380 ms event, images spaced by 200 ms are provided (images u-aa).

The rate of domain reversion was determined through an analysis of the still video frames. (This process is described more thoroughly in Section 7.5.6, and additional information about each stress experiment is provided in Figure 7.9a.) For the stress

experiments described, the crystal was held so that the mother was in the extinguishing position; daughter domains emerging in the stress experiment were therefore observable as bright regions in the crystal. There are two types of daughter domain that preserve epitaxy with surrounding mother domain. These are described in Figure 4.3a. Daughters grown along a {130}{130} boundary run parallel to $[310]_{mother}$, and generally run normal to the growth face. Daughters grown along a {110}{110} boundary run parallel to $[110]_{mother}$, and generally intersect the growth face at an angle of 60°. Because extinguished mother and non-extinguished daughter domains transmit light differently, reversion kinetics were measured by following changes in crystal luminosity. (This process is described in Section 7.5.6.) In previous experiments[48] the motions of the domain walls were measured, but this work[49] has demonstrated a linear correspondence between domain wall position and luminosity (a measure of brightness) for domain reversion in a crystal containing (nominally) an 85:15 mixture of diketone and monoketone. The experiment is described in Figure 4.24a-k. In this stress experiment (performed[50] by Mark Abel and Alexis Black), the crystal broke, and the reversion process of a broken fragment was recorded at 125 fps but stored at 30 fps (Figure 4.24a-i). The visible "width" of the domain (which is proportional to its volume) was measured (using ImageJ, v. 1.33u, for Macintosh) by drawing line profiles across the domain, as demonstrated in Figure 4.24a and measuring the full width at half maximum (FWHM) of each profile. For comparison, the mean luminosity was measured (using Adobe Photoshop, v. 7.0, for Macintosh) for the same 56 × 93 $px^2$ region outlined by the dashed box in Figure 4.24a. A plot of FWHM and mean luminosity vs. time (Figure 4.24j) demonstrates very similar behavior for both methods; furthermore, a plot of FWHM vs.

mean luminosity (Figure 4.24k) shows a very linear correlation between the two measurements. Thus, luminosity can be scaled to the size (volume) of the daughter domain. This process is outlined in Section 7.5.6.

Although both methods appear applicable for measuring domain reversion kinetics, the method based on mean luminosity is considered more reliable because the same region of each video frame can be sampled using available computer software such as Adobe Photoshop (v. 5.5 and 7.0, for the Macintosh). (In practice, many daughter domains do not revert over a simple domain front. Since it does not measure the shape of the domain, the measurement of mean luminosity is also not affected by changes in the shape of the domain or domain boundary that can affect simple measurements of domain "width".) In this fashion, daughter content was analyzed over sequential video frames by drawing a sample marquee of suitable size around the region of interest and recording the mean luminosity for that region in each frame. (For each entry the sample region was chosen based on its coverage of the daughter domain of interest, lack of interference from other domains, and inclusion within each video frame of the video sequence. The process is demonstrated in Figure 4.24l-z. Because the crystals typically jump or move following fast retraction of the stress anvil, a static analysis region does not accurately measure reversion for a particular daughter domain. This problem was addressed by applying a thin film of paratone oil to the bottom of the crystal (to provide some adhesion to the microscope sample slide) and by manually relocating the sample marquee according to visible crystal landmarks. Although relocation of the marquee does not correct for vertical crystal movement (towards the microscope objective), careful positioning of the marquee produced results that are thought to be as accurate as possible. (This topic is

revisited below.) An account of each ultrafast video sequence is provided in the next sections.

### 4.4.1 Reversion Behavior and Kinetics

A discussion of the kinetic data obtained from this analysis follows the discussion of crystal behavior and data collection. For each experiment, the slow axis of the mother domain, {100}, was oriented horizontally so the mother was extinguished. In each experiment the stress bars were oriented either 60° CW or CCW from horizontal, as was the slow axis of the daughter domain; this orientation is denoted for each experiment. (In every case, the daughter domain slow axis is oriented parallel to the stress bars.) Figures 4.12 through 4.23 provide images collected during the reversion events and schematic diagrams of the stressed crystals are provided in Figure 4.26b-m. Additional information about domain orientation is provided in the following discussion and in the fifth column of Figure 4.26a, which summarizes details about each stress experiment.

#### 4.4.1.1 Crystal Behavior

Beginning with entry 1 (Figure 4.12), the crystal (4.7% 2-undecanone) was compressed by 0.76% along the NW to SE diagonal. (See the white "stress bar" in the figure.) Immediately prior to stress, photomicrographs (Figure 4.12a) indicate several striped daughter domains in the viewing area. (These domains are labeled 1-3 in Figure 4.12b.) This photomicrograph was taken between crossed polars but without the λ plate, which is the same set of conditions used for the fast video capture. Of interest is the closely spaced pair of daughter domains that span the length of the crystal (labeled 3 in

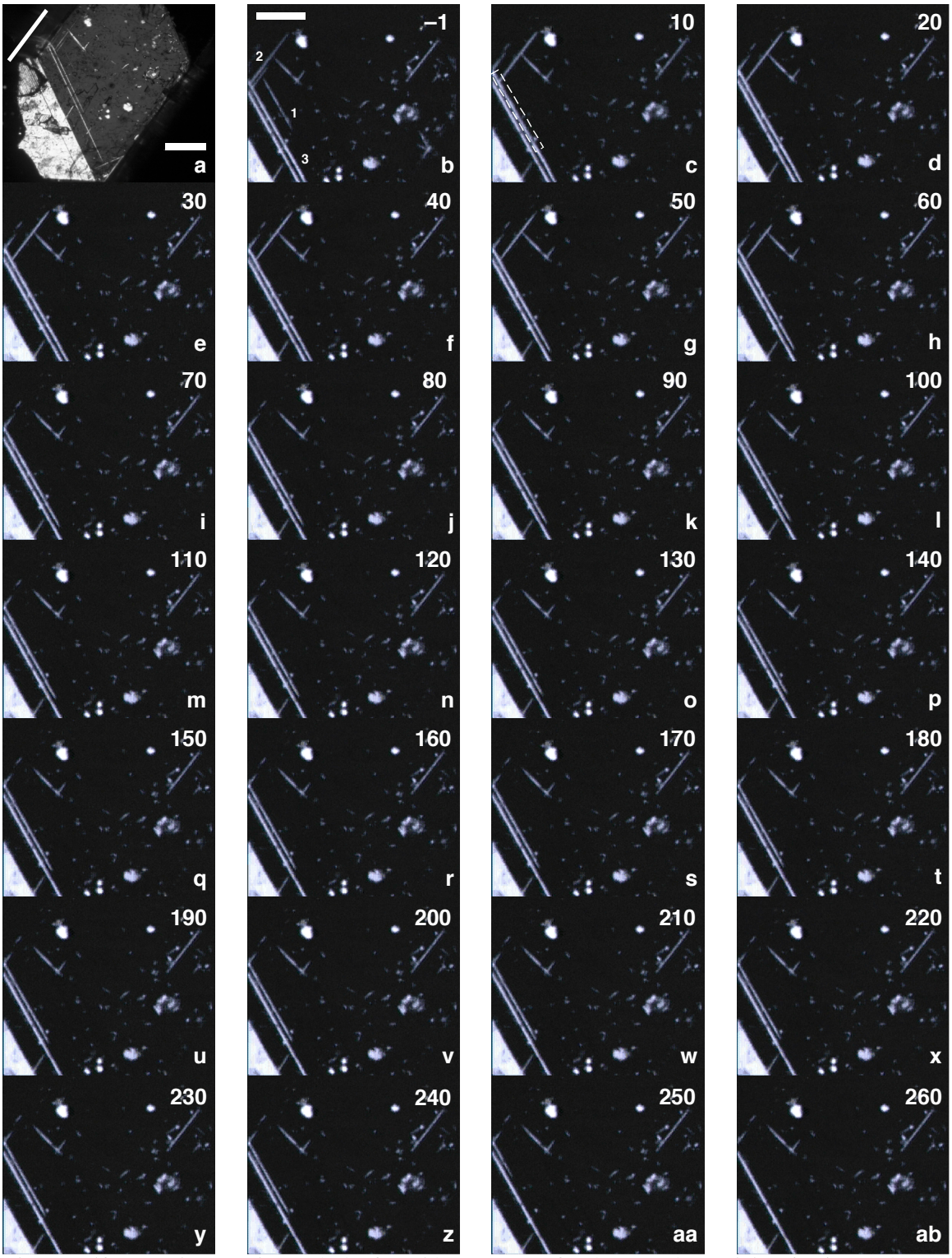



**Figure 4.12** Domain reversion and ultrafast video sequence for the crystal containing 4.7% monoketone (entry 1 in Figure 4.26) following 0.76% compression. **(a)** Photomicrograph (crossed polars) of the crystal taken immediately before stress release. The orientation of the active stress bar is indicated at top left of the crystal. Here, mother domain (extinguished) surrounds bright stripes of daughter domain (labeled 1 through 3 in **b**). Scale bar = 0.25 mm (Nikon 5x). **(b-x)** Ultrafast (1000 fps) video frames, beginning 1 ms prior to stress release (**b**) and in 10 ms increments thereafter (**c-ab**). In each image the time from stress release (time = 0) is presented in the upper right-hand corner. The box in frame **c** indicates the sample region for this frame, which was repositioned according to crystal motion (see text). Scale bar = 0.20 mm (Kodak 5x).

the figure; see also boxed region in c). As illustrated by the schematic in Figure 4.26b, the daughter domains run along [110] and border the surrounding mother domain at {110}{110} type boundaries (Figure 4.3a). In the video frame collected 1.0 ms before stress release (Figure 4.12b), portions of both of these daughters can be seen at lower left. At stress release (time 0, frame not shown) the crystal jumps rapidly so that the first video frame (collected at 1000 fps) appears blurred. (At the time of this experiment, the relatively slow video capture speed was predicted to be adequate for this crystal containing a small amount of monoketone. Most of the reversion experiments that followed were performed at faster rates, typically 3000 to 5000 fps, and are not as subject to blurring.) For this reason, the first video frame collected after stress release (at 1.0 ms) was discarded from the kinetic analysis, and this entry is said to have a dwell time of 1 ms. (This was the only experiment for which there was a dwell time.)

In the second frame collected following stress release (t = 1 ms, not shown), daughter 1 had already disappeared (it was not located within the integration box, anyway), and its behavior was not analyzed. For the large pair of daughters (labeled 3), one stripe of daughter domain reverts over a span of 254 ms, while the other does not revert at all. With the exception of entry 7, this is the only case in which a plastic daughter was generated in this series of crystals. The region that did exhibit pseudoelastic reversion was analyzed for luminosity within the sample area outlined in Figure 4.12c. This area, which spans an area of 30 × 360 $\mu m^2$, was positioned so that it would sample predominantly one daughter (3); however, some interference from the adjoining daughter (2) was unavoidable because the two daughters were not completely separable. Their behavior is discussed below.

For entries 2 and 3 (10.8 and 11.3% 2-undecanone, Figures 4.13 and 4.14; schematics in Figure 4.26c-d), a single band of daughter is observed toward the top of the crystal. In each case the daughter domains run along [310] (defined in Figure 2.6e) and border surrounding mother domain at a {130}{130} type boundary (Figure 4.3a). However, unlike the thin daughter in entry 1, which appears to withdraw parallel to its longest axis, the domain switching process for entries 2 and 3 clearly occurs at {130}{130} domain walls. For entry 2, compressive force (to 0.90%) was applied along the SW to NE diagonal. Upon release, domain reversion spans 1.0 ms, or three frames at the 3000 fps capture rate. (The area analyzed for luminosity measured 280 × 56 $\mu m^2$.) This event provides only three data points for kinetic analysis; over these frames, domain wall motion appears much faster than in the crystal containing 4.7% 2-undecanone (entry 1). However, it is demonstrated below that, in terms of mole guest $s^{-1}$, the rates observed for this crystal are comparable to rates of reversion for other crystals. For entry 3 (also compressed by 0.90%, but along the NW to SE diagonal), the fast video was captured at 500 fps (an error on the part of the experimentalist); in this trial the reversion event spans five frames, or 10.0 ms. For this crystal, luminosity was recorded within a 210 × 210 $\mu m^2$ sample area (Figure 4.14b).

Entry 4 (11.4% 2-undecanone, Figure 4.15; schematic on Figure 4.26e) exhibits two parallel daughter domains prior to stress release from 0.85% compression (Figure 4.15a-b). Force was applied to this crystal along the SW to NE diagonal; the daughter domains run along [310] (Figure 2.6e) and border surrounding mother domain at a {130}{130} type boundary (Figure 4.3a). Upon retraction of the stress anvil, both daughters decay with the same approximate overall rate; here, luminosity decays over a

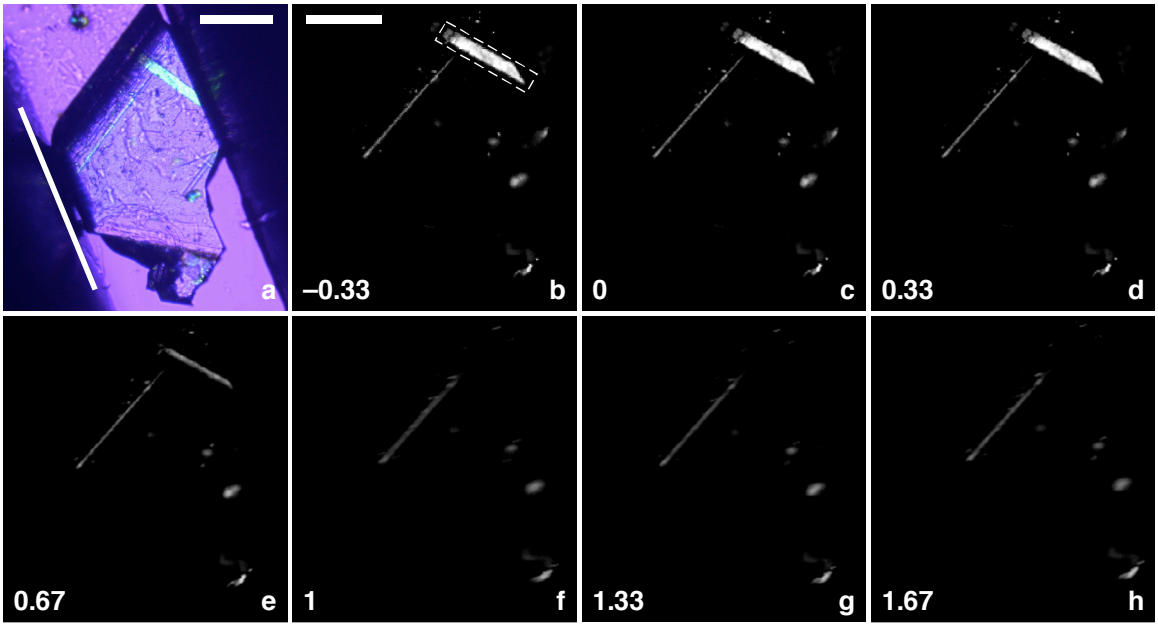



**Figure 4.13** Domain reversion and ultrafast video sequence for the crystal containing 10.8% monoketone (entry 2 in Figure 4.26) following 0.90% compression. **(a)** Photomicrograph (λ plate, crossed polars) of the crystal taken immediately before stress release. Here, mother domain (extinguished) surrounds bright stripes of daughter domain along {130}{130} domain boundaries. The orientation of the active stress bar is indicated. Scale bar = 0.25 mm (Nikon 5x). **(b-h)** Ultrafast (3000 fps) video frames (crossed polars), beginning 0.33 ms prior to stress release (**b**) at stress release (**c**) and in 0.33 ms increments thereafter (**d-h**). In each image, the time from stress release (time = 0, frame **c**) is presented in the lower left-hand corner. The box in frame **b** indicates the sample region for this frame, which was repositioned according to crystal motion (see text). Scale bar = 0.20 mm (X-Stream XS-4 10x). The aspect of the video frames was altered during accumulation of this video; this imperfection does not affect the measured reversion rates (see text).

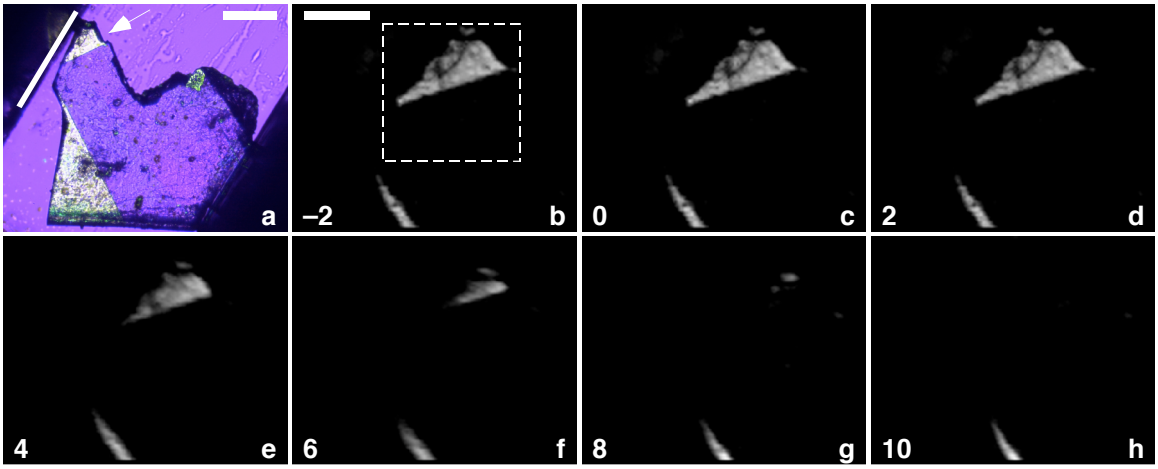



**Figure 4.14** Domain reversion and fast video sequence for the crystal containing 11.3% monoketone (entry 3 in Figure 4.26) following 0.90% compression. **(a)** Photomicrograph (λ plate, crossed polars) of the crystal taken immediately before stress release. At the upper tip of this crystal, the daughter (see arrow) forms a bright wedge above the adjacent mother domain (extinguished). (The resulting domain boundary is {130}{130}.) The orientation of the active stress bar is indicated. Scale bar = 0.25 mm (Nikon 5x). **(b-h)** Fast (500 fps) video frames (crossed polars), beginning 2 ms prior to stress release (**b**) at stress release (**c**) and in 2 ms increments thereafter (**d-h**). In each image the time from stress release (time = 0, frame **c**) is presented in the lower left-hand corner. The box in frame **b** indicates the sample region for this frame, which was repositioned according to crystal motion (see text). Scale bar = 0.10 mm (X-Stream XS-4 10x). The aspect of the video frames was altered during accumulation of this video; this imperfection does not affect the measured reversion rates (see text).

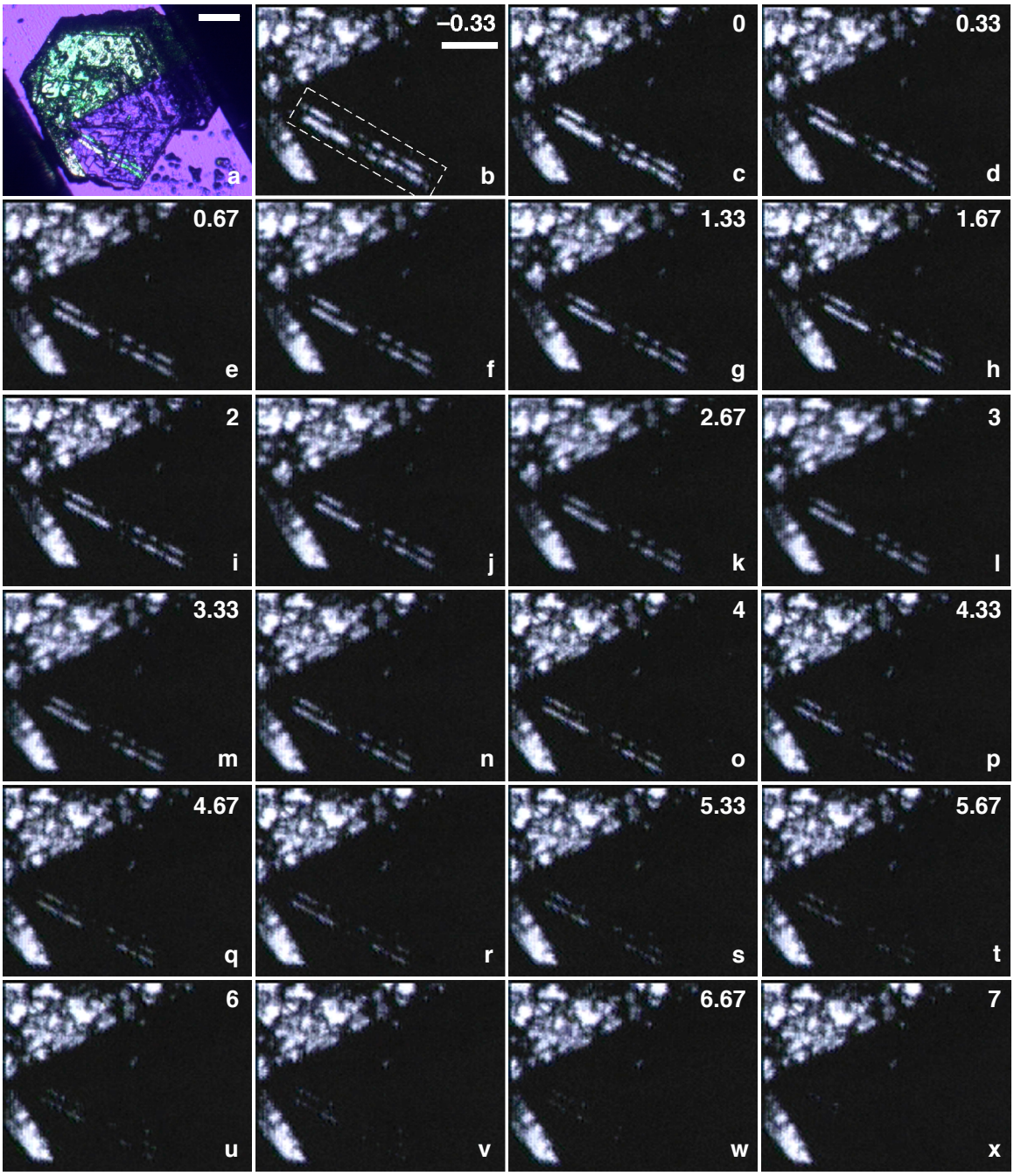



**Figure 4.15** Domain reversion and ultrafast video sequence for the crystal containing 11.4% monoketone (entry 4 in Figure 4.26) following 0.85% compression. **(a)** Photomicrograph (crossed polars, λ plate) of the crystal taken immediately before stress release. Here, mother domain (extinguished) surrounds bright stripes of daughter domain. Scale bar = 0.25 mm (Nikon 1.3x). **(b-x)** Ultrafast (3000 fps) video frames, beginning 0.33 ms prior to stress release (**b**) at stress release (**c**) and in 0.33 ms increments thereafter (**d-x**). In each image, the time from stress release (time = 0, frame **c**) is presented in the upper right-hand corner. The box in frame **b** indicates the sample region for this frame, which was repositioned according to crystal motion (see text). Scale bar = 0.20 mm (Kodak MotionCorder 1.3x).

period of 7.0 ms, or 21 frames at 3000 fps. Analysis was conducted for the 140 × 570 $\mu m^2$ region denoted in Figure 4.15b.

When compressed by 0.44% along the SW to NE diagonal, entry 5 (11.5% 2-undecanone, Figure 4.16) exhibits two daughter domains that intersect at an angle of approximately 30° (see Figure 4.16b and schematic in Figure 4.26f). This crystal exhibits daughters along both possible domain fronts: {110}{110} (larger portion) and {130}{130} (smaller portion); these are presented schematically in Figure 4.26f. Although less common than daughters that form along {110}{110}, growth of {130}{130} daughter regions such as this has been described by Hollingsworth, et al.[21] As the schematic in Figure 4.26f shows, strain within the {130}{130} daughter is not oriented parallel to the stress bars; instead, the strain is oriented 60° from the applied stress and this domain is degenerate to the mother (with respect to the applied stress). This daughter is therefore known as an *anomalous* daughter; the formation and possible function of anomalous daughters is discussed in Chapter 5.

The 72 × 560 $\mu m^2$ sample region (Figure 4.16b) was chosen so that it included predominantly the larger {110}{110} domain, though the apparent rate measured for this portion should be influenced by reversion within the anomalous daughter domain. (This results from an unfortunate choice of location for the integration box.) This process occurs over a span of 26.0 ms and was captured at 3000 fps (78 frames). A second large stripe of daughter domain observed throughout the frame sequence does not appear to revert. Although it consists of channels whose orientation is not the same as in the mother, this domain was not created in the stress experiment: it was observable before stress was applied.[51]

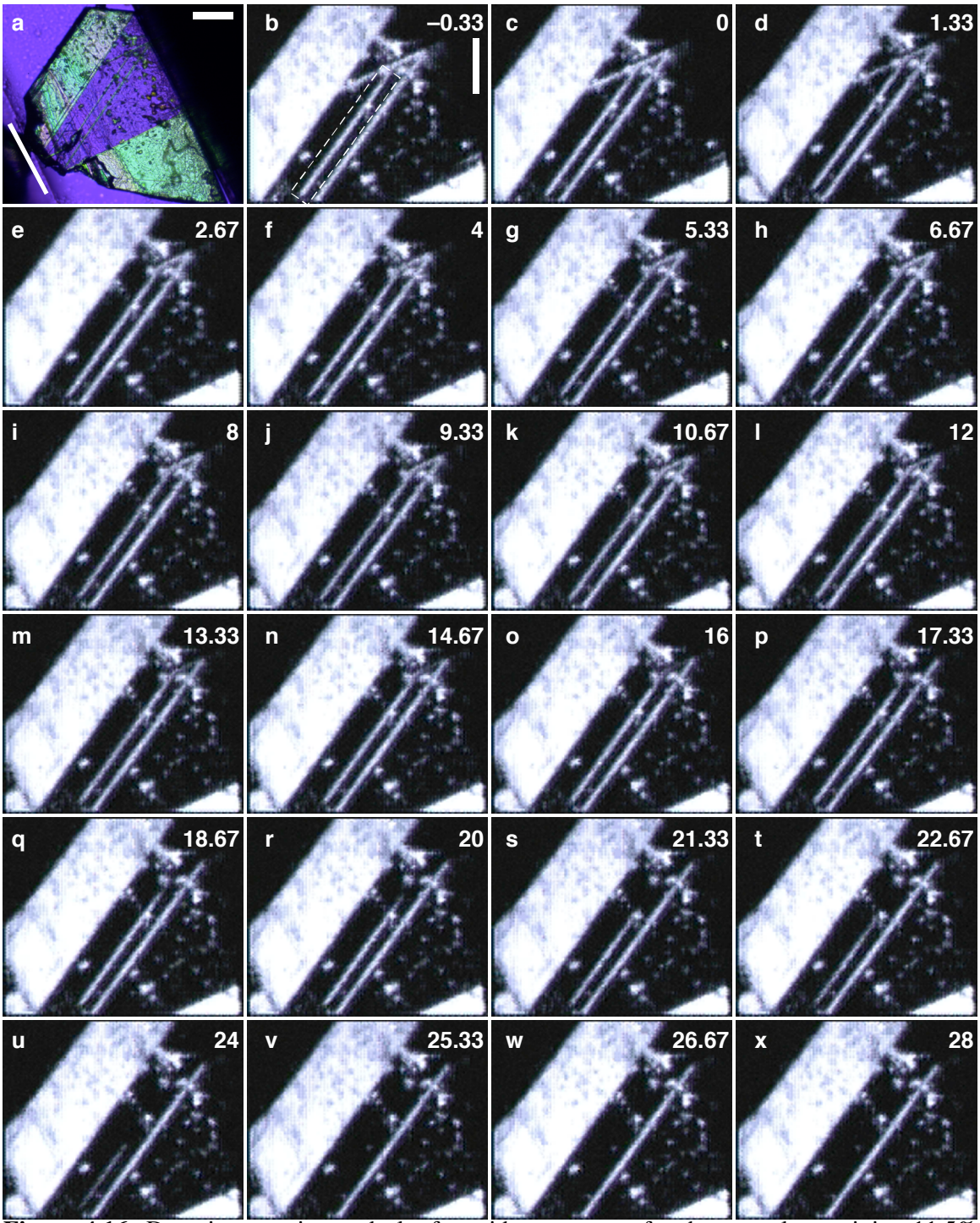



**Figure 4.16** Domain reversion and ultrafast video sequence for the crystal containing 11.5% monoketone (entry 5 in Figure 4.26) following 0.44% compression. **(a)** Photomicrograph (λ plate, crossed polars) of the crystal taken immediately before stress release. The orientation of the active stress bar is indicated. Here, mother domain (extinguished) surrounds bright stripes of daughter domain. Scale bar = 0.25 mm (Nikon 5x). **(b-x)** Ultrafast (3000 fps) video frames (crossed polars), beginning 0.33 ms prior to stress release (**b**), at stress release (**c**), and in 1.33 ms increments thereafter (**d-x**). In each image the time from stress release (time = 0, frame **c**) is presented in the upper left-hand corner. The box in frame **b** indicates the sample region for this frame, which was repositioned according to crystal motion (see text). Scale bar = 0.20 mm (Kodak MotionCorder 1.3x).

Figure 4.17 depicts the domain reversion for a crystal containing 11.8% 2-undecanone (entry 6). When stressed by 1.21% along the SW to NE diagonal, this crystal exhibits several striped {110}{110} daughter domains running along [110] (as well as an anomalous daughter along [310]); a schematic is provided in Figure 4.26g. These appear to emanate from a high spot that contacts the live stop of the stress device (Figure 4.17a). Although photomicrographs taken after stress release indicate complete pseudoelastic reversion, the video camera recorded only a portion of the largest of these (see arrow). Luminosity was recorded within the 30 × 170 $\mu m^2$ sample region outlined in Figure 4.17b. (Because of poor video resolution and lack of identifiable crystal landmarks, precise location of this sample area is not known. This leads to difficulties in marquee positioning for frames where the crystal is in motion, which could affect the measured reversion rates.) In the figure, video still frames are presented to 74.0 ms following stress release; after this time the decrease in luminosity is hardly noticeable visually, but it is observed in the analysis described below. The captured video spans a duration of 78.0 ms, at which time the video capacity of the Kodak MotionCorder was reached. (In total, the reversion event spanned 235 frames at 3000 fps.) As discussed below, the luminosity is still decreasing at this time, so the entire reversion process was not observed in this experiment. However, by 78 ms, the rate of change in luminosity has slowed appreciably, and most of the reversion event is accounted for in the analysis.

Entry 7 (12.5% 2-undecanone, Figure 4.18) represents the second of two crystals in which complete pseudoelastic reversion was not observed. (Entry 1, Figure 4.12, is the other.) This crystal was compressed to 2.12% (the largest stress value for crystals in this study) along the SW to NE diagonal. At maximum compression, this crystal appears as

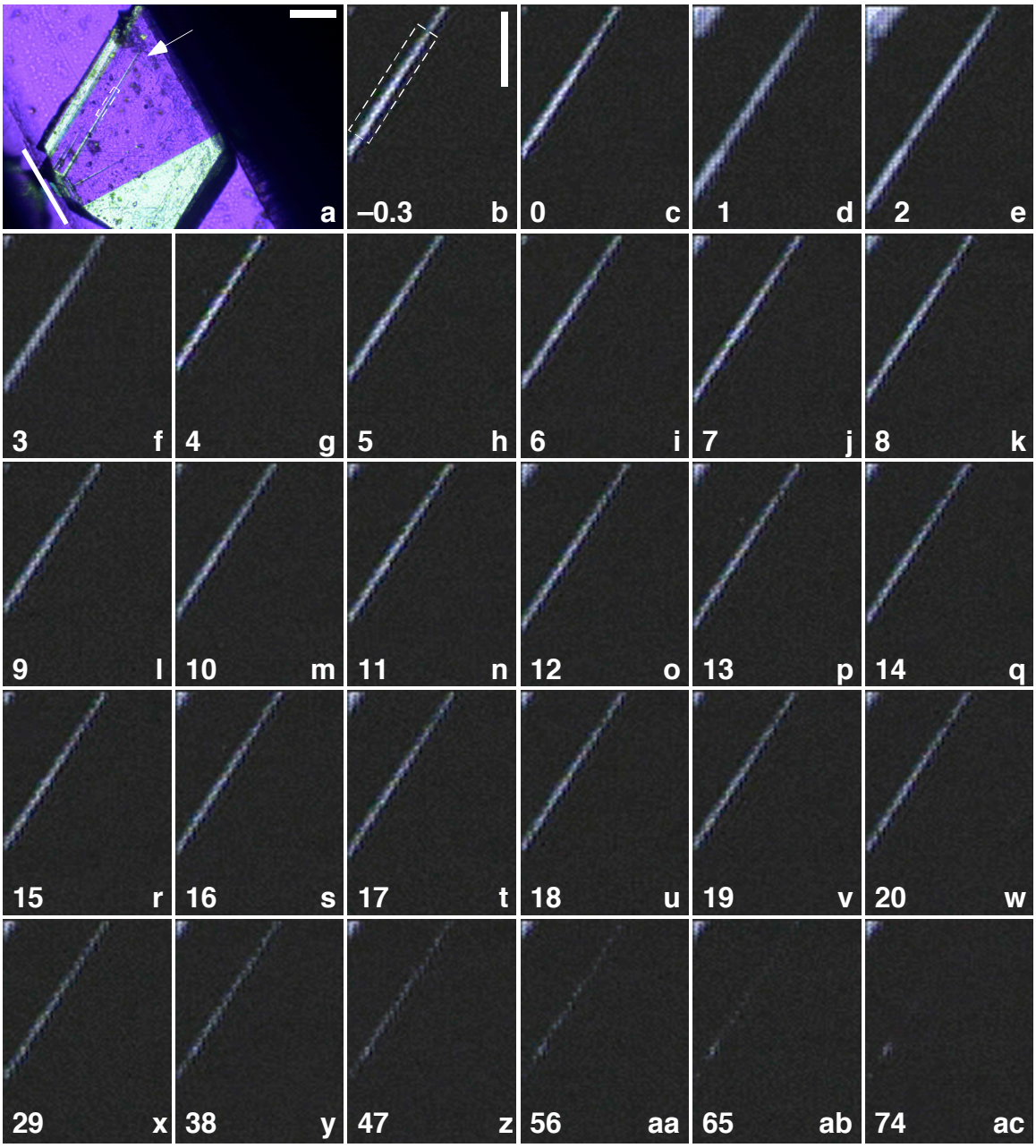



**Figure 4.17** Domain reversion and ultrafast video sequence for the crystal containing 11.8% monoketone (entry 6 in Figure 4.26) following 1.21% compression. **(a)** Photomicrograph (λ plate, crossed polars) of the crystal taken immediately before stress release. The orientation of the active stress bar is indicated. Here, mother domain (extinguished) surrounds bright stripes of daughter domain. The daughter domain analyzed is denoted by the arrow. Scale bar = 0.25 mm (Nikon 5x). **(b-ac)** Ultrafast (3000 fps) video frames (crossed polars), beginning 0.33 ms prior to stress release (**b**), at stress release (**c**), and in 1 ms (**d-w**) and 9 ms (**x-ac**) increments thereafter. In each image the time from stress release (time = 0, frame **c**) is presented in the lower left-hand corner. The box in frame **b** indicates the sample region for this frame, which was repositioned according to crystal motion (see text). Although the precise location of the sample area is not known, its approximate location is provided in **a**. Scale bar = 0.10 mm (Kodak MotionCorder 5x).

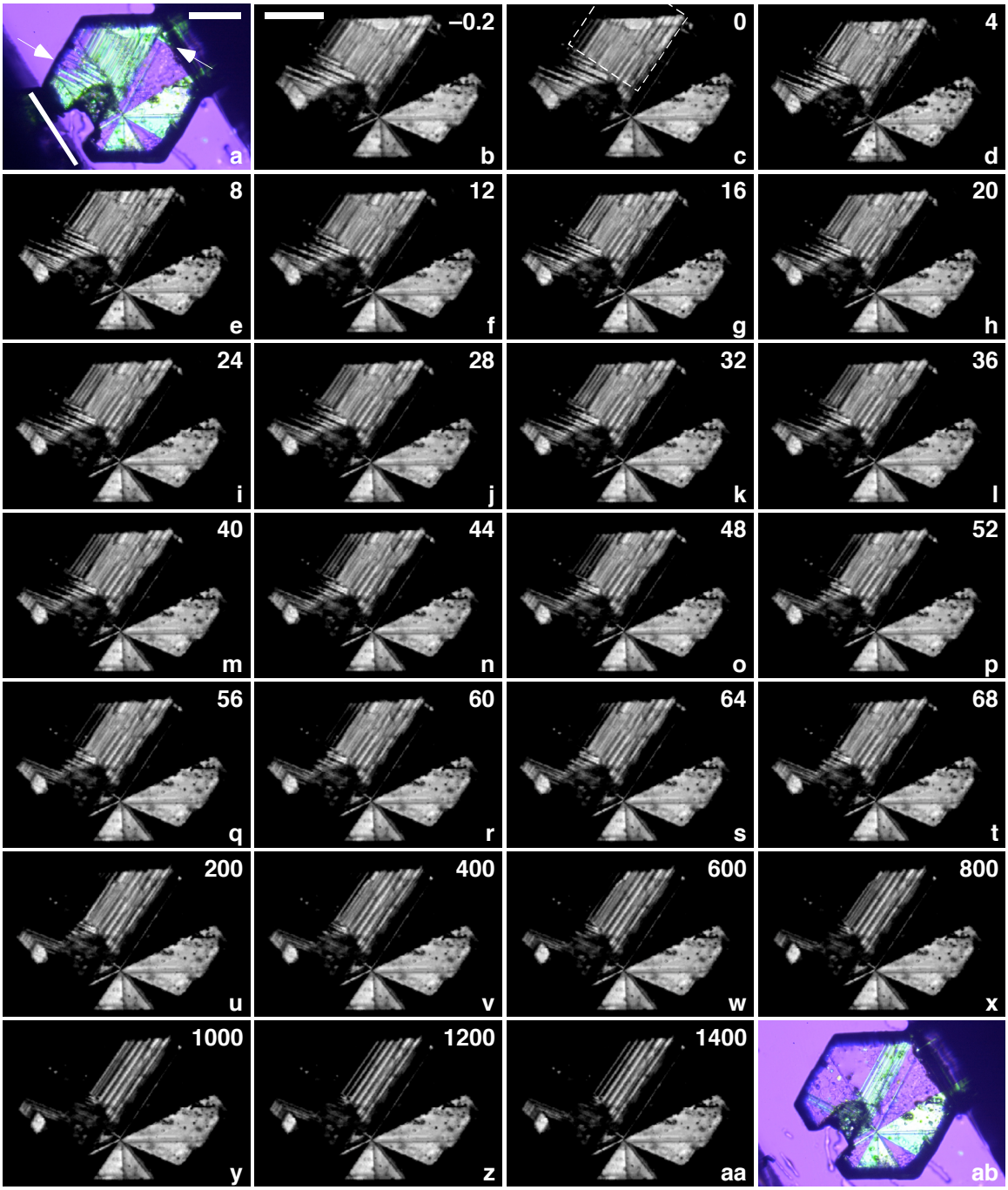



**Figure 4.18** Domain reversion and ultrafast video sequence for the crystal containing 12.5% monoketone (entry 7 in Figure 4.24) following 2.12% compression. **(a)** Photomicrograph (λ plate, crossed polars) of the crystal taken immediately before stress release. The orientation of the active stress bar is indicated. Here, mother domain (extinguished) surrounds bright stripes of daughter domain. Scale bar = 0.25 mm (Nikon 5x). **(b-aa)** Ultrafast (5000 fps) video frames (crossed polars), beginning 0.2 ms prior to stress release (**b**), at stress release (**c**), and in 4 ms (**c-t**) and 200 ms (**u-aa**) increments thereafter. In each image, the time from stress release (time = 0, frame **c**) is presented in the upper right-hand corner. The box in frame **c** indicates the sample region for this frame, which was repositioned according to crystal motion (see text). Scale bar = 0.20 mm (X-Stream XS-4 10x). The aspect of the video frames was altered during accumulation of the video; this imperfection does not affect the measured reversion rates (see text). **(ab)** Photomicrograph (λ plate, crossed polars) taken following stress release demonstrates incomplete domain reversion for this crystal. Scale as in **a**.

in Figure 4.18a; here, the top sector contains many striped {110}{110} daughter domains that have grown together so that that sector consists predominantly of switched channels (see schematic in Figure 4.26h). Sectors to the left and right contain {130}{130} daughters, as well (see arrows in Figure 4.18a). Release of stress gives rise to rapid pseudoelastic reversion during the initial 70 ms (Figure 4.18c-t) followed by slower activity for the remainder of the 1.5 s of ultrafast footage (Figure 4.18u-aa). Luminosity was measured for multiple {110}{110} daughters in the region spanning 280 × 300 $\mu m^2$ (outlined in Figure 4.18c); the 1.5 s of captured video at 5000 fps produced 7500 still images, of which every tenth was analyzed. Thus, the time "resolution" for this experiment is 1/500 s, or 2.0 ms. Figure 4.18aa presents a photomicrograph (crossed polars) taken approximately 2 minutes after stress release. Here, the crystal exhibits plastic daughter domains.

In a fashion similar to entry 7, the crystal containing 15.0% 2-undecanone was compressed to 1.96%, a value much greater than most of the crystals studied. This crystal produced two {110}{110} daughter regions suitable for analysis; these are examined in Figures 4.19 and 4.20 and are identified as entries 8 and 9. The smaller of the two regions (entry 8, Figure 4.19b) was analyzed using a 52 × 330 $\mu m^2$ sample area. Relaxation of this daughter spanned 2.6 ms (13 frames at 5000 fps). The larger daughter (entry 9, Figure 4.20) relaxed over a period of 101.4 ms. This daughter was analyzed (using a 70 × 420 $\mu m^2$ sample area) in every third frame for the initial 93.8 ms following stress release; here, the time resolution is 3/5000 s, or 0.6 ms. For the remainder of the 101.4 ms event, every frame was analyzed. (Note that, near the top of the crystal, both daughters adjoin a {130}{130} daughter; see schematic in Figure 4.26j. Although the

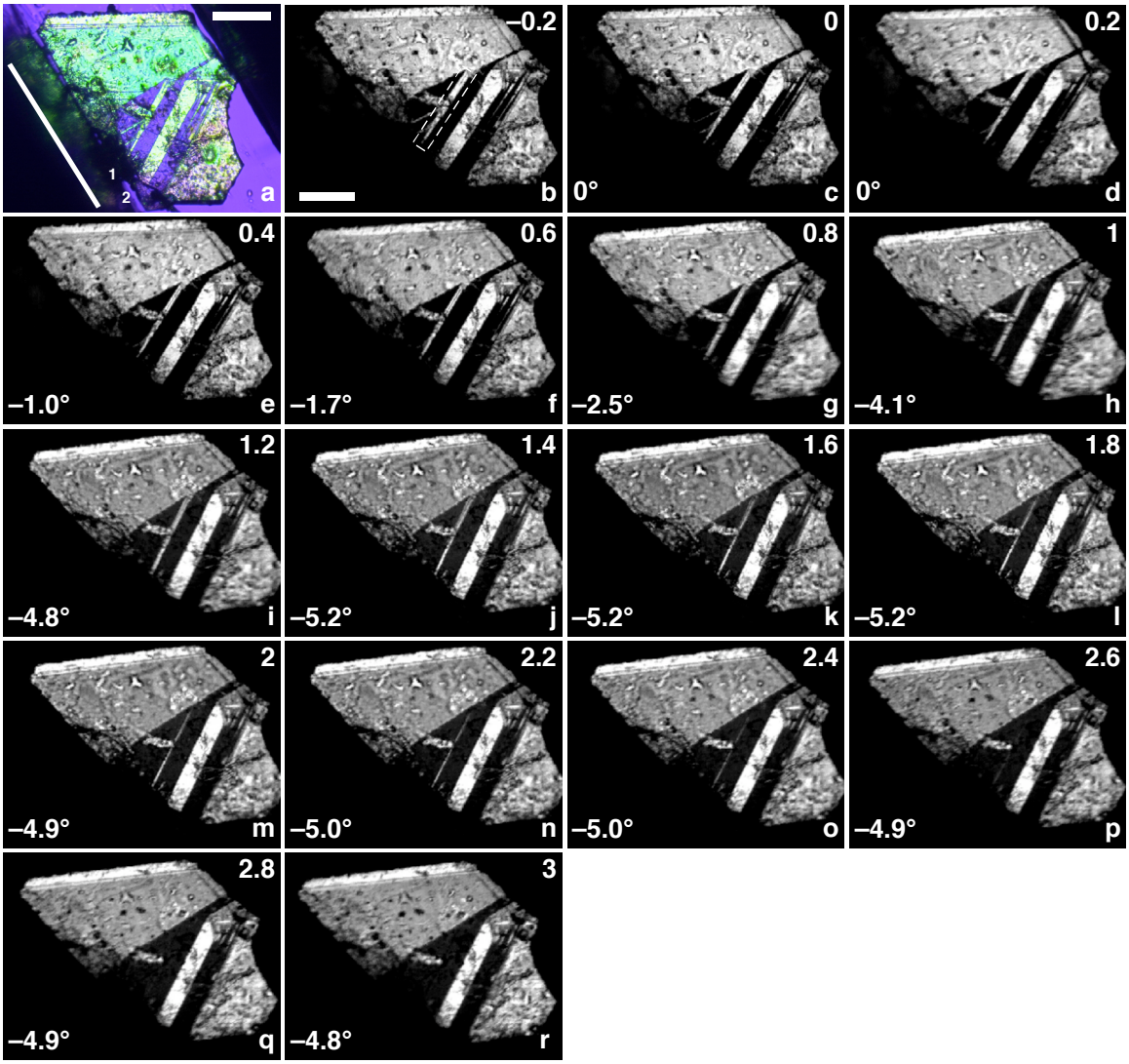



**Figure 4.19** Domain reversion and ultrafast video sequence for the crystal containing 15.0% monoketone (entry 8 in Figure 4.24) following 1.96% compression. **(a)** Photomicrograph (λ plate, crossed polars) of the crystal taken immediately before stress release. The orientation of the active stress bar is indicated. Here, mother domain (extinguished) surrounds bright stripes of daughter domain. Scale bar = 0.25 mm (Nikon 5x). **(b-aa)** Ultrafast (5000 fps) video frames (crossed polars), beginning 0.2 ms prior to stress release (**b**), at stress release (**c**), and in 0.2 ms (**c-r**) increments thereafter. In each image the time from stress release (time = 0, frame **c**) is presented in the upper left-hand corner. The box in frame **b** indicates the sample region for this fram (daughter 1), which was repositioned (and reoriented) according to crystal motion (see text). Crystal orientations, measured from the top face of the crystal, are provided in the lower left corner of each frame. Scale bar = 0.20 mm (X-Stream XS-4 10x). The analysis of the larger daughter region (2) is illustrated in Figure 4.20. The aspect of the video frames was altered during accumulation of the ultrafast video; this imperfection does not affect the measured reversion rates (see text).

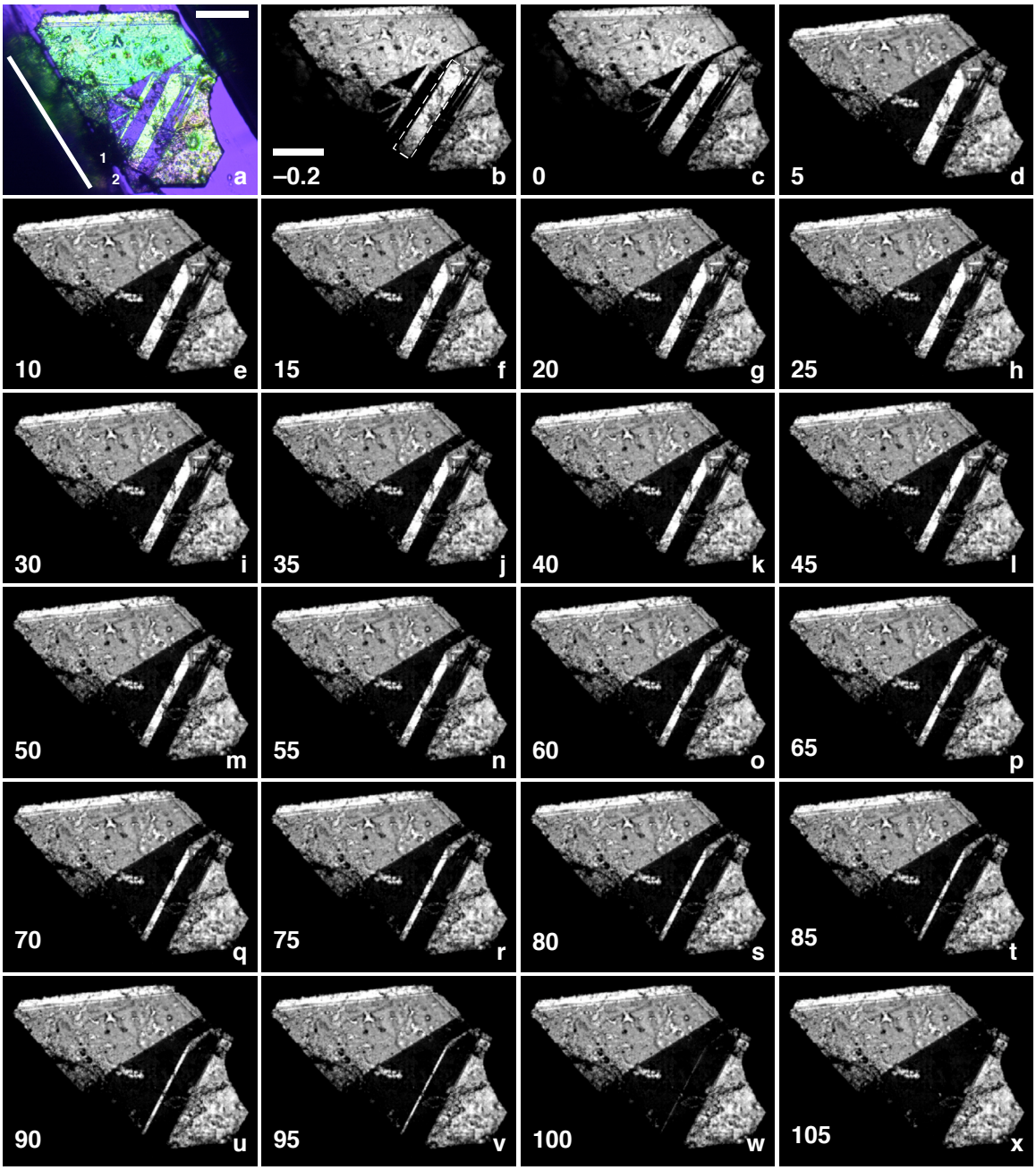



**Figure 4.20** Domain reversion and ultrafast video sequence for the crystal containing 15.0% monoketone (entry 9 in Figure 4.26) following 1.96% compression. **(a)** Photomicrograph (λ plate, crossed polars) of the crystal taken immediately before stress release. The orientation of the active stress bar is indicated. Here, mother domain (extinguished) surrounds bright stripes of daughter domain. Scale bar = 0.25 mm (Nikon 5x). **(b-x)** Ultrafast (5000 fps) video frames (crossed polars), beginning 0.2 ms prior to stress release (**b**), at stress release (**c**), and in 5 ms (**c-x**) increments thereafter. In each image, the time from stress release (time = 0, frame **c**) is presented in the lower left-hand corner. The box in frame **c** indicates the sample region for this frame (daughter 2), which was repositioned (and reoriented) according to crystal motion (see text). As illustrated in Figure 4.19, crystal rotation occurs during the first 3.0 ms of this event. In frames **d**-**x**, the crystal is oriented –4.8° from its starting position (in **b** and **c**). Scale bar = 0.20 mm (X-Stream XS-4 10x). The analysis of the smaller daughter region (1) is illustrated in Figure 4.19. The aspect of the video frames was altered during accumulation of the ultrafast video; this imperfection does not affect the measured reversion rates (see text).

regions over which the reversion kinetics were measured contain primarily {110}{110} daughters, their intersection with {130}{130} daughters may influence domain reversion; this will be discussed below.)

It is interesting to note the large difference in "lifetimes" exhibited by the pair of daughters that comprise entries 8 and 9. These events were observed in the same crystal sector so they presumably had similar guest stoichiometries and were subject to the same treatment both before and during the stress experiment. A comparison of the kinetic behavior for this pair of domains is important to the discussion of energetics for pseudoelasticity in this crystal. This will be addressed below.

Figure 4.21 examines the domain reversion in a crystal containing 15.8% 2-undecanone (entry 10). For this crystal, compression by 0.68% along the NW to SE diagonal led to ferroelastic reorientation in the extinguished sector (Figure 4.21a). A long, thin stripe of daughter domain (produced along {110}{110} boundaries; see schematic in Figure 4.26k) was analyzed using a 42 × 540 $\mu m^2$ sample area (Figure 4.21b). Luminosity from this daughter decayed over 2.4 ms (12 frames at 5000 fps).

The final crystal used in this experiment, which contained 17.0% guest impurity in the stressed sector, produced two {110}{110} daughter domains when stressed to 1.05% along the NW to SE diagonal. Entries 11 and 12, respectively, are described in Figures 4.22 and 4.23, while a schematic of the crystal is provided in Figure 4.26k-l. (This crystal was also presented in Figure 4.1.) Figure 4.22 (entry 11) depicts the domain reversion of the larger of the pair, which reverted over 246 ms. The video of this event, (captured at 5000 fps) contains over 1200 frames, of which every tenth frame was sampled in the 210 × 1570 $\mu m^2$ region outlined in Figure 4.22b. As with entry 7 (Figure

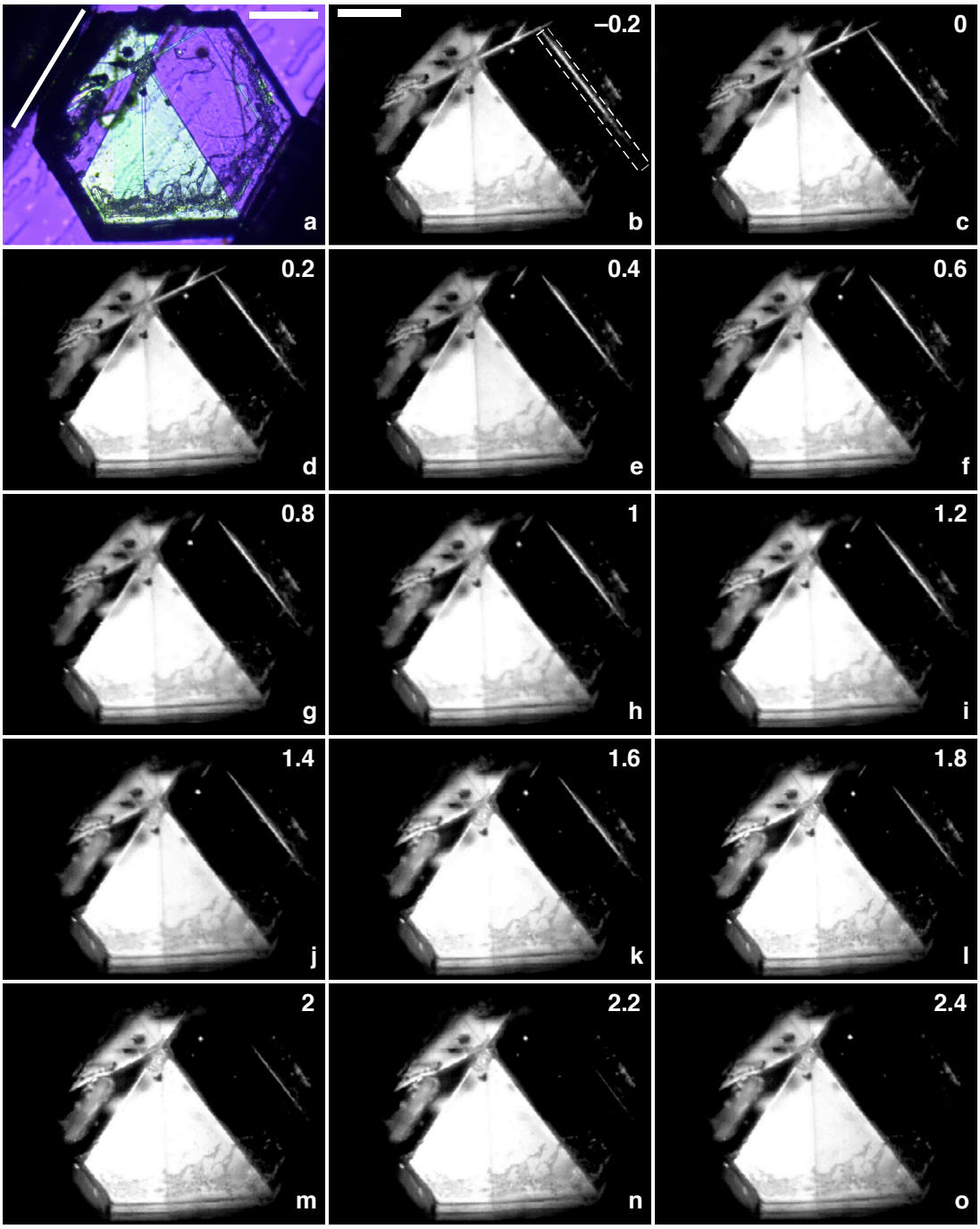



**Figure 4.21** Domain reversion and ultrafast video sequence for the crystal containing 15.8% monoketone (entry 10 in Figure 4.26) following 0.68% compression. **(a)** Photomicrograph (λ plate, crossed polars) of the crystal taken immediately before stress release. The orientation of the active stress bar is indicated. Here, mother domain (extinguished) surrounds bright stripes of daughter domain. Scale bar = 0.25 mm (Nikon 5x). **(b-o)** Ultrafast (5000 fps) video frames (crossed polars), beginning 0.2 ms prior to stress release (**b**), at stress release (**c**), and in 0.2 ms (**c-o**) increments thereafter. In each image the time from stress release (time = 0, frame **c**) is presented in the upper right-hand corner. The box in frame **c** indicates the sample region for this frame, which was repositioned according to crystal motion. Scale bar = 0.20 mm (X-Stream XS-4 10x). The aspect of the video frames was altered during accumulation of the ultrafast video; this imperfection does not affect the measured reversion rates (see text).

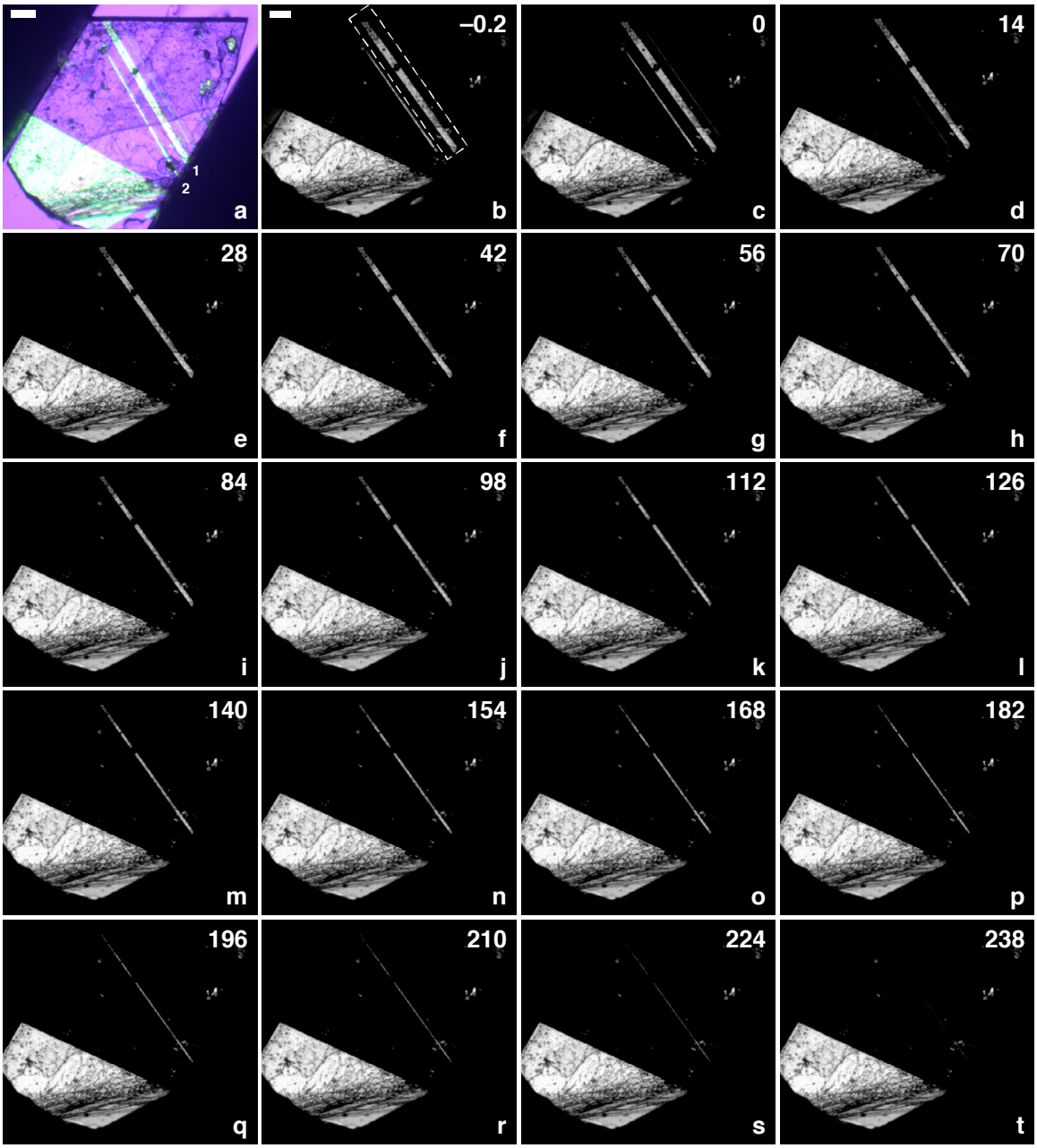



**Figure 4.22** Domain reversion and ultrafast video sequence for the crystal containing 17.0% monoketone (entry 11 in Figure 4.26) following 1.05% compression. (This crystal was also presented in Figure 4.1.) **(a)** Photomicrograph (crossed polars, λ plate) of the crystal taken immediately before stress release. Here, mother domain (extinguished, magenta) surrounds bright stripes of daughter domain; the stress bars are visble on both sides of the crystal. Scale bar = 0.25 mm (Nikon 1.3x). **(b-t)** Ultrafast (5000 fps) video frames, beginning 0.2 ms prior to stress release (**b**), at stress release (**c**), and in 14 ms (**c-t**) increments thereafter. (Although the reversion process for this crystal spanned 246 ms, the daughter domain is not readily visible in the concluding frames; footage from the final 8 ms have been excluded from this figure.) In each image the time from stress release (time = 0, frame **c**) is presented in the upper right-hand corner. The box in frame **b** indicates the sample region for this frame (daughter 1), which was repositioned according to crystal motion (see text). A second daughter domain (2), visible in images **a**-**c**, was analyzed similarly; this work is described in 4.23. Scale bar = 0.20 mm (X-Stream XS-4 5x). The aspect of the video frames was altered during accumulation of the ultrafast video; this imperfection does not affect the measured reversion rates (see text).

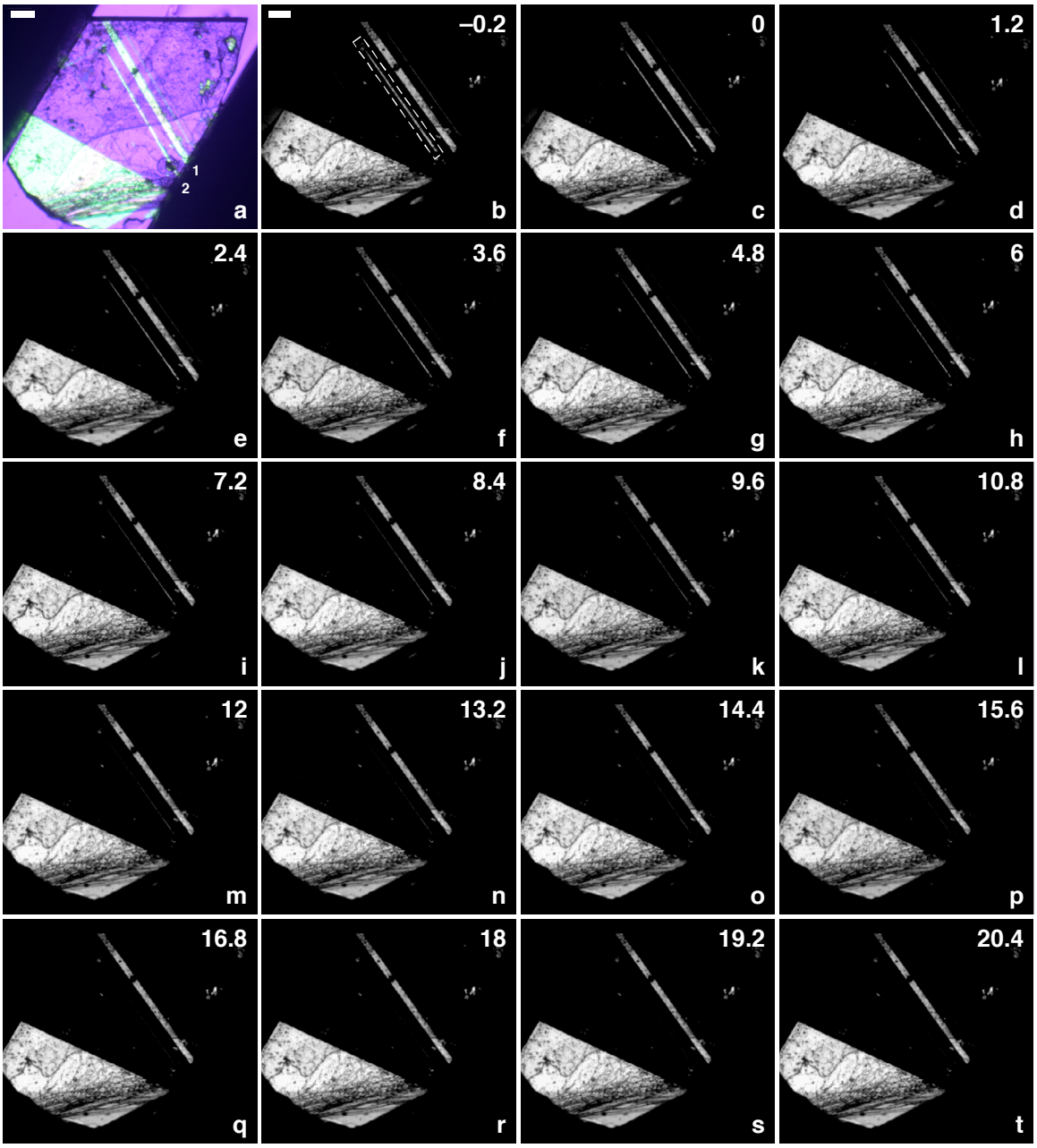



**Figure 4.23** Domain reversion and ultrafast video sequence for the crystal containing 17.6% monoketone (entry 12 in Figure 4.26) following 1.05% compression. (This crystal was also presented in Figure 4.1.) **(a)** Photomicrograph (crossed polars, λ plate) of the crystal taken immediately before stress release. Here, mother domain (extinguished, violet) surrounds bright stripes of daughter domain; the stress bars are visble on both sides of the crystal. Scale bar = 0.25 mm (Nikon 1.3x). **(b-t)** Ultrafast (5000 fps) video frames, beginning 0.2 ms prior to stress release (**b**), at stress release (**c**), and in 1.2 ms (**c-t**) increments thereafter. (Although the reversion process for this crystal spanned 22.6 ms, the daughter domain is not readily visible in the concluding frames; footage from the final 2.2 ms have been excluded from this figure.) In each image the time from stress release (time = 0, frame **c**) is presented in the upper right-hand corner. The box in frame **b** indicates the sample region for this frame (daughter 2), which was repositioned according to crystal motion (see text). A second daughter domain (1) that reverted on a longer time scale was analyzed similarly; this work is described in Figure 4.22. Scale bar = 0.20 mm (X-Stream XS-4 5x). The aspect of the video frames was altered during accumulation of the ultrafast video; this imperfection does not affect the measured reversion rates (see text).

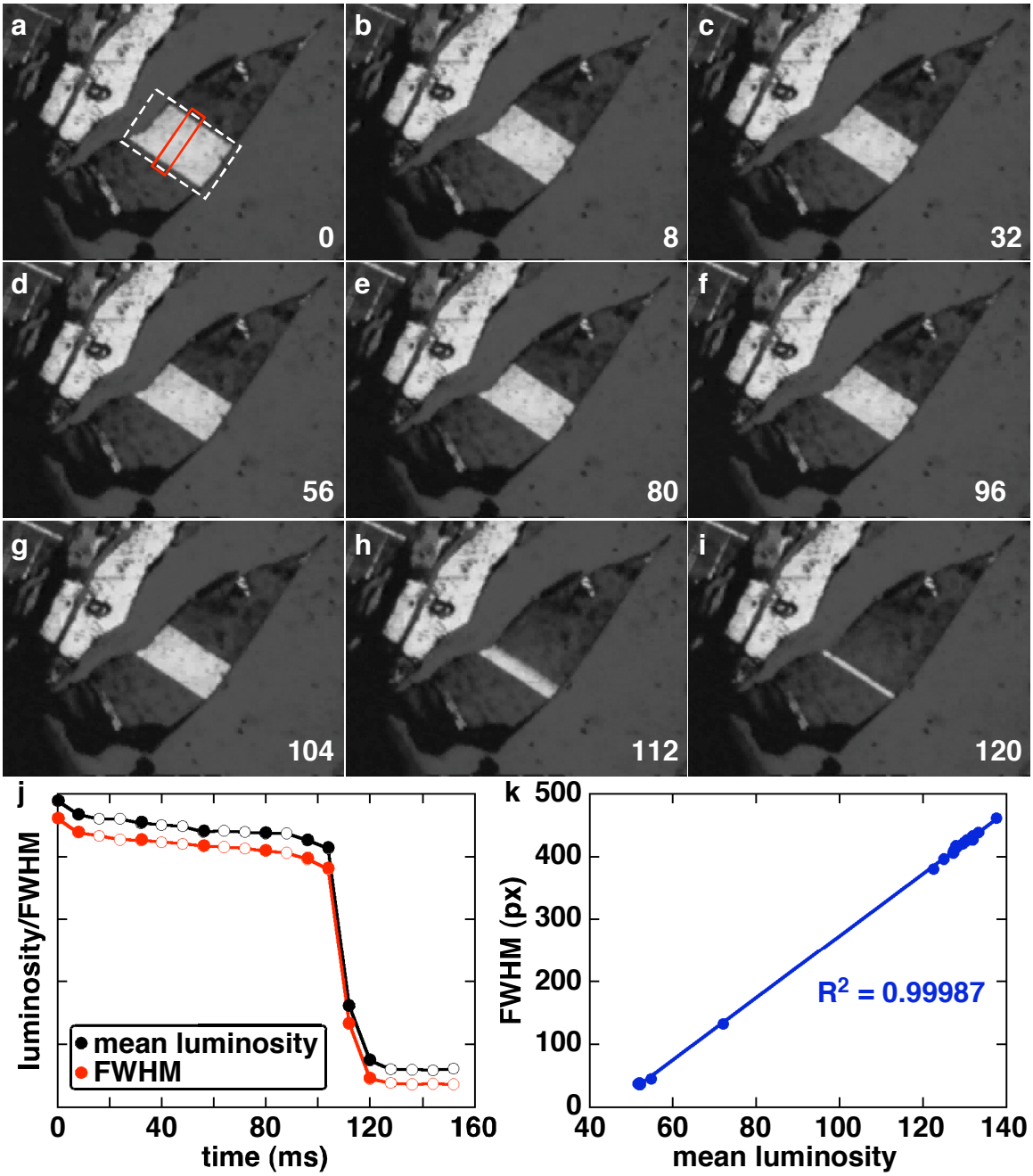
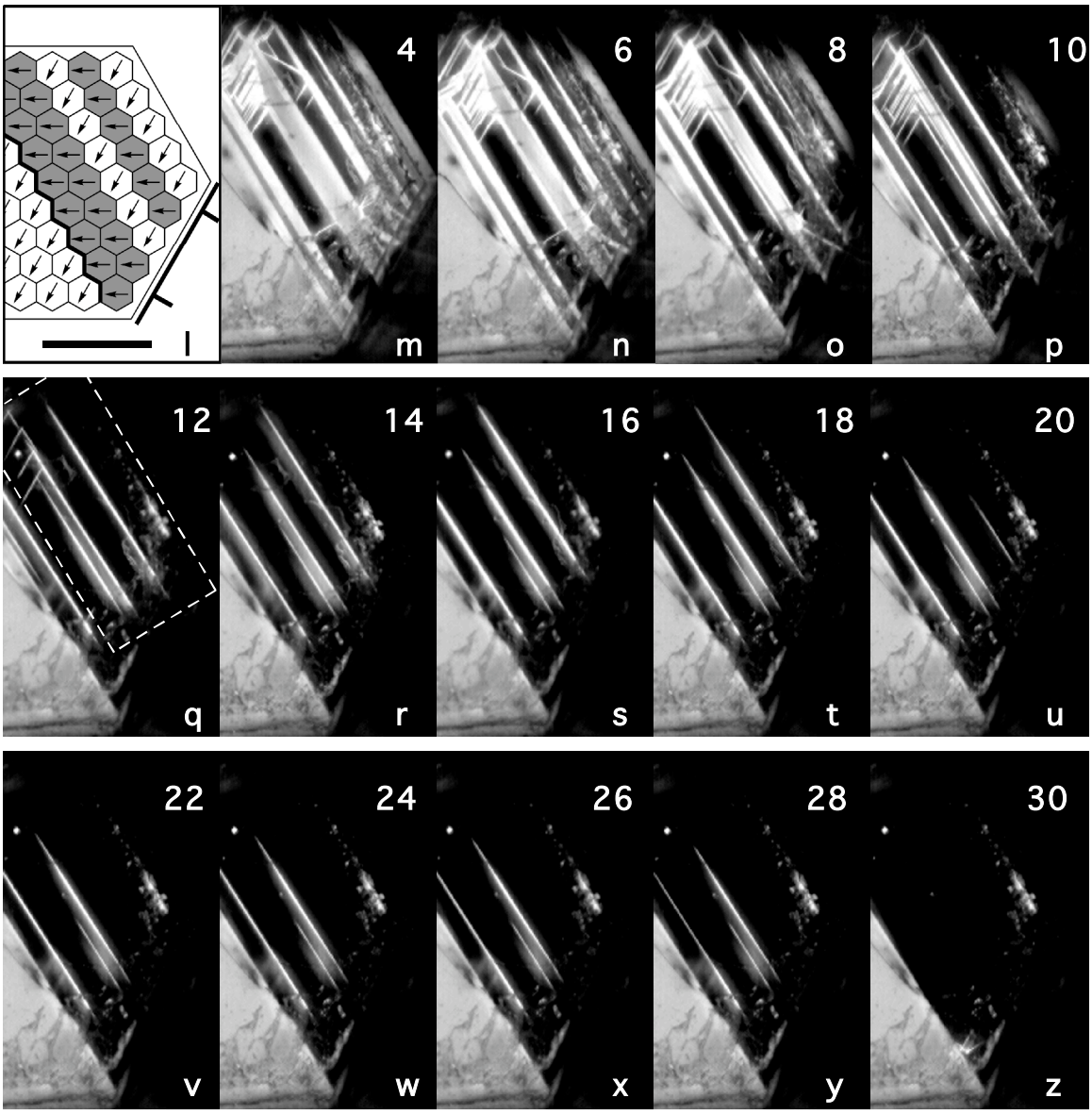



**Figure 4.24** A comparison of methods used to quantify domain reversion kinetics. Here, a video sequence of pseudoelastic reversion for a UIC crystal grown in a solution containing an 85:15 mixture of 2,10-undecanedione and 2-undecanone is analyzed in two ways: by monitoring the location of the domain wall (which provides an estimate of the domain size), and by measuring the mean luminosity of a region containing the daughter. **(a-i)** Still images from the video (recorded at 125 fps), over 120 ms of the domain reversion event. (Time, relative to the first frame, is provided (in ms) in the lower right corner of each image.) For domain wall measurements, a line profile (12 px wide) was drawn for the area outlined by the red box in **a**. For luminosity measurements, the 56 x 93 $px^2$ region outlined in the white box in **a** was sampled. **(j)** Plot of mean luminosity and FWHM (of plot profiles) vs. time, for 20 frames spanning 152 ms. (Ordinate scales are not provided.) Filled symbols correspond to still images **a** through **i**. This graph illustrates that these methods provide very similar estimates of "domain size" for this daughter. **(k)** Plot of FWHM vs. mean luminosity demonstrates a linear correlation (see text).




Analysis of domain reversion kinetics for a UIC crystal containing an 84.2:15.8 mixture of 2,10-undecanedione and 2-undecanone. This is the third stress attempt for the crystal described in Figure 4.21 (entry 10). This crystal was strained by 0.68, 0.69 and 1.38%. **(l)** Schematic of the stressed crystal. Stress is applied to the crystal by the stress bars, which are oriented as shown. In the images collected, the mother is in the extinguishing position and therefore appears dark. The daughter, however, is not extinguished; the luminosity of each frame (or a region of each frame) is a measure of the amount of daughter domain. By following the decay of luminosity it is therefore possible to measure the rate of reversion of that domain. Scale bar (for the video frames) = 0.50 mm. **(m-z)** Video frames collected at 10,000 fps. Here, every 20th frame (2.0 ms increments) is presented, spanning 26.0 ms. The numbers at top right indicate the time, in ms intervals. The stress bar was released between **m** and **n**, at 5.4 ms. Kinetics measurements were performed by quantifying the average luminosity within the region enclosed by the box in **q**. Because of crystal movement, the location of this box was repositioned manually according to landmarks on the crystal so that the same region was sampled throughout the experiment. Although portions of the box move into and out of the video frame, the luminosity measurement is affected to a minimal extent (see text). Figure and caption adapted from Hollingsworth, *et al*., *Cryst. Growth Des*., **5**, 2100 (2005).

4.18), the time "resolution" for this analysis is 1/500 s, or 2 ms. Figure 4.23 (entry 12) examines the relaxation of this crystal's second daughter, which reverted over 22.6 ms (113 frames, all of which were analyzed, at 5000 fps). For this daughter, luminosity was recorded for the 98 × 1310 $\mu m^2$ sample area outlined in Figure 4.23b. In the figure, video stills from every sixth frame (or every 1.2 ms) are provided.

4.4.1.2 Measurement of Domain Reversion Kinetics

Before discussing the kinetic information extracted from these experiments, some technical details should be addressed. First, periodic variations in frame brightness were noted for all of the ultrafast videos, although they depend on which camera was utilized. For video sequences collected using the X-Stream camera (entries 2, 3 and 7 through 12), every fifth frame appears dim. In these experiments, luminosity is used as a measure of daughter concentration; therefore, variations in frame brightness introduce error in the determination of reversion rates. When this was the case, these data were not retained for the final analysis.

Videos recorded using the Kodak MotionCorder (entries 1 and 4 through 6) exhibit a time-dependent variation in luminosity in the moments *prior* to stress release. Because the crystal is held fixed in the stress device at this time, such variations cannot arise from domain reversion or crystal movement. In fact, similar oscillations of luminosity are observed within portions of the viewing area that do not include the crystal (background regions).[52] Figures 4.25a-b demonstrate this behavior for the crystal containing 11.5% monoketone (entry 5). In Figure 4.25a, the mean luminosity for a 30 × 40 $\mu m^2$ background area oscillates between 17.2 and 17.9 luminosity units in the 23 ms

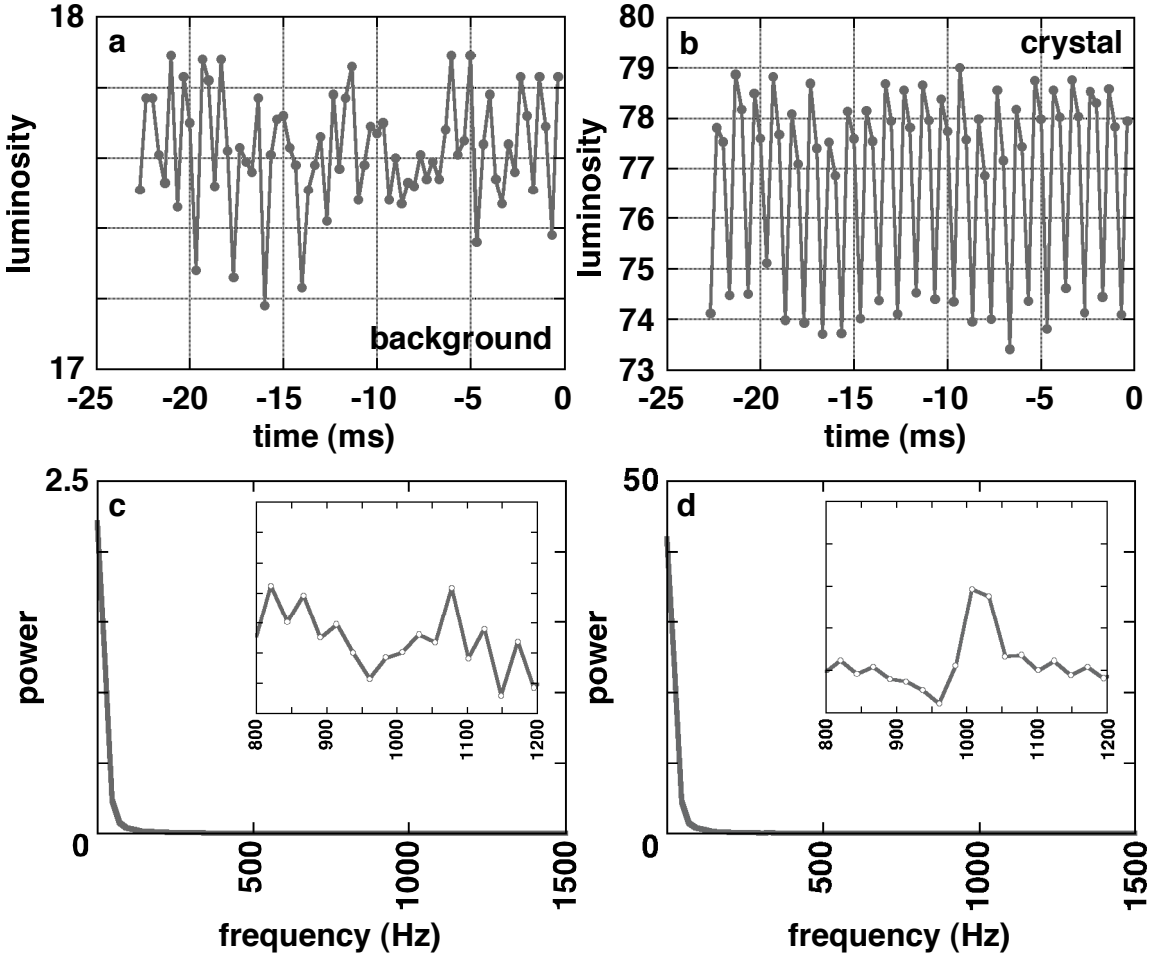
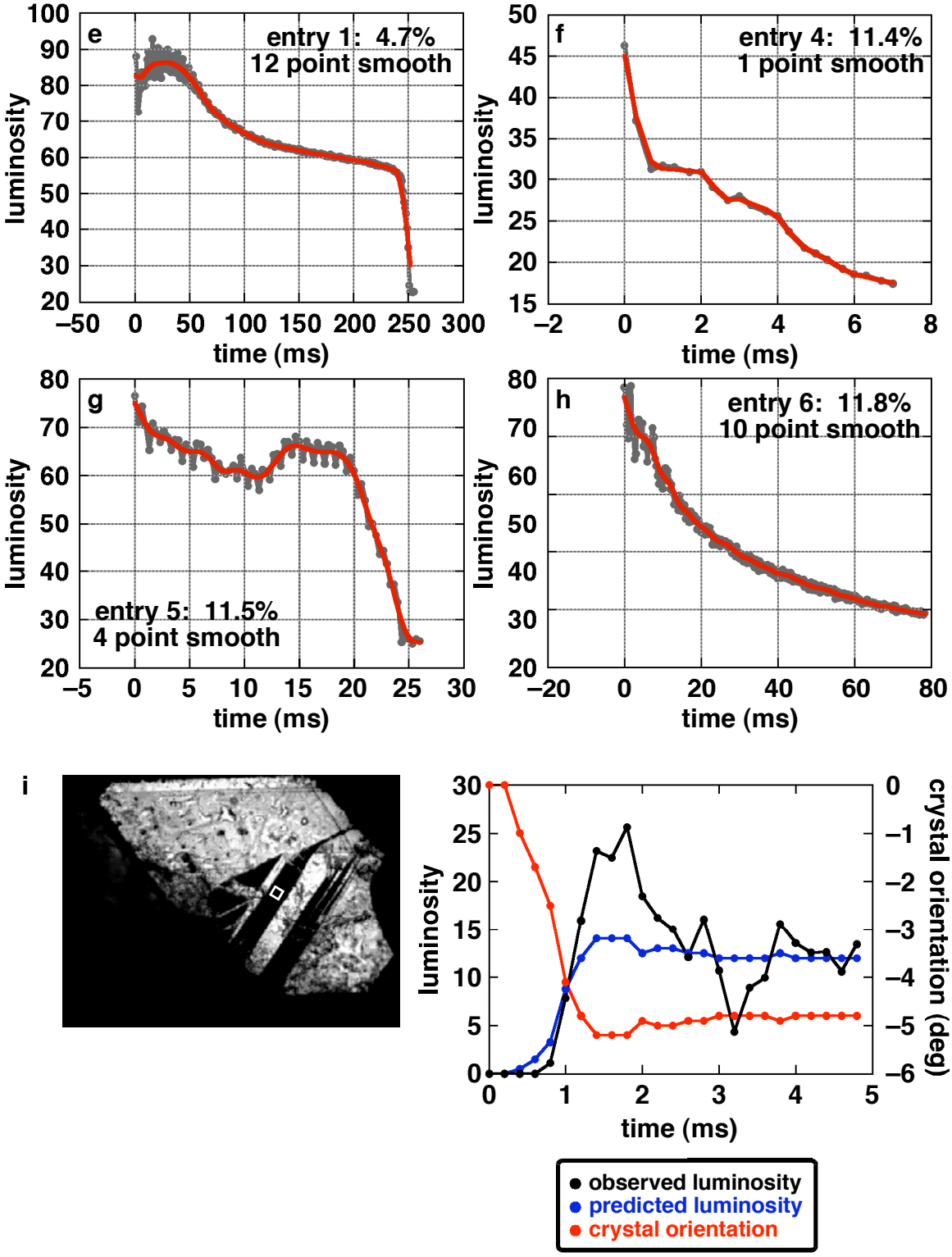



**Figure 4.25** Noise in the analysis of domain reversion. For high-speed video recorded using the Kodak MotionCorder camera there is a periodic variation in the brightness of the video frames. In these graphs, mean luminosity is plotted as a function of time. **(a,b)** The analysis of high-speed footage recorded as the crystal is held still (for 23 ms leading up to stress release). In **a**, a background region was sampled from the video for entry 5 (Figure 4.16). Here, the luminosity varies by as much as 0.7 units (average ~17.6 units). In **b**, the crystal sample region was analyzed for the same video. Here, changes in luminosity span almost 6 units (average ~76 units). **(c,d)** Fourier analysis of the data plotted in **a** and **b**. Here, power spectra are plotted for the background region (**c**) and the crystal region (**d**). Note the flat response of the background region (**c**); however, the crystal (**d**) exhibits a peak at approximately 1008 Hz (see inset). **(e-h)** For four crystals studied using the MotionCorder, plots of luminosity (grey circles) *vs.* time reveal a similar periodicity. The periodic variation in luminosity leads to incorrect reversion rates. By utilizing a Fourier smoothing routine (see text), the effect of these variations can be minimized. In **e-h**, the smoothed luminosity values are presented in red. **(i)** For entries 8 and 9, the observed luminosity was affected by crystal rotation during the first 3 ms of the reversion event. Here, luminosity data for an extinguished region are corrected for rotation. See text for details.


e
entry 1: 4.7%
12 point smooth
luminosity
time (ms)
f
entry 4: 11.4%
1 point smooth
luminosity
time (ms)
g
entry 5: 11.5%
4 point smooth
luminosity
time (ms)
h
entry 6: 11.8%
10 point smooth
luminosity
time (ms)
i
luminosity
crystal orientation (deg)
time (ms)
observed luminosity
predicted luminosity
crystal orientation

leading up to stress release (in these graphs, at time = 0). Assuming no contamination from other light sources, perfectly crossed polarizers, and no dark current in the recording apparatus, the background should have a constant luminosity of zero. In Figure 4.25b, the mean luminosity for the crystal's sample region (described in Figure 4.16b) oscillates from 73.5 to 79 units over the same time period. Because these variations are not observed in images recorded with the X-Stream camera (which were recorded using the same microscope and light source and do reveal a "background" of zero luminosity units[53]), they are thought to originate from the Kodak camera or from some aspect of processing the images collected using the MotionCorder. (As discussed in Section 7.5.6, these images were exported from the MotionCorder to Adobe Premiere (v. 5, for Windows) via S-video. This transfer requires a conversion of the digital video data to an analog format; the video is then reconverted to digital by the Premiere software, so this may be the source of the anomalous background luminosity.) In Figure 4.25a, and especially Figure 4.25b, the luminosities appear to oscillate periodically. This periodicity was examined[54] via Fourier analysis of the data, using Origin (v. 7.0, for Windows). The data were sampled over the 68 frames (22.7 ms, sample rate = 3000 Hz) immediately preceding stress release. Fourier transformation of the time-dependant luminosities plotted in Figures 4.25a and b provides frequency-dependent luminosities; a power spectrum for each region is plotted in Figure 4.25c and d. For the background region (Figure 4.25c), no discernible maxima were observable in the Fourier data; however, the crystal region (Figure 4.25b) produced a strong peak at approximately 1008 Hz. (See insets in Figure 4.25c and d.) Thus, the variations in luminosity for this static crystal are periodic, with a frequency of approximately 1008 Hz. Since these variations are thought

to arise from the recording process, they should also be present in the background data plotted in Figure 4.25a; perhaps a longer sampling time would reveal them.

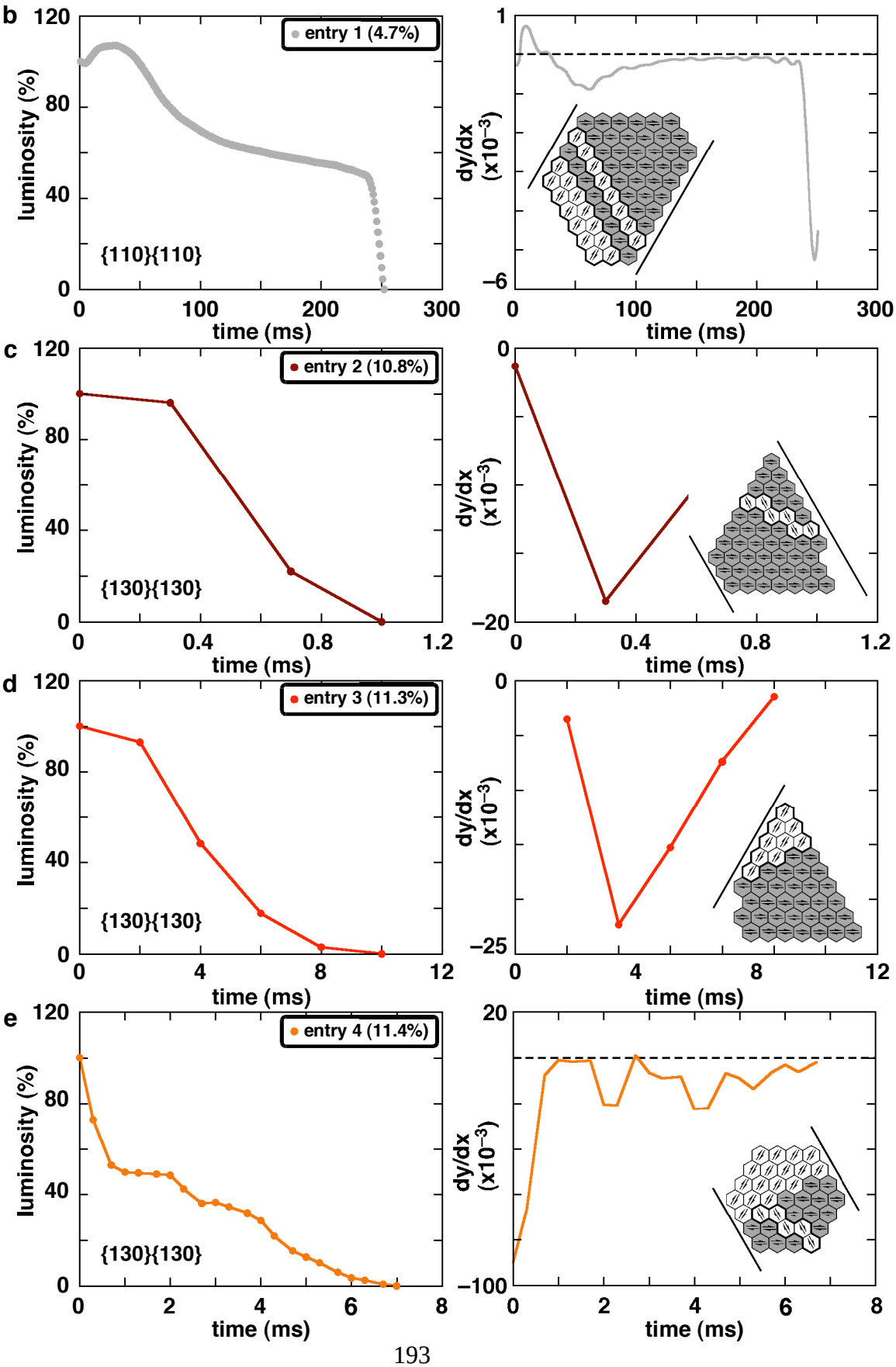
As the plots in Figure 4.25a-b illustrate, these variations can be quite dramatic. For frames with anomalously low luminosities, the rate obtained by comparison with the preceding frame will be erroneously fast. Rates determined using an anomalously low measurement and the datum following it will be anomalously slow (or in some cases, less than zero). For this reason, the luminosity data from entries 1 and 4 through 6 were fitted using a Fourier smoothing algorithm included in the Origin software package (v. 7.0 for Windows). In this procedure, the data are "smoothed" so that periodic variations in the luminosity data that were not attributable to domain reversion are minimized. The smoothed results are provided in Figure 4.25e-h; here, the grey points represent the uncorrected luminosity data and the red lines represent the smoothed data. For each entry, the total number of data points used in the smoothing routine is provided. In each case, a minimum number of smoothing points were used to visually remove the high frequency modulations in luminosity while attempting to retain the physically meaningful aspects of the data. It is likely that this procedure has removed some changes in luminosity arising from changes in daughter population, but this could not be avoided. However, the relative insensitivity of the smoothed curves to the number of smoothing points used suggested that this procedure is reasonable.

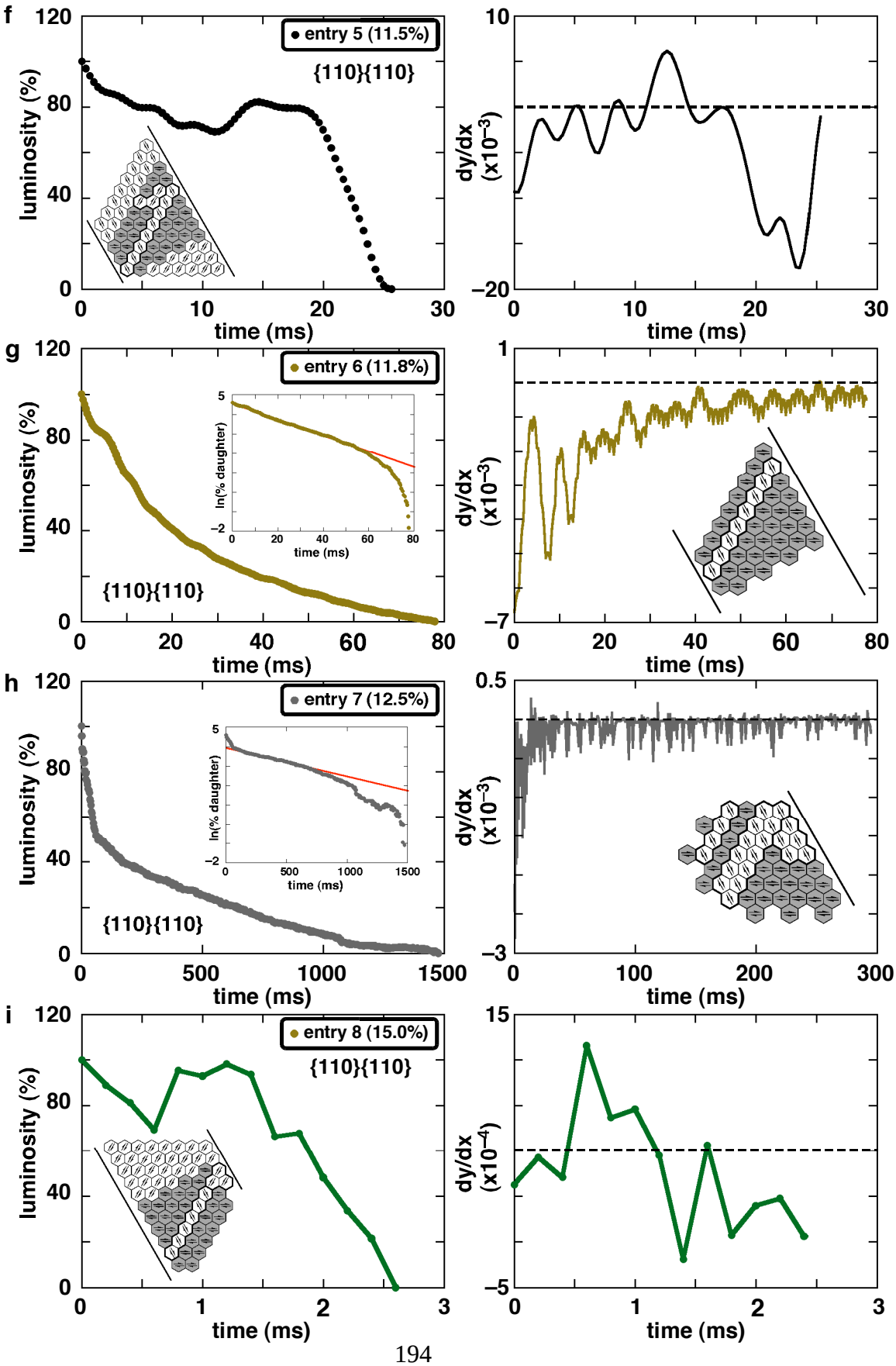
Inspection of the resulting plots indicates that this process does not remove non-periodic variations in luminosity. As shown in Figure 4.25, for crystals containing 4.7% (entry 1, Figure 4.26e) and 11.5% (entry 5, Figure 4.26g) monoketone, the luminosity appears to increase substantially for a period of time during the reversion event in a

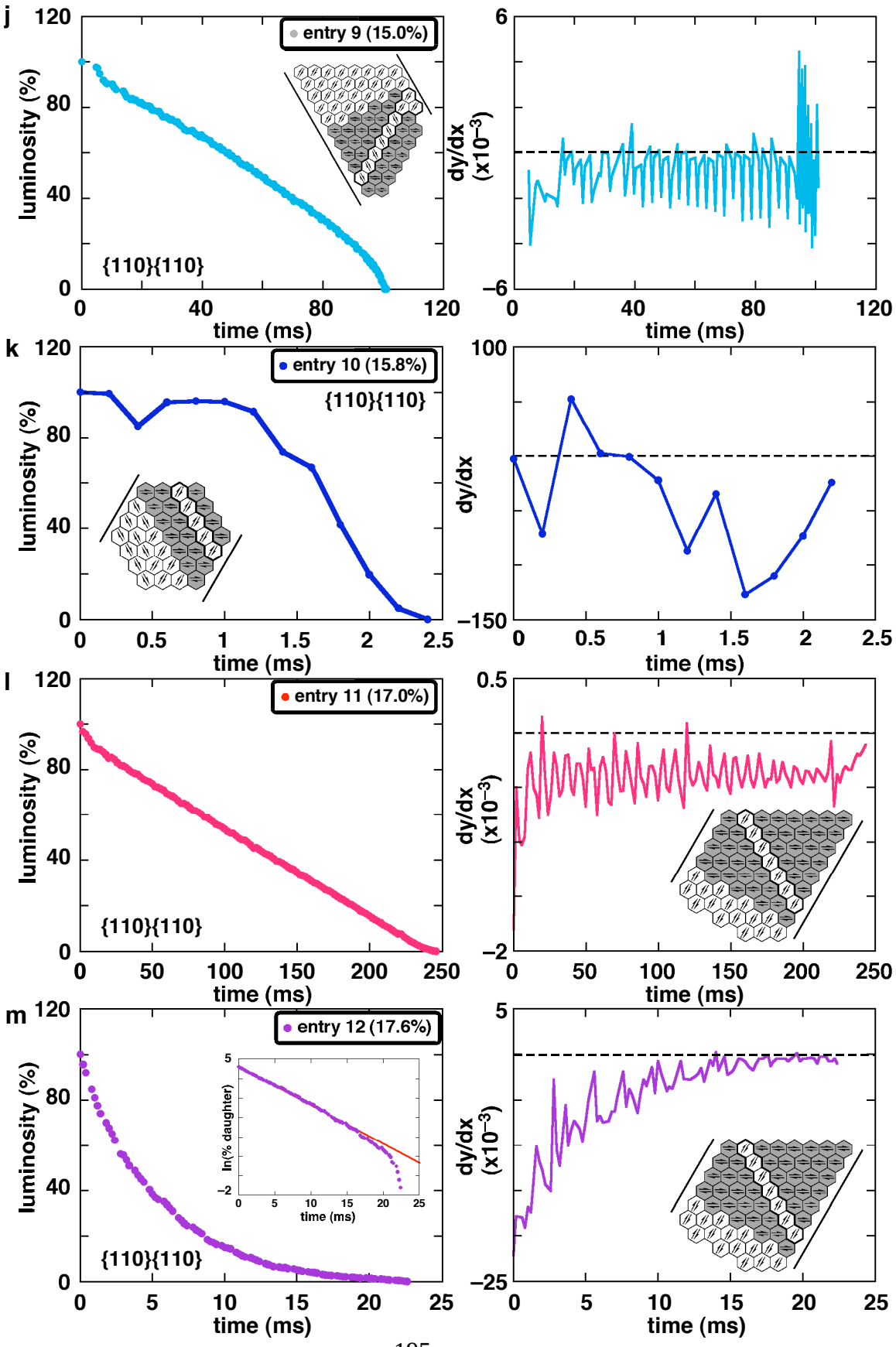
**Figure 4.26** **(a)** A summary of domain reversion kinetics measured in initial stress attempts for UICs containing 2,10-undecanedione and 2-undecanone. This table presents information pertinent to each stress experiment. (A *, for entries 1, 4, 5 and 6, indicates these videos were collected using the Kodak MotionCorder camera; these data were smoothed, as described in the text and Figure 4.25. All other experiments utilized the X-Stream camera.) As discussed in the text, instantaneous rate data from entry 8 were discarded, so they not shown here. Rates of reversion were measured as outlined in Figure 4.25. On the following pages: **(b-m)** Kinetic plots. On the left: plots of luminosity (as a percent of the total luminosity change) vs. time; on the right: first derivatives of % luminosity, with respect to time. These data are described in the text. Within each plot legend, % 2-undecanone and the percent strain (in parentheses) are provided. The color scheme used here coincides with the color scheme of Figure 4.27 (with the exception of entries 5 and 7). Schematic diagrams of the domain structure of each stressed crystal illustrate domain boundaries and orientations. **(n)** A power output curve for the Exfo X-Cite 120 light source used for illumination in the domain reversion experiments. **(o)** A plot of intensity vs. retardation calculated for this light source. **(p)** Cumulative intensities, plotted as a function of retardation. Plots **n** and **o** include a scale of crystal thickness (in μm), which can be used to estimate the maximum retardation for a daughter (see text).

**a**

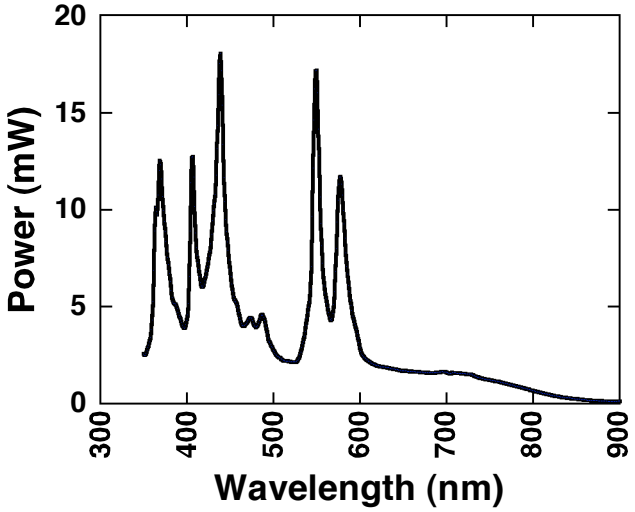
| entry | minor guest (%) | thickness (μm) | strain (%) | domain front | capture rate (fps) | reversion time (ms) | daughter fraction | frames sampled | sample size ($px^2$) | sample size ($\mu m^2$) | max. rate (mol guest $s^{-1}$) | delay to max. rate (ms) | min. rate (mol guest $s^{-1}$) | zero rates? |
|---|---|---|---|---|---|---|---|---|---|---|---|---|---|---|
| * 1 | 4.7 | 114 | 0.76 | {110} | 1000 | 254 | 0.437 | 255 | 10 × 119 | 30 × 360 | $4.83 \times 10^{-08}$ | 248 | $5.26 \times 10^{-10}$ | no |
| 2 | 10.8 | 138 | 0.90 | **{130}** | 3000 | 1.0 | 0.640 | 4 | 16 × 80 | 56 × 280 | $\mathbf{5.24 \times 10^{-06}}$ | 0.3 | $\mathbf{2.82 \times 10^{-07}}$ | no |
| 3 | 11.3 | 111 | 0.90 | **{130}** | 500 | 10.0 | 0.190 | 6 | 60 × 60 | 210 × 210 | $3.49 \times 10^{-07}$ | 2.0 | $2.30 \times 10^{-08}$ | no |
| * 4 | 11.4 | 136 | 0.85 | **{130}** | 3000 | 7.0 | 0.188 | 22 | 23 × 95 | 140 × 570 | $2.80 \times 10^{-06}$ | 0 | $3.45 \times 10^{-08}$ | no |
| * 5 | 11.5 | 160 | 0.44 | {110} | 3000 | 25.7 | 0.258 | 78 | 12 × 94 | 72 × 560 | $5.12 \times 10^{-07}$ | 23.7 | $1.94 \times 10^{-08}$ | yes |
| * 6 | 11.8 | 203 | 1.21 | {110} | 3000 | 78.0 | 0.363 | 235 | 10 × 56 | 30 × 170 | $\mathbf{4.29 \times 10^{-08}}$ | 0 | $\mathbf{3.64 \times 10^{-10}}$ | yes |
| 7 | 12.5 | 157 | 2.12 | {110} | 5000 | 1476 | 0.310 | 739 | 80 × 85 | 280 × 300 | $1.94 \times 10^{-07}$ | 2 | $1.85 \times 10^{-10}$ | yes |
| 8 | 15.0 | 76 | 1.96 | {110} | 5000 | 2.6 | 0.320 | 14 | 15 × 95 | 52 × 330 | – | – | – | – |
| 9 | 15.0 | 76 | 1.96 | {110} | 5000 | 101.4 | 0.822 | 198 | 20 × 120 | 70 × 420 | $1.64 \times 10^{-07}$ | 0 | $1.26 \times 10^{-09}$ | yes |
| 10 | 15.8 | 221 | 0.68 | {110} | 5000 | 2.4 | 0.226 | 13 | 12 × 155 | 42 × 540 | $2.46 \times 10^{-06}$ | 1.6 | $1.48 \times 10^{-08}$ | no |
| 11 | 17.0 | 161 | 1.05 | {110} | 5000 | 246 | 0.241 | 124 | 30 × 225 | 210 × 1580 | $3.61 \times 10^{-06}$ | 0 | $1.64 \times 10^{-07}$ | yes |
| 12 | 17.6 | 161 | 1.05 | {110} | 5000 | 22.6 | 0.142 | 114 | 14 × 188 | 98 × 1320 | $1.13 \times 10^{-06}$ | 0 | $1.29 \times 10^{-08}$ | no |


b
entry 1 (4.7%)
luminosity (%)
{110}{110}
time (ms)
dy/dx (x10⁻³)
c
entry 2 (10.8%)
{130}{130}
d
entry 3 (11.3%)
e
entry 4 (11.4%)

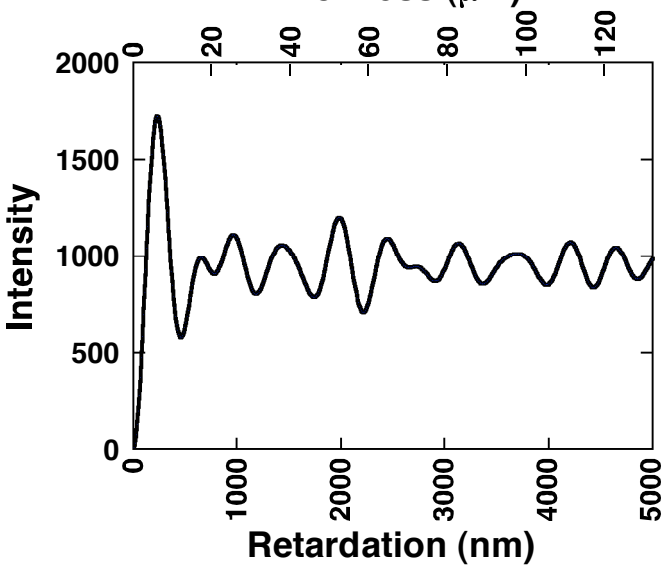

f
entry 5 (11.5%)
{110}{110}
luminosity (%)
dy/dx (x10$^{-3}$)
time (ms)
g
entry 6 (11.8%)
{110}{110}
ln(% daughter)
time (ms)
h
entry 7 (12.5%)
{110}{110}
i
entry 8 (15.0%)
{110}{110}
dy/dx (x10$^{-4}$)


j
entry 9 (15.0%)
{110}{110}
luminosity (%)
time (ms)
dy/dx (x10$^{-3}$)
k
entry 10 (15.8%)
{110}{110}
luminosity (%)
time (ms)
dy/dx
l
entry 11 (17.0%)
{110}{110}
luminosity (%)
time (ms)
dy/dx (x10$^{-3}$)
m
entry 12 (17.6%)
{110}{110}
luminosity (%)
time (ms)
ln(% daughter)
dy/dx (x10$^{-3}$)

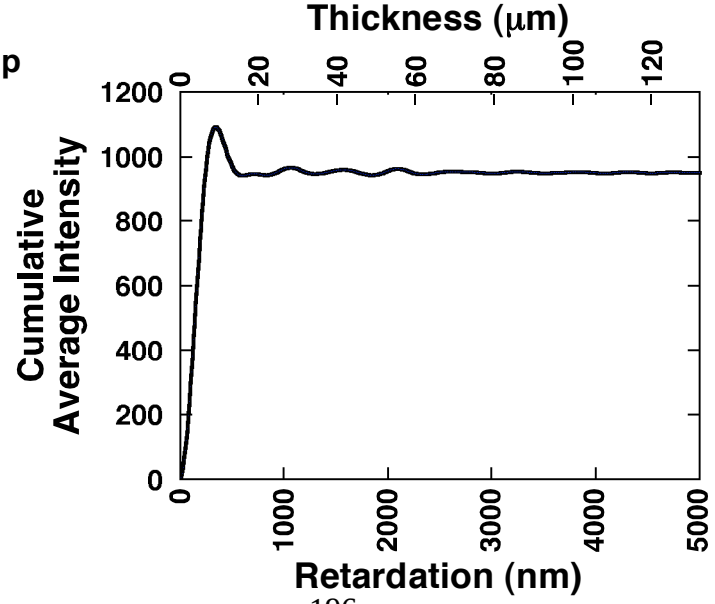
n


Power (mW)
Wavelength (nm)

o


Thickness (μm)
Intensity
Retardation (nm)

p


Thickness (μm)
Cumulative Average Intensity
Retardation (nm)

fashion that does not appear related to the variations demonstrated in Figure 4.25a and b. Similar behavior was observed for entries 8 and 9, which were recorded using the X-Stream camera. This sort of behavior is therefore not attributable to the camera or some other aspect of the recording process, but appears to indicate crystal movement. (However, there was at least one case in which the intensity increased anomalously even though the crystal was still.) There are two kinds of motion envisioned: crystal rotation and crystal jumping. These are discussed below.

During the reversion event, rotation of the crystal changes the orientation of the slow axis with respect to the orientation of the polarizer and analyzer. This leads to an increase in the luminosity of "extinguished" regions (because they are no longer oriented correctly) so that the measured concentration of daughter becomes overestimated. Although the problem of crystal rotation was addressed by rotating the analysis region for frames sampled during this period (e.g. entries 8 and 9), the inability to account for the resulting optical effects in regions that should be extinguished makes the data collected during periods of rotation unreliable. As discussed below, the crystals used in entries 1 and 5 do not rotate by more than 0.2º and 0.4°, respectively; however, the crystal used in entries 8 and 9 rotates substantially during the period of apparent daughter growth. This effect is therefore operative.

Crystal jumping, tilting, or other motion perpendicular to the microscope stage, perhaps unnoticeable in the video images, can also lead to unexplained changes in the luminosity recorded by changing the crystal focal depth, transmission properties, and apparent size of the daughter. Such increases in luminosity can be interpreted erroneously as growth of the daughter. Although the relatively poor resolution of the fast

video images precludes a definitive answer, the crystals shown in entries 1 and 5 do not appear to jump during their reversion events. On the other hand, the crystal studied in entries 8 and 9 can be seen to jump in the initial moments following stress release. Here, jumping and rotation appear to occur simultaneously (compare, for instance, the crystal orientation in Figure 4.19b and r), leading to the apparent growth of the daughter domain. The correction for rotation is deferred to the discussion of entries 8 and 9, below.

The third technical detail involves the use of ultrafast images collected using the X-Stream XS-4 camera. This camera was capable of exporting video directly to an .avi file for later examination. One will note that in video frames collected using this camera (entries 2, 3 and 7 through 12), the crystal appears flattened (along the vertical direction) when compared to the still photomicrographs taken during the stress experiment. This is most readily noticed in Figure 4.18. In the ultrafast video images the horizontal:vertical aspect ratio is unnaturally large so that the crystal appears squashed. Thus, it appears that the (nominally square) pixels have become rectangular in the video output. This distortion was not noticed until after the raw image data had been deleted from the computer used to control this camera and export videos. However, since the rates determined rely only on the *change* in luminosity between the values recorded at the beginning and at the end of the reversion experiment, and all pixels were presumably distorted to the same extent, this distortion should not affect the rates observed.

To determine the concentration of daughter, the number of bright (daughter) pixels and the change in luminosity attributable to them was estimated using Photoshop. This information was combined with the crystal thickness to determine the volume of daughter; dividing this value by the unit cell volume provides the number of unit cells in

the daughter orientation. (The process is illustrated in Section 7.5.6.) For ease of concept, the rates presented herein are expressed in moles of *guest* (of which there are four per mole unit cell) per second (mol guest $s^{-1}$).

A final concern, central to deriving the population of an orientation state from measured luminosity, involves the relationship between domain size and luminosity. This is especially important for understanding whether or not anomalous increases in daughter population (entries 1, 5, 8 and 9) are due to effects other than crystal motion. During pseudoelastic reversion, domain switching must occur both within the channel (intrachannel motion) and perpendicular to the channel (lateral motion), and either mechanistic process might be rate limiting. One might imagine two limiting cases. In one scenario, intrachannel motion is fast and lateral motion is rate limiting. Here, a given channel will exist in one of two (observable) states (daughter or mother) and will therefore exhibit either a large (bright) or small (extinguished) luminosity, both of which contribute to the luminosity observed for a given pixel. In the other limiting case, intrachannel motion is rate determining, and lateral motion is fast. Here, each channel will contribute to a distribution of retardations (and intensities) that, in each case, depends on the fraction of the channel that has reverted. Although the screw-like motion of guests and concomitant high degree of intrachannel cooperativity (Section 4.2.2) makes it intuitively satisfying that lateral propagation of the domain wall would be slower than intrachannel reorientation of guest and host molecules, the low resolutions available in the ultrafast video experiments makes these mechanisms indistinguishable. (At 10x, each pixel spans 1.5 × 1.5 $\mu m^2$ for the Kodak MotionCorder and 3.5 × 3.5 $\mu m^2$

for the X-Stream XS-4; see Section 7.5.4. For both cameras, each pixel contains on the order of $10^6$ channels.)

For the first proposed mechanism (all or nothing within each channel), a large number of pixels whose luminosities are changing (at a given point in time) should exhibit an even distribution of retardations. In the analyses described, the sample area consists of hundreds or thousands of pixels, so this condition may be met. However, in the kinetic measurements, it is the pixels that lie on the domain front that contribute to the changes in luminosity that are interpreted as changes in the population of daughter domain. When domain reversion is occurring within only a small number of pixels, an even distribution of retardations may not be present. As discussed below, this case could lead to anomalous changes in luminosity (that may be observed in crystals once they have become stationary), if the first mechanism is operative.

In the second proposed mechanism, domain reversion does not necessarily occur along the entire channel length, so that a given channel may contain both mother and daughter populations. Here, the appreciable number of channels within each pixel allows for an even distribution of retardations within each pixel. In this case, anomalous changes in luminosity should not arise from perturbations of that distribution, but from other effects.

These arguments underscore the importance of understanding the relationship between crystal luminosity and domain size. At the resolutions employed, it is not possible to distinguish between either of these mechanisms, although the possible optical effects may be described. (The topic of crystal optics was also discussed in Section

2.2.3.2.) For a crystal held between crossed polars, the intensity, I, of transmitted light is described[55,56] by the expression,

$$I = I_0 \sin^2(2\theta)\sin^2(\delta/2). \quad (3)$$

Here, $I_0$ is the intensity of the incident radiation, $\theta$ is the angular difference between the crystal slow axis and the microscope polarizers and $\delta$ is the phase shift between the eigenrays at a given wavelength, $\lambda$. When passing through a birefringent crystal, these waves become out of phase, and their separation, or *retardance*, is defined[55,57] as,

$$\Gamma = \frac{\delta\lambda}{2\pi} = L \cdot \Delta n, \quad (4)$$

where $L$ is the path length and $\Delta n$ is the difference in refractive index between perpendicular waves. From expression 4 it is clear that $\Gamma$ (often referred to as *retardation*), is expressed units of distance. Combining expressions 3 and 4,

$$I = I_o \sin^2(2\theta)\sin^2(\Gamma\pi/\lambda). \quad (5)$$

In equations 3 and 5, the first trigonometric term provides a scaling factor between the slow axis orientation of the crystal and the microscope polarizers. For a crystal whose slow axis is oriented at 45° (to the polarizers), this term equals unity; for all other orientations, this term is less than unity and the transmission intensity becomes attenuated accordingly. Thus, the scaling factor,

$$I \propto I_o \sin^2(2\theta), \quad (6)$$

can provide corrected intensities for crystals that rotate during the domain reversion event. (This will be described below.)

By summing contributions from all wavelengths and intensities emitted by a particular light source, one can construct a curve that describes the relationship between

intensity and retardance (for a given wavelength) expressed in equation 5.[58] To this end, Mark Hollingsworth digitized the output curve[59] for the EXFO X-Cite 120 metal halide light source used in the kinetic experiments to 1 nm resolution in the range between 350 and 900 nm (the predominant portion of the emission curve that passes through the optical train of the microscope). This curve is reproduced in Figure 4.26n. Although there was a small emission below 350 nm, this region of the spectrum is thought to be effectively filtered by the materials in the optical train, so it was excluded from the digitization procedure. (Although equivalent data for the Nikon microscope were not available, many glasses used in optical applications have transmission curves that drop off around 350 nm.[60]) Using the digitized curve, output intensities ($I_0$) were calculated for each wavelength; then, with equation 5 it is possible to determine the transmitted intensity (I) for each wavelength ($\lambda$) as a function of $I_0$. By summing the intensities of all wavelengths at a given retardation (in 10 nm increments, to 5080 nm) the plot of intensity versus retardation in Figure 4.26o was obtained. (This curve was generated using $\theta = 45°$ in equation 5. Because, in each case, the daughter domain was oriented at 30° or 60° with respect to the crossed polarizers, $\theta = 30°$. From equation 6, the maximum intensity of a daughter at this orientation is $\sin^2(2 \times 30°) = 0.75$. Since this correction affects the intensities at all values of $\Gamma$ by the same scaling factor, it affects only the absolute values of intensity and not the overall shape of the curve or the conclusions that follow.)

The wavelength dependence of the MotionCorder and X-Stream cameras was not known at the time of this analysis, and it was assumed that their responses are wavelength-independent (flat). Although the response of the X-Stream camera is now known not to be flat, the variations in this detector response are much smaller than the

variations in the output curve of the lamp, so effects from this camera should not change the general conclusions of this analysis.

Thus, with the assumption of a flat detector response, the curve in Figure 4.26o provides the transmission intensity observed for a crystal as a function of its retardation. Here, the maximum intensity for a crystal appears at retardations near 230 nm. For higher retardations the intensity oscillates about some intermediate value; for lower retardations, the intensity drops rapidly to zero. Because retardation is dependent on path length, it is possible to derive a scale of intensity vs. crystal thickness. This was conducted using birefringence data from the crystal described in Figure 4.5, which was grown in a solution containing an 83:17 mixture of 2,10-undecanedione and 2-decanone. For this crystal, which is approximately 7.3 μm thick, the birefringence map (Figure 4.5c) demonstrates a maximum phase shift (δ) of around 3 at an incident wavelength of 580 nm. (Since this is the only data available on such a thin crystal, it is unknown how much crystal optical properties vary over the range 4.7% to 17.6% 2-undecanone. Although the remaining discussion will assume so, future studies should address whether this analysis is applicable to crystals with different guest compositions.) From equation 4, the retardance of this crystal is approximately 277 nm, and $\Delta n = 0.0379$. Since the relationship between $\Gamma$ and $L$ is linear (equation 4), it is a simple matter to create a scale of intensities based upon crystal thickness. Such a scale is provided along the upper x-axis in Figure 4.26o.

The optical characteristics of each pixel include contributions from all of the channels that it incorporates (each kind contributing differently to the observed luminosity). Thus, it is the *cumulative average* of all retardations (up to the maximum

possible value for a given crystal thickness) that provides the overall, observed intensity of a given frame. In this fashion, the curve in Figure 4.26p was drawn by calculating a running average of all of the intensities for all smaller values of retardation. For a given crystal retardation (or thickness), this curve predicts the *observed* intensity (assuming an even distribution of retardations discussed above).

The scale of thickness is applicable only to those crystals that exhibit a similar birefringence. It was created using data from one crystal (Figure 4.5) and has not been validated against data from others. Since it was grown from a solution containing 17% monoketone, the crystal in Figure 4.5 should be at the low end of the retardation range for the crystals whose kinetics were studied. Thus, the thickness scale probably underestimates the retardation for a given crystal thickness. Nevertheless, it is useful in approximating the changes of retardation that should be operative in the crystals studied, which range in thickness from 76 to 221 μm (see Figure 4.26a).

With the above assumptions concerning even distribution of retardations, Figure 4.26p defines the intensity that is ideally observed at a given retardation. It is clear that crystals with thicknesses greater than approximately 20 μm will transmit, *on average*, a similar intensity of white light. Since, for these experiments, the crystal is oriented so that the mother domain is in the extinguishing position, transmission should occur in the daughter domains. Following stress release, domain reversion within some portion of the daughter channels that compose a given pixel will reduce the average intensity for that pixel. It therefore becomes important to address the contribution of each channel (or domain) to the observed luminosity. At any instant during the domain reversion event, the observed birefringence (and therefore luminosity) is somewhere between zero

(extinguished) and the maximum value established by the thickness and composition of the crystal (Figure 4.26o). As discussed above, the low resolution of the video images means that only the combined effect of large numbers of channels is measured, and anomalous optical behavior can depend on the mechanism by which reversion occurs.

As the region within a pixel reverts from daughter to mother, Figure 4.26p predicts that the intensity should not change appreciably until the retardation drops to 580 nm. Between $\Gamma$ = 580 and 340 nm, the intensity increases (by as much as 15%), and then decreases quickly for smaller values. For crystals thick enough for the stress-strain experiment (for the twelve sectors studied, 76 μm or greater), this plot demonstrates that a large fraction of daughter must revert to mother before the retardation enters this range. In other words, under crossed polarizers and with the EXFO light source, domain switching is only observable once it has neared completion. Since the maximum retardation is a function of crystal thickness, the *extent* of conversion required to produce changes in luminosity will vary with crystal thickness; however this should not affect the comparison of behavior from different crystals because each daughter should revert via the same mechanism, as long as the sampling methods are consistent (a condition that may not always be met). For example, a crystal that is 76 μm thick exhibits a maximum retardation of approximately 2880 nm, whereas the thickest crystal studied, 221 μm, has a maximum retardation of about 8380 nm. For these, approximately 80% and 93% of the reversion process should have occurred before the retardation reaches the threshold of 580 nm.) Based on the scale in Figure 4.26p (and assuming that it is correct), it is only for crystals with $\Gamma_{max}$ of less than the curve maximum at 340 nm (about 9 μm thick) that

the entire domain reversion event is accompanied by decreasing luminosity and may therefore be monitored in a straightforward manner using this light source.

The above discussion is important because it illustrates that the changes in luminosity are only observable for a very small fraction of the reversion event. In the retardation regime between 580 and 240 nm, the increase in intensity might be manifested as oscillations or other increases in luminosity measured for groups of pixels. It is also important to remember that the resolutions employed do not permit one to discriminate between fast reversion of a few channels and slow reversion of many. Therefore, it remains unclear what the distribution of retardations is for a given pixel. If the distribution is shifted to low retardations, then domain reversion of such pixels can give rise to anomalous changes in the observed luminosity. An example of this may occur if mechanism 1 (all or nothing) is operative: if retardation for pixels near the domain front was much lower (for instance, near 580 nm) than that of the bulk, then their reversion could lead to anomalous changes in intensity. For mechanism 2 (partial reversion along the channel), the presence of partially reverted channels could give rise to the same effect. Thus, the possible distribution of retardations can play an important role in the measurement of domain reversion kinetics. In the studies described below, crystal translation was accounted for by moving the sample region, while rotation was addressed by scaling the observed luminosity using equation 6. (These measures will be described as necessary.) For entries 5 and 8, anomalous changes in luminosity were recorded that could not be attributed to crystal motion; these will be discussed below.

4.4.1.3 Reversion Kinetics

The results from the kinetic analysis are tabulated in Figure 4.26a. In addition to information on the guest content and experimental parameters, this table provides the maximum and minimum "instantaneous" rates measured between consecutive data points. (The temporary arrest of the domain wall (a rate of zero) was observed for four crystals; these are identified in the final column.) The decay kinetics (and first derivatives) are plotted in Figure 4.26b-m. Here, smoothed rate data have been used for entries 1 and 4 through 6, Figure 4.25b and e-g. (As discussed below, an analysis of kinetic data from entry 8 was not conducted because of anomalous changes in luminosity that could not be accounted for based on simple crystal rotation; however, the data are included in Figure 4.26i.) In general, the length of time required for complete decay of daughter fell into one of three regimes: 2-12 ms (entries 2-4, 6, 8 and 10), 25-80 ms (entries 5, 6 and 12) or 100-250 ms (entries 1, 7 and 11); one crystal (entry 7) relaxed over 1.5 s (Figure 4.26h). Many of the crystals exhibited discontinuous changes in their decay curves. Members of this laboratory have observed stepwise reversion in other crystals containing 2,10-undecanedione and 2-undecanone.[21] Thus, for a given crystal, the relaxation event can exhibit a variety of rates that may include temporary arrest of domain wall motion. Certainly, average rates are useful in describing the reversion process, but in some cases it was difficult to make the distinction between different rate regimes. For this reason, instantaneous rates provide a quantitative picture of the domain reversion process. A discussion of the domain reversion event for each crystal studied is provided below.

As outlined in Figure 4.26a, the daughter in entry 1 was formed along {110}{110} boundaries. For this daughter, the measured mean luminosity increases over approximately 30 ms following stress release (Figure 4.26b), which provides an apparent increase in the amount of daughter domain observed over that period of time. This behavior may result from crystal motion; during this event, noticeable translation was noted for the first 70 ms. (However, no rotation is observable.) Frames that indicated an increase in daughter domain (i.e., a negative rate of domain reversion) were discarded from the kinetic analysis.

Following the period of increased luminosity, the daughter domain reverts to mother over a variety of rates. The still frames indicate complete disappearance of daughter 2 and some reversion of daughter 3 (the larger of the pair, Figure 4.12). After approximately 75 ms, the rates slow gradually, and the kinetic plot appears quite curved. Between 125 and 225 ms a fairly linear regime is observed with an average rate of $9.63 \times 10^{-10}$ mol guest $s^{-1}$ ($R^2 = 0.997$ for 101 data points). (Nearly linear decay is evident in the first derivative plot of Figure 4.26b, which indicates a consistent derivative during this period.) This time period corresponds to relaxation within daughter 3 as the mother overtakes this domain on three sides and the daughter appears to withdraw from the extinguished mother in much the same way a blade is withdrawn from its sheath. Such motion is commonly observed in daughter domains that do not stretch across the entire crystal and are surrounded on three sides by mother domain. (Entries 5 and 6 provide additional examples of this behavior.) Finally, the last frames of this video demonstrate the fastest rates and the disappearance of daughter 3; over the last 10 ms, the rate of reversion increases rapidly. Such behavior might be expected for a daughter whose

volume has become quite small in relation to the surface area it exposes to the surrounding mother. This appears to concur with the hypothesis that domain walls are destabilized relative to the bulk domain (Sections 4.2.4 and 4.3.3).

For entry 2, the band of daughter domain reverts over three frames at the 3000 fps capture rate employed. For this daughter, domain wall motion occurs on both sides (Figure 4.13) and the fastest instantaneous rate ($5.24 \times 10^{-6}$ mol guest $s^{-1}$) is observed in the first frame. The small number of data points does not permit a detailed analysis of the data, although this crystal exhibited the fastest instantaneous rates (discussed below and tabulated in Figure 4.26a). This daughter appears to decay from both {130}{130} fronts (which probably contributes to the relatively fast reversion kinetics); such behavior contrasts that of entry 3 (Figure 4.14), in which reversion occurs along a single {130}{130} domain front (Figure 4.26c).

Prior to release, the daughter domain of entry 3 extends to a crystal edge so that it is bordered by mother domain only on one side. The kinetic data (Figure 4.26d, 500 fps frame rate) reveal a variety of instantaneous reversion rates, starting with $5.50 \times 10^{-8}$ mol guest $s^{-1}$ between the first two frames (2.0 ms span). Between 2.0 and 6.0 ms, faster rates are observed (see derivative plot in Figure 4.26d). Towards the conclusion of the reversion event, the measured rate gradually slows, as indicated in the first derivative plot.

Entry 4 exhibits a variety of rates (Figure 4.26e). For this crystal a pair of {130}{130} daughter domains with similar size and orientation were measured collectively. Although pseudoelastic reversion should follow a domain front that traverses the daughter domain, such a front is not observable at the resolution employed

for the ultrafast video capture (Figure 4.15). Instead, these daughters appear to fade in intensity until no longer observed. At 3000 fps, the fastest rates are observed immediately following stress release. After this, reversion exhibits a variety of slower rates (some nearing 0 moles guest $s^{-1}$), as indicated by the first derivative plot (Figure 4.26e).

In a fashion similar to entry 1, the domain reversion event (recorded at 3000 fps) for entry 5 (Figure 4.26f) exhibits an apparent increase in the concentration of daughter domain between 10.7 and 20.0 ms following stress bar retraction. During this time, the crystal does not rotate by more than 0.4° (measured using Photoshop). As discussed above, this behavior should not arise from an actual increase in daughter concentration, which is not expected to occur *after* the release of stress. Furthermore, changes in pixel retardation that occur during the reversion event (Figure 4.26p) appear ruled out on the grounds that they do not occur over the entire reversion event, but are noted 10.7 ms following release. In any event, this increase in luminosity is not currently understood. The data that exhibit *decreasing* daughter population exhibit three rate regimes. Over the 1.33 ms immediately following stress release, the measured rates reflect changes in luminosity both for the daughter of interest ({130}{130} boundary. (See the box in Figure 4.16b and for the {130}{130} daughter that lies nearly horizontal.) What follows is a variety of instantaneous rates (ranging $1.94 \times 10^{-8}$ to $1.46 \times 10^{-7}$ mol guest $s^{-1}$) between 1.67 and 11.0 ms. Following the anomalous increase in daughter concentration (between 11.33 and 18.0 ms), domain reversion proceeds at its greatest rates (see derivative plot, Figure 4.26f), and these changes become readily apparent in the still images. The slowest apparent rates occur at the maximum of the anomalous luminosity

measurements, recorded between t = 17 and 18 ms, and are probably not accurate. (The luminosity data collected between 10.7 and 20.0 ms were discarded.) Thus, the slowest *reliable* rate, $1.94 \times 10^{-8}$ mol guest $s^{-1}$, is observed 8.0 ms following release.)

The decay plot for entry 6 (Figure 4.26g) exhibits no abrupt changes in rate, but rather a smooth curve of moles of daughter vs. time. For this {110}{110} daughter, no discrete domain front was visible in the still images (Figure 4.17); like the daughters in entry 4, this domain appears to fade away. The fastest reversion rates are observed in the initial moments following stress release. What follows is a gradual reduction in the rate of reversion: between 9.3 and 60.0 ms, the instantaneous rates slow by approximately one order of magnitude. Although the luminosity data were smoothed (Figure 4.25h), oscillations are evident in the linear and first order derivative plots of Figure 4.26g. Nevertheless, the kinetic data have the appearance of a first-order process. To test this, ln(%daughter) was plotted vs. time (see inset in Figure 4.26g). This gave a linear correlation ($R^2 = 0.998$) for 55.0 ms following stress release; during this period, the first-order rate constant is 40.7 $s^{-1}$. Although first order kinetic behavior is not expected for a solid-state reaction such as this,[61,62] similar regions of first order decay were also observed for entries 7 and 12.

During the final portion of entry 6, reversion has slowed appreciably. At 78.3 ms, the memory buffer for the ultrafast camera became full so that the remaining portion of the event was not recorded. However, the mean luminosity measured for the sample region for the last five frames collected (29.3(3) units) is comparable to the mean luminosity for an extinguished region (28.5 units, in a sample measurement). The difference in these values (about 0.8 units) is much smaller than the change in luminosity

observed over the course of the reversion event (41.8 units); thus, the majority of reversion has occurred before 78.3 ms elapsed time, and the kinetic analysis is *nearly* complete.

Entry 7 produced multiple {110}{110} daughters (Figure 4.18) for which domain reversion was analyzed collectively (at a frame sample rate of 500 $s^{-1}$; see below). The rate data (Figure 4.26h) shows a rapid decrease in daughter population during the first 68.0 ms followed by several regions of increasingly slower decay. The first order derivative of that data indicates large oscillations in rate for most of the reversion event. This crystal provided the slowest instantaneous rates (see Figure 4.26a), which could arise from the sampling of a large number of domains or because it was stressed more than any other (to 2.12%). (This will be discussed below.) It is interesting that, like entries 6 and 12, this daughter appears to exhibit first-order reversion kinetics. A plot of ln(%daughter) vs. time (see inset in Figure 4.26h) produces a linear correlation ($R^2$ = 0.995) between t = 150 and 650 ms; during this period, the first-order rate constant is 1.46 $s^{-1}$. Although this rate constant is much slower than those observed in entries 6 and 12, it represents the averaged decay of many daughter domains. Between these, there are probably a multitude of rates that may or may not exhibit first-order kinetics *individually*.

Like entries 1 and 5 (and, below, entries 9 and 10), the entry 8 exhibits a period of apparent growth for the daughter domain. The kinetic plot for entry includes increases in luminosity that are thought to arise from tilting of the crystal, which leads to an increase in observed luminosity that could not be accounted for with the available information. Although it is difficult to assess the amount of tilting, rotation along an axis parallel to the light path can be measured. This was conducted[63] by drawing a line parallel to a

growth face of the crystal and recording its orientation (in Photoshop, v. 7.0, for Macintosh). Using equation 6 (above), it is possible to account for crystal rotation (along an axis perpendicular to the stage) in the observed luminosity data. This correction was applied to data from a nominally extinguished region in the crystal. (See boxed region in Figure 4.25i. This region spans $7 \times 7$ px$^2$, or $25 \times 25$ μm$^2$.) Since no observable domain switching is occurring in this region, any changes in the observed luminosity should be caused by crystal motion; this provides a check on the applicability of the correction as well as an indicator of the effects of motion other than crystal rotation. The data are plotted in Figure 4.25i. During the first 1.4 ms, the crystal rotates by -5.2°; this rotation is clearly observable by comparing the top edge of the crystal in Figure 4.19b and j. As expected, one measures no luminosity prior to stress release; once the crystal has rotated by 2.5° (at t = 0.8 ms), the extinguished region begins transmitting light and the luminosity increases. Using equation 6, the predicted luminosity for this region was identified, and scaled as follows: between 3 and 10 ms, the observed luminosity assumes an average value of 12.[64] By this time the crystal has stopped rotating (and has settled at -4.8° from its initial orientation[65]), so the predicted luminosity for the extinguished region is constant (= 0.028). The scaling factor is determined by the ratio of the "terminal" observed luminosity (= 12) to the predicted luminosity (= 0.028); its application (to the each predicted data point) allows a direct comparison between the measured and the predicted luminosities. For these data, this factor was 430.

In Figure 4.25i, one notes fair agreement between the predicted and observed values up through t = 1.0 ms. After t = 1.0 ms, the observed luminosity is appreciably greater than that predicted by simple crystal rotation. This behavior may arise from

crystal tilting (rotation along an axis not parallel to the light path) or other sorts of motion. Since these motions have not been measured, it is impossible to correct for them adequately, and no further corrections have been applied. For entries 8 and 9, all data collected between t = 1.0 to 3.0 ms are considered unreliable. After 3.0 ms, the predicted and observed luminosities for the extinguishing region are reasonably close, so a correction (applied in the same fashion as for the extinguished region) should be applicable to entry 9 (Figures 4.20 and 4.26j). Unfortunately, the daughter in entry 8 (Figure 4.19) completely reverted at t = 2.6 ms, so proper analysis of the kinetic data is not possible. The decay curve (and the first derivative curve) is provided in Figure 4.26i.

Entry 9 produces the same apparent growth of {110}{110} daughter domain during the frames immediately following stress bar retraction as entry 8. As discussed above, luminosity data collected between 1.0 and 3.0 ms were discarded and all other data were corrected for rotation using equation 6. In addition, the ultrafast video sequence contains oscillations in the overall brightness of each frame. On average, data from every fifth frame was discarded because the frames were anomalously dim. The kinetic data collected after this period (Figure 4.26j) consists of rapid reversion in the first few frames, followed by a long, and more gradual decay. From t = 10-80 ms (approximately), the rate plot appears somewhat linear; however, the first order derivative plot demonstrates large oscillations in the reversion rate for the entire process. During this time period, the crystal does not move noticeably, and the band of daughter domain is traversed by a domain front from both sides. As reversion proceeds the average rate of reversion increases quite slowly before it speeds up (following t = 94.6 ms) as the daughter disappears.

For entry 10, longitudinal jumping between 0.4 and 0.6 ms produced a decrease in luminosity for the region analyzed (Figure 4.21b). (This motion is discernible in the 5000 fps ultrafast video as the crystal moves into and out of focus.) These data were discarded from the final kinetic analysis. Between 1.2 and 2.2 ms, domain reversion occurs at its fastest rates; at the end, the {110}{110} daughter gradually fades in intensity before it disappears.

As outlined above, entries 11 and 12 were measured on the same crystal (capture rate = 5000 fps). The largest of the pair, entry 11 (Figure 4.26l), exhibits a very long region of linear decay. (For this crystal, every tenth of the ultrafast frames measured at 5000 fps were analyzed to yield a sample rate of 500 $s^{-1}$.) To 9.8 ms following stress release, the fastest rates are observed. What follows is a very linear regime of appreciable duration: frames measured between 11.8 and 235.8 ms indicate an average rate of $8.64 \times 10^{-8}$ mol guest $s^{-1}$ ($R^2 = 1.000$ for 113 data points). (Although the first derivative plot in Figure 4.26l shows oscillation in reversion rate, the average rate is quite consistent throughout this range.) During this time, domain wall motion is visible on both sides of the daughter (Figure 4.22d-s). In frames collected after this period, the daughter domain is barely visible (see Figure 4.22t). However, luminosity measurements indicate small changes in transmission that are likely to arise from domain reversion. During the last 8.0 ms of the reversion event, the slowest rates are observed; this is reflected in the first derivative plot, which tends toward zero.

For entry 12, the daughter domain disappears gradually in a process that exhibits a smooth transition from fast to slow rates (Figure 4.26m). (Although it lies very close to the sector boundary between the top and left sectors in Figure 4.23a, this daughter was

wholly formed within the top sector.) As with entry 9, every fifth frame of the ultrafast video exhibited decreased brightness. These luminosity data were therefore discarded from the kinetic analysis. (Although entry 11 was measured from the same video sequence, the series of frames analyzed was chosen so that they did not include the anomalous frames.) As with entry 6, these data appear to describe a first-order process. This is confirmed by a plot of ln(%daughter) vs. time (inset in Figure 4.26m), which illustrates a very linear correlation ($R^2 = 0.998$) for 16.4 ms following stress release; during this period, the first-order rate constant is 199 $s^{-1}$.

4.4.1.4 Instantaneous Rates of Reversion

As described above, instantaneous rates provide a description of the domain reversion kinetics. For most of the experiments described, the time resolution is limited by the video capture rate. Exceptions are as follows: entries 7 and 11 (5000 fps capture rate) were sampled for every tenth frame for a resolution of 1/500 s (2.0 ms) and, for the majority of the reversion event, entry 9 (5000 fps capture rate) was analyzed for every third frame for a resolution of 3/5000 s (0.6 ms). (During the last 9.6 ms of this reversion event every sequential frame was sampled.) As discussed above, certain other data were discarded because of crystal motion or anomalously low brightness in the video frames.

The maximum and minimum observed instantaneous rates are tabulated in the last several columns of Figure 4.26a. When only the nine sectors stressed to 1.21% strain or less (excluding entries 7-9) are included, the range of observed rates spans a factor of approximately 14,400 ($3.64 \times 10^{-10}$ to $5.24 \times 10^{-6}$ mol guest $s^{-1}$; entries 6 and 2, respectively). (The fastest and slowest rates observed in these nine sectors are presented

in bold in Figure 4.26a.) These data differ significantly from values published[21] by Hollingsworth, et al., for the same experiments because additional analyses have been conducted since that time. These include data smoothing to the Kodak MotionCorder data (entries 1 and 4 through 6), corrections for crystal rotation (entry 9) and the analysis of additional frames (entries 6 and 7).

Although the fastest rates span over four orders of magnitude, the fastest rates vary by only a factor of 120 ($4.29 \times 10^{-8}$ to $5.24 \times 10^{-6}$ mol guest $s^{-1}$; entries 6 and 2, respectively). These values demonstrate no obvious correlation with monoketone concentration or percent strain. Inclusion of entries 7 and 9 (strained to 2.12 % and 1.96%, respectively) does not change the fastest rates, but it does widen the range of observed rates to a factor of 28,200. Now, the smallest instantaneous rate observed in a crystal is $1.85 \times 10^{-10}$ mol guest $s^{-1}$ (entry 7).

The apparent independence of reversion rate on the amount of 2-undecanone might suggest that the kinetic barrier to domain reversion is not affected by this impurity. However, for reactions in the solid state there may be many kinds of centers that must react, each with its own energetic barrier and distinct "slow step" in the observed reaction progress.[8] Such behavior is reflected in the variety of rates observed in the kinetic plots of Figure 4.26. It was reasoned that perhaps the *distribution* of instantaneous rates could provide insight into the effect of 2-undecanone impurity on observed ferroelastic behavior. Histograms of the measured instantaneous rates are therefore provided in Figure 4.27. For these, instantaneous rates were binned into half log unit portions (which correspond to rate partitions of a factor of close to three), and the percentage of daughter that relaxed within each rate range was plotted against those rates. (For instance, the

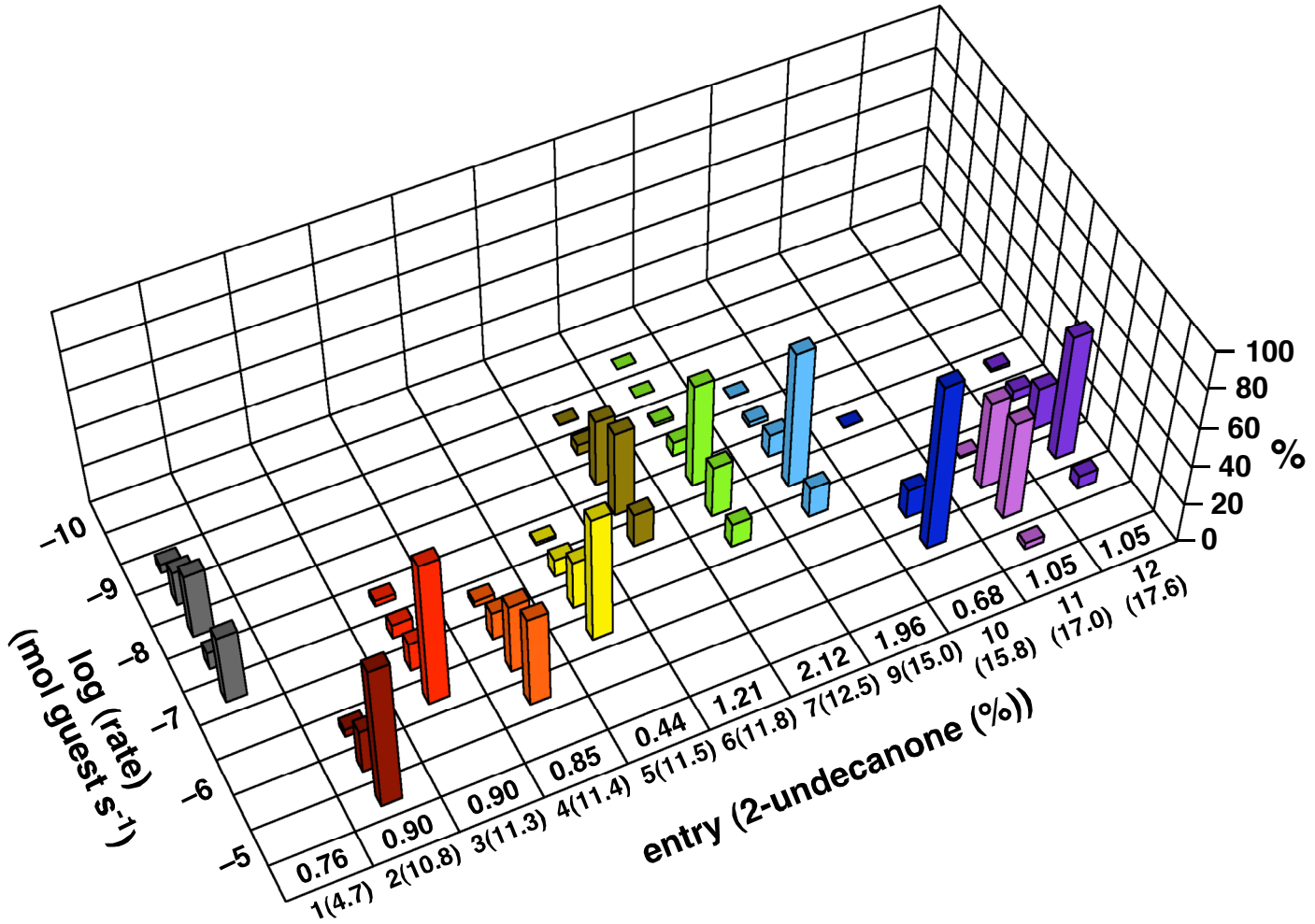



**Figure 4.27** Instantaneous rates of pseudoelastic domain reversion in UICs containing mixtures of 2,10-undecanedione and 2-undecanone. For each stressed sector, the percentage of 2-undecanone guest was determined by HPLC following the stress experiment. The vertical axis represents the percentage of daughter domain that reverted within a given range of rates (binned in half log units). Values in the first row along the horizontal axis indicate the percent strain applied to the crystal prior to stress release. The color scheme used here coincides with the plots in Figure 4.26 (except for entry 5, 11.5% 2-undecanone). As discussed in the text, instantaneous rates from entry 8 (15.0%) have been discarded.

fastest rate recorded for entry 1 (4.7% monoketone) is $4.83 \times 10^{-8}$ mol guest $s^{-1}$, or log(rate) = -7.316. This datum is included in the range from -7.5 to -7.0 so that in Figure 4.27 it is counted in the "-7.0" bin.

The histograms of instantaneous rates differ for each of the crystals studied. Some, such as entries 7 and 12, exhibit a distribution of rates that is somewhat centered around the mode; others, such as entries 2 through 4, produce a "tailing" histogram as a majority of reversion occurs at rates near their maximum. Indeed, for many of these, a majority of domain reversion occurs over a small range of rates, the magnitude of which is fairly consistent between samples: the histogram maxima (Figure 4.27) for all twelve entries span 2.5 log units, or a factor of approximately 300. The critical dependence of pseudoelastic behavior on 2-undecanone concentration indicates that monoketone incorporation does affect the reversion process, but the small range of maximum rates observed in this study suggests that the fastest rates are relatively insensitive to the incorporation of monoketone relaxive impurity.

Comparing pairs of stressed sectors in the same crystal (entries 11 and 12), presents a unique opportunity to compare reversion behavior in regions that have been subjected to identical treatment. For this crystal, one daughter (entry 11) was much larger than the other (entry 12), yet similar rate maxima are observed. However, close inspection of Figure 4.22a (or 4.23a) shows that these daughters were formed on different growth sectors that possessed different monoketone concentrations (17.0% and 17.6% for entries 11 and 12, respectively). This difference in concentration could make entry 12 revert more quickly; however, this is not the case. The maximum rate observed for entry 11 ($3.61 \times 10^{-6}$ mol guest $s^{-1}$) is over three times faster than the maximum rate observed

for entry 12 ($1.13 \times 10^{-6}$ mol guest $s^{-1}$); their slowest rates differ by approximately an order of magnitude (Figure 4.26a). In addition, the histogram for entry 11 (Figure 4.27) is visibly shifted to higher rates in comparison to entry 12. For these sectors, which presumably were subject to identical treatment, reversion rates appear dependant upon factors other than monoketone concentration. Some possible factors are identified below.

The kinetic experiments were initially confusing because they don't indicate any obvious correlation between impurity concentration and relaxation rate. Nor do they suggest that daughters formed *in the same crystal* will exhibit similar reversion kinetics. Furthermore, these kinetic data do not elucidate the nature of the rate-limiting step. Although variations in strain occur from crystal to crystal, the data do suggest the monoketone impurity provides no measurable increase in the rate of relaxation of the fastest sites; instead, as illustrated in Section 4.3, this impurity appears to affect only whether or not pseudoelastic reversion occurs at all.

In Section 4.3.3, stressed defects were hypothesized to control domain reversion. If this hypothesis is true, it appears reasonable that those same defects may have an appreciable effect on the rate at which domain reversion occurs. In the absence of pinned defects, the reversion of 2,10-undecanedione/urea should proceed at some maximum intrinsic rate. From the kinetic data above, this intrinsic maximum is on the order of $10^{-5}$ moles of guest $s^{-1}$ (or greater) at room temperature and appears somewhat independent of guest stoichiometry within the range of 4.7 to 17.6% monoketone. From the histograms in Figure 4.27, it is clear that for many crystals (for instance, entries 2, 4 and 10 through 12), appreciable fractions of daughter channels revert at or near the intrinsic rate maxima. The *range* of rates observed also suggests the presence of a variety of reversion barriers

that could arise from different combinations of defects that favor and resist domain reversion. The nature of such defects will be discussed in Chapter 5.

In summary, UICs containing mostly 2,10-undecanedione exhibit spontaneous domain reversion, and the driving force for this process is sometimes counterintuitive. One might expect the energetic barrier to domain switching (Figure 4.11) to depend on the concentration of relaxive impurity so that the rates of reversion should correlate with the incorporated amount of the relaxive impurity 2-undecanone. However, the stress experiment is not perfect: the act of physically applying force to the crystal can produce stressed defects that make the daughter less stable than the mother or resist domain wall motion. It appears that pseudoelasticity depends on a combination of factors, which includes the formation defects and the ability of relaxive impurity to anneal them.

### 4.4.2 The Effect of Repeated Stress

If pinned sites are created during the stress process, their concentration (or potential to inhibit domain wall motion) might be increased as a crystal is subjected to multiple cycles of stress and release. If so, the effect of pinned sites (or other changes in crystal domain structure) might be addressed via study of kinetics of pseudoelastic reversion. This hypothesis was tested by stressing the crystal containing 11.5% 2-undecanone (entry 5, Figure 4.16) five times in succession. (Data from the initial stress attempt were used in the preceding discussion and in Figures 4.26h and 4.27). The experiment is summarized in Figure 4.28; the table provides relevant information for each stress attempt, and Figures 4.29 through 4.32 depict the second, third, fourth and fifth stress attempts, respectively. For each cycle of stress and release, the applied strain

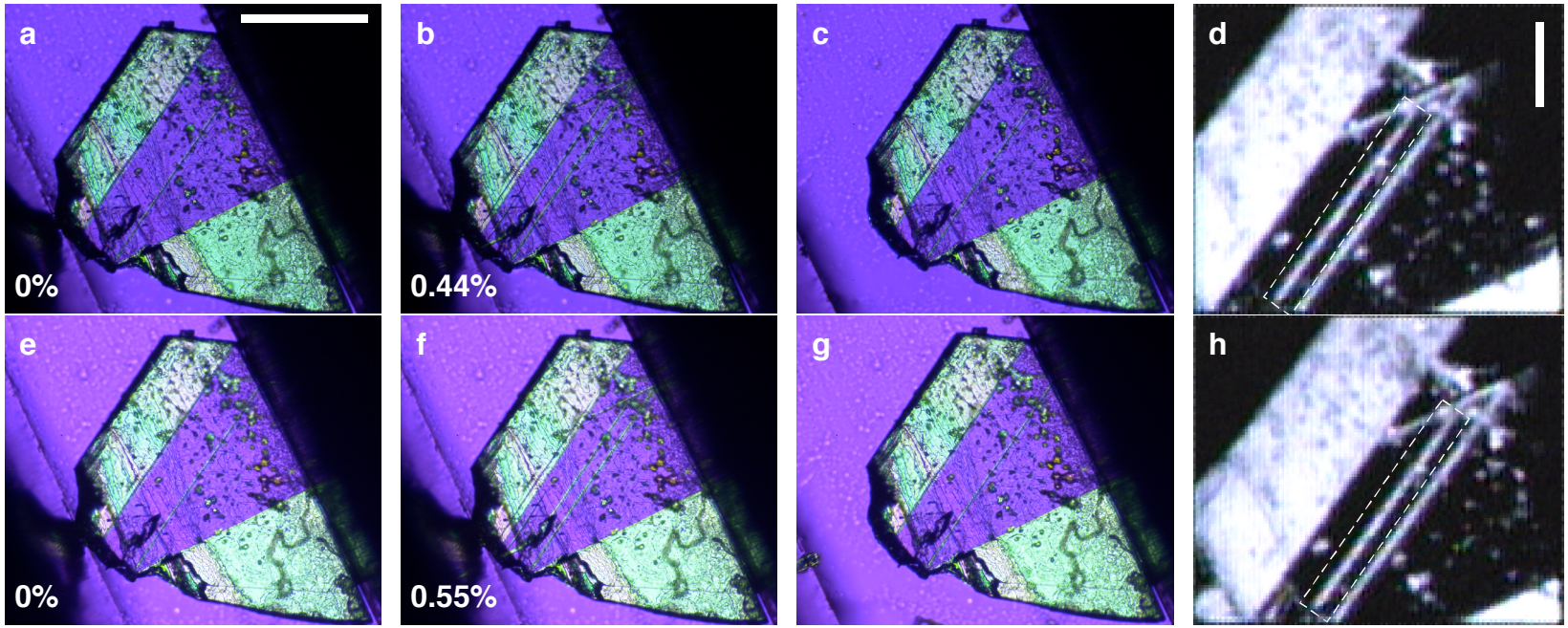
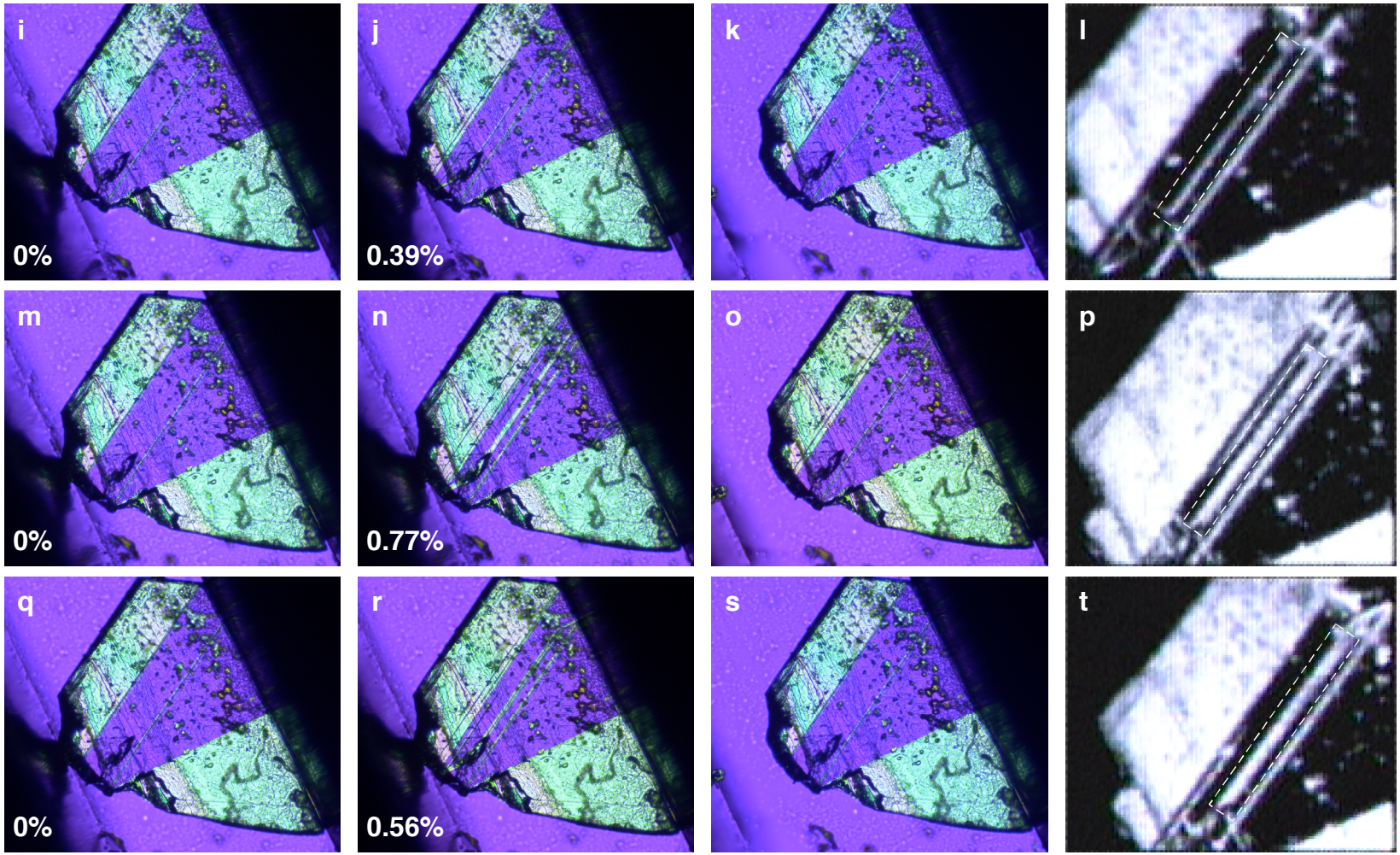



**Figure 4.28** Multiple stress attempts for a UIC crystal containing a mixture of 88.5:11.5 2,10-undecanedione and 2-undecanone. (**a-d**) Initial stress attempt. Photomicrographs, taken between crossed polars and with λ plate, of the crystal at first contact with the stress bar (**a**), at maximum strain (**b**), and following release of stress (**c**). The measured strain is provided in **a** and **b**. Scale bar = 0.50 mm (Nikon 5x). (**d**) Video frame, recorded between crossed polars, preceding stress bar retraction. Here, the mother domain is in the extinguishing position, and the daughter appears as a bright band. The daughter region analyzed is denoted by the box. The bright band that lies outside of the sample region and runs parallel to the daughter was present prior to stress (see **a**). Scale bar = 0.20 mm (Kodak MotionCorder 1.3x). A similar series of images is provided for stress attempts II (**e-h**), III (**i-l**), IV (**m-p**) and V (**q-t**), some of which are on the following page.

| attempt | strain (%) | capture rate (fps) | dwell time (ms) | event length (ms) | frames sampled | maximum rate (mol $s^{-1}$) | delay to max. rate (ms) | minimum rate (mol $s^{-1}$) | delay to min. rate (ms) | frames excluded (ms) |
|---|---|---|---|---|---|---|---|---|---|---|
| **I** | 0.44 | 3000 | 0 | 25.7 | 78 | $5.12 \times 10^{-07}$ | 23.7 | **$1.94 \times 10^{-08}$** | 8.0 | 10.7–20.0 |
| **II** | 0.55 | 3000 | 0 | 25.3 | 77 | $6.52 \times 10^{-07}$ | 22.3 | $4.42 \times 10^{-09}$ | 1.7 | 13.7–18.7 |
| **III** | 0.39 | 3000 | 0 | 31.0 | 94 | $5.92 \times 10^{-07}$ | 30.0 | $1.85 \times 10^{-08}$ | 17.7 | 0–17.3 |
| **IV** | 0.77 | 3000 | 0 | 730.0 | 279 | **$3.32 \times 10^{-07}$** | 0.3 | **$3.56 \times 10^{-10}$** | 250.0 | none |
| **V** | 0.56 | 3000 | 0 | 24.7 | 75 | **$8.48 \times 10^{-07}$** | 23.3 | $8.04 \times 10^{-09}$ | 12.0 | 18.0–21.0 |


i
0%
j
0.39%
k
l
m
0%
n
0.77%
o
p
q
0%
r
0.56%
s
t

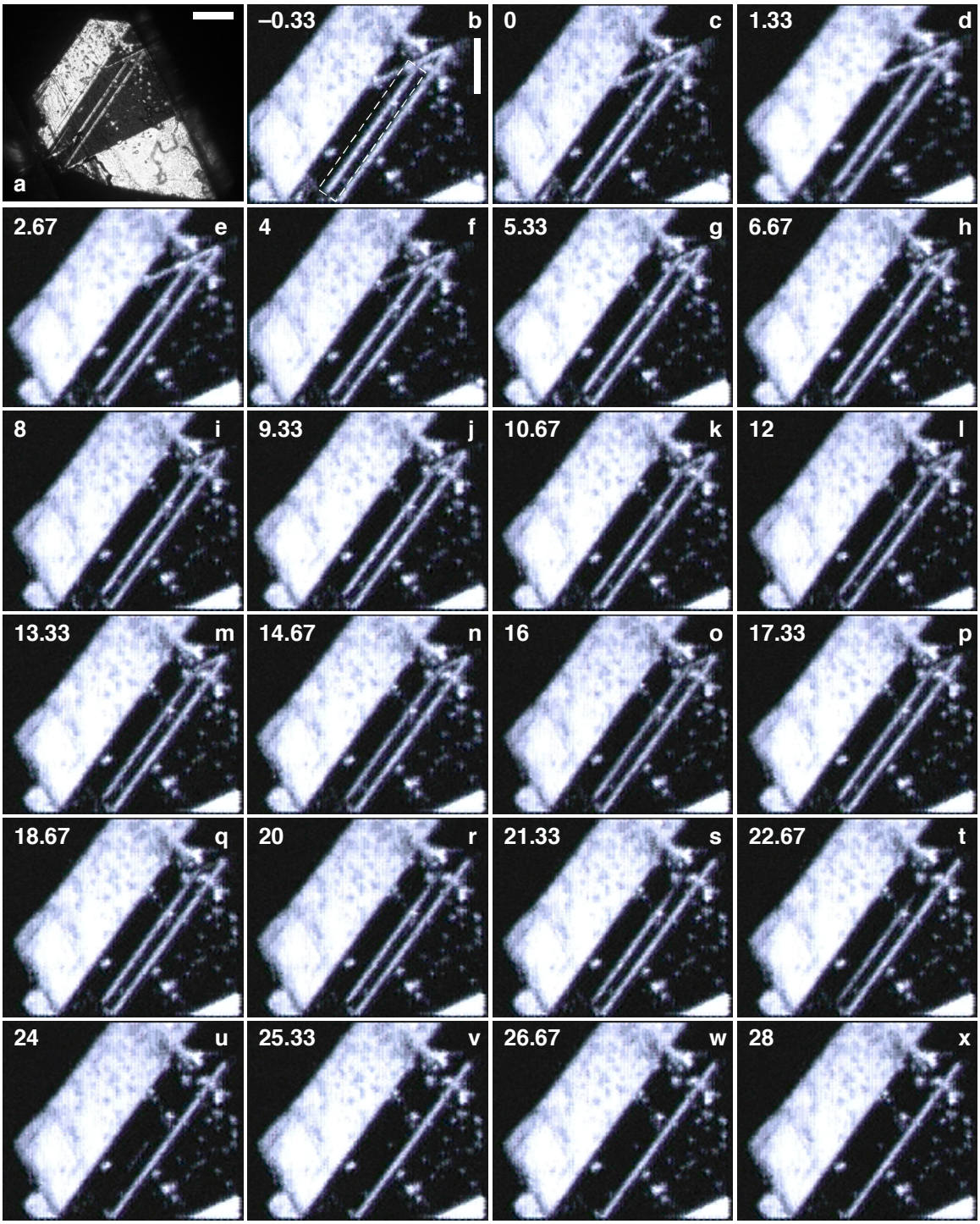



**Figure 4.29** Domain reversion and ultrafast video sequence for the second stress attempt for the crystal containing 11.5% monoketone, following 0.55% compression. The experimental setup is similar to the description provided in Figure 4.16. **(a)** Photomicrograph (crossed polars) of the crystal taken immediately before stress release. Scale bar = 0.25 mm (Nikon 5x). **(b-x)** Ultrafast (3000 fps) video frames, beginning 0.33 ms prior to stress release (**b**), at stress release (**c**), and in 1.33 ms increments thereafter (**d-x**). In each image the time from stress release (time = 0, frame **c**) is presented in the upper left-hand corner. The box in frame **b** indicates the sample region for this frame, which was repositioned according to crystal motion (see text). Scale bar = 0.20 mm (Kodak MotionCorder 1.3x).

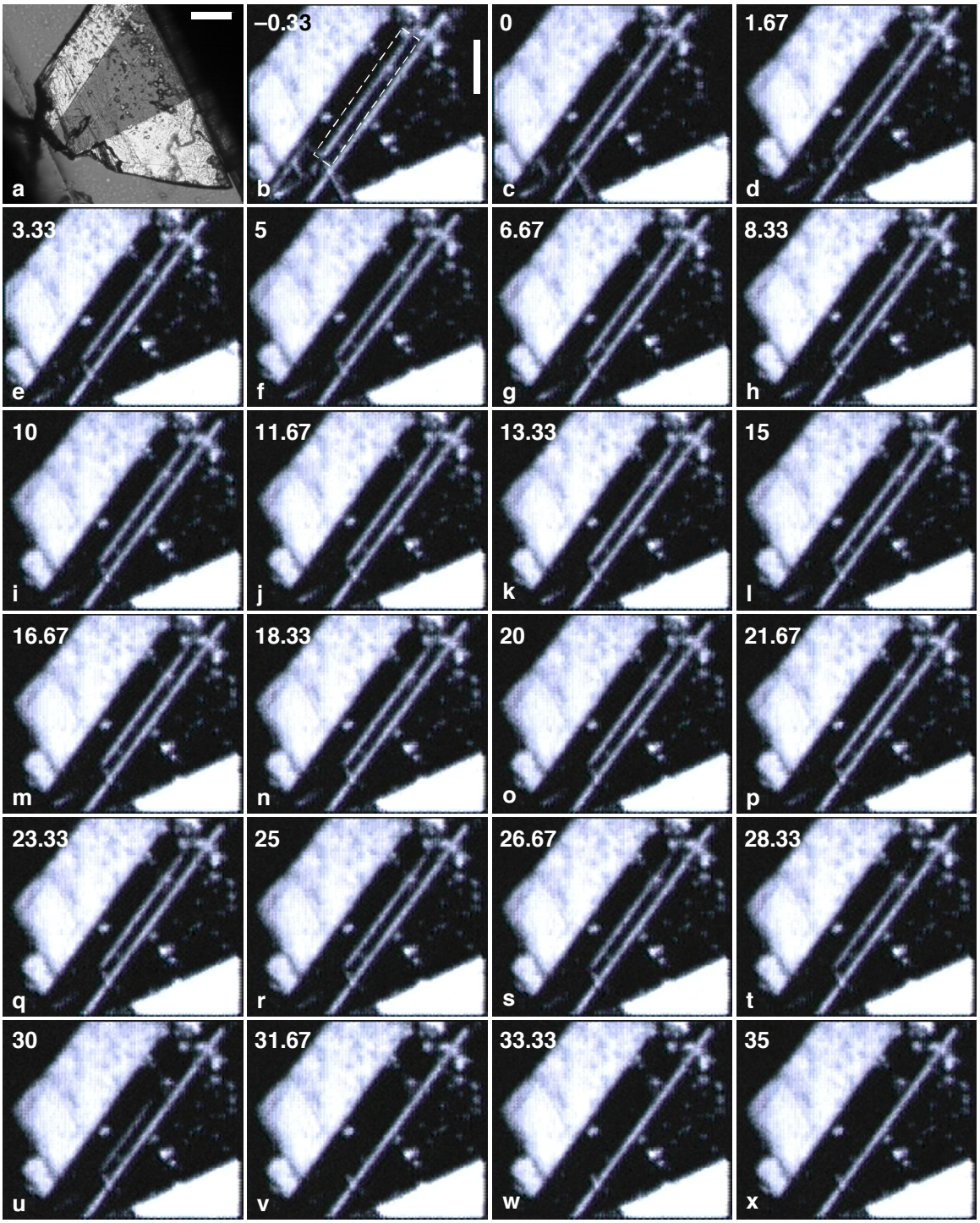



**Figure 4.30** Domain reversion and ultrafast video sequence for the third stress attempt for the crystal containing 11.5% monoketone, following 0.39% compression. The experimental setup is similar to the description provided in Figure 4.16. **(a)** Photomicrograph (crossed polars) of the crystal taken immediately before stress release. Scale bar = 0.25 mm (Nikon 1.3x). **(b-x)** Ultrafast (3000 fps) video frames, beginning 0.33 ms prior to stress release (**b**), at stress release (**c**), and in 1.67 ms increments thereafter (**d-x**). In each image the time from stress release (time = 0, frame **c**) is presented in the upper left-hand corner. The box in frame **b** indicates the sample region for this frame, which was repositioned according to crystal motion (see text). Scale bar = 0.20 mm (Kodak MotionCorder 1.3x).

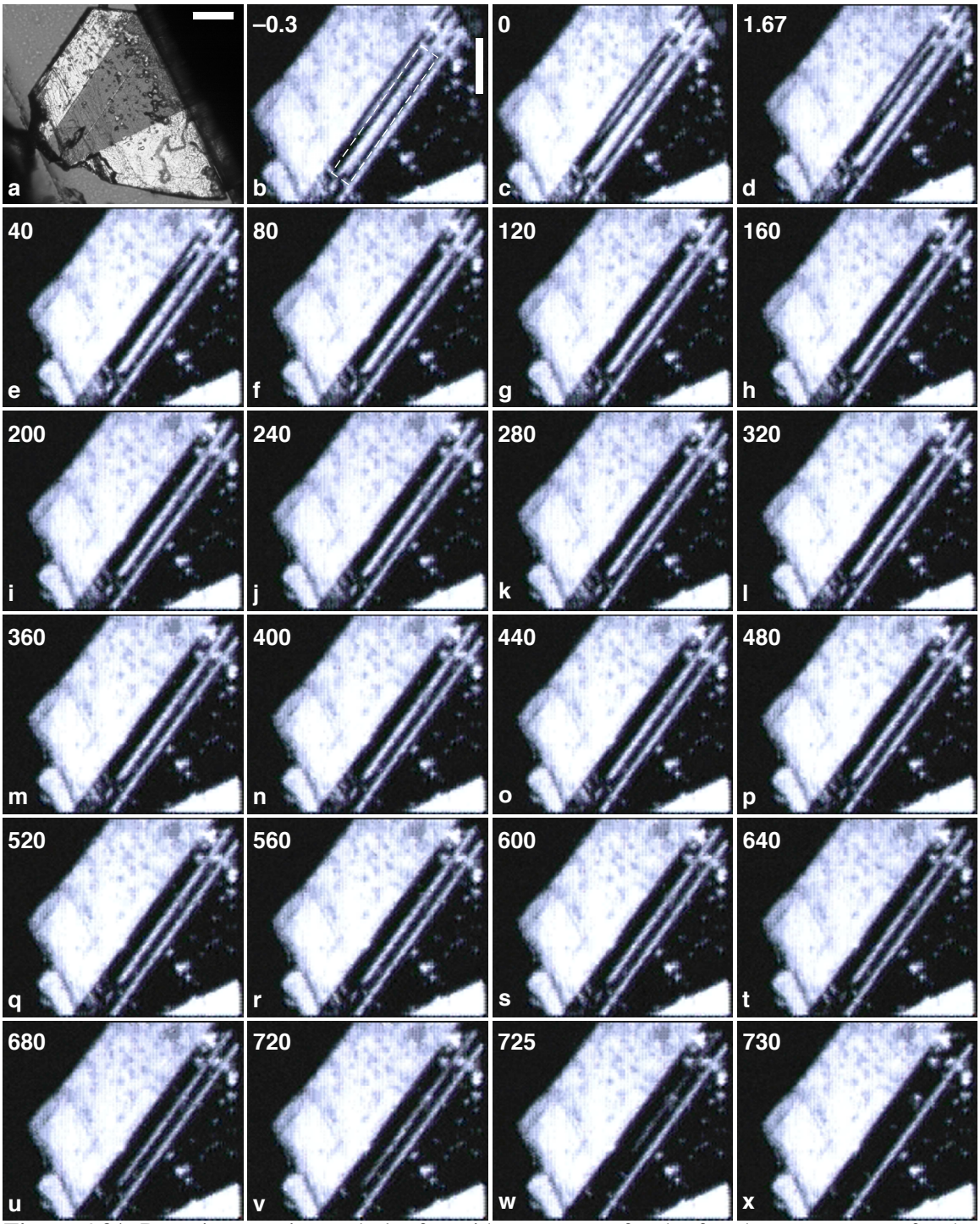



**Figure 4.31** Domain reversion and ultrafast video sequence for the fourth stress attempt for the crystal containing 11.5% monoketone, following 0.77% compression. The experimental setup is similar to the description provided in Figure 4.16. **(a)** Photomicrograph (crossed polars) of the crystal taken immediately before stress release. Scale bar = 0.25 mm (Nikon 5x). **(b-x)** Ultrafast (3000 fps) video frames, beginning 0.33 ms prior to stress release (**b**), at stress release (**c**), after 1.67 ms **(d)**, and in 40 ms increments thereafter (**d-v**). The last two images **(w-x)** are spaced by 5 ms and illustrate the last portion of the domain reversion event. In each image the time from stress release (time = 0, frame **c**) is presented in the upper left-hand corner. The box in frame **b** indicates the sample region for this frame, which was repositioned according to crystal motion (see text). Scale bar = 0.20 mm (Kodak MotionCorder 1.3x).

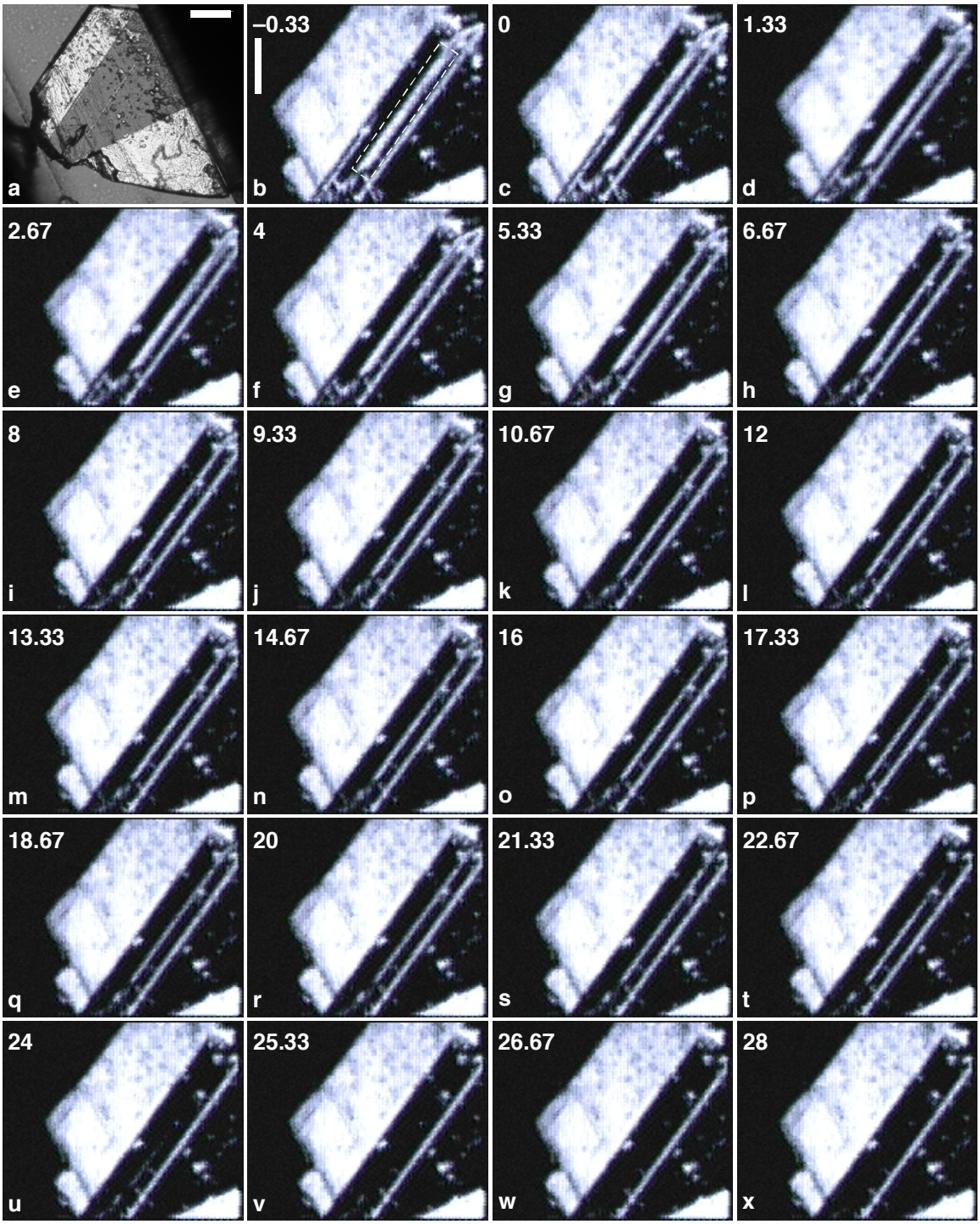



**Figure 4.32** Domain reversion and ultrafast video sequence for the fifth stress attempt for the crystal containing 11.5% monoketone, following 0.56% compression. The experimental setup is similar to the description provided in Figure 4.16. **(a)** Photomicrograph (crossed polars) of the crystal taken immediately before stress release. Scale bar = 0.25 mm (Nikon 5x). **(b-x)** Ultrafast (3000 fps) video frames, beginning 0.33 ms prior to stress release (**b**), at stress release (**c**), and in 1.33 ms increments thereafter (**d-x**). In each image the time from stress release (time = 0, frame **c**) is presented in the upper left-hand corner. The box in frame **b** indicates the sample region for this frame, which was repositioned according to crystal motion (see text). Scale bar = 0.20 mm (Kodak MotionCorder 1.3x).

was varied from 0.39 to 0.77%, and a {110}{110} daughter was grown in approximately the same region of the crystal (Figure 4.28). In each stress attempt, pseudoelastic reversion was observed.

This experiment utilized the Kodak MotionCorder to capture ultrafast video of each domain reversion event. In the analysis of the video frames, a 72 × 560 $\mu m^2$ sample region was positioned so that the same daughter region was examined in each case. Since these data were collected using the Kodak MotionCorder, it was necessary to remove time-dependent variations in the luminosity data using the Fourier smoothing routine discussed in Section 4.4.1. The raw and smoothed data are provided in Figure 4.33a-e. (Here, data from the first stress attempt, entry 5, are reproduced.) As with previous experiments, the number of data points used in each smoothing routine was kept to a minimum. So that data from each attempt was treated in the same fashion, each run was smoothed using four data points. Although the smoothing routine should qualitatively reduce the periodic variations in luminosity that arise from the use of the Kodak camera, they should not eliminate artifactual changes in luminosity.

In stress attempts I, II, III and V, unexpected luminosity increases were observed. For attempts I and II, the increases began around 12 ms following stress bar retraction (Figure 4.33a,b), while for attempt III the luminosity began to increase almost immediately (Figure 4.33c); for stress attempt V, the luminosity appears to jump near 20 ms following stress bar retraction (Figure 4.33e). During each attempt the crystal does not appear to rotate or jump. (An investigation[66] of images collected at stress release, at 1.33 ms, and much later in the sequence, revealed rotations of 0.1° or less in each stress attempt. In addition, as described in Sections 4.4.1.2 and 7.5, stress bar retraction should

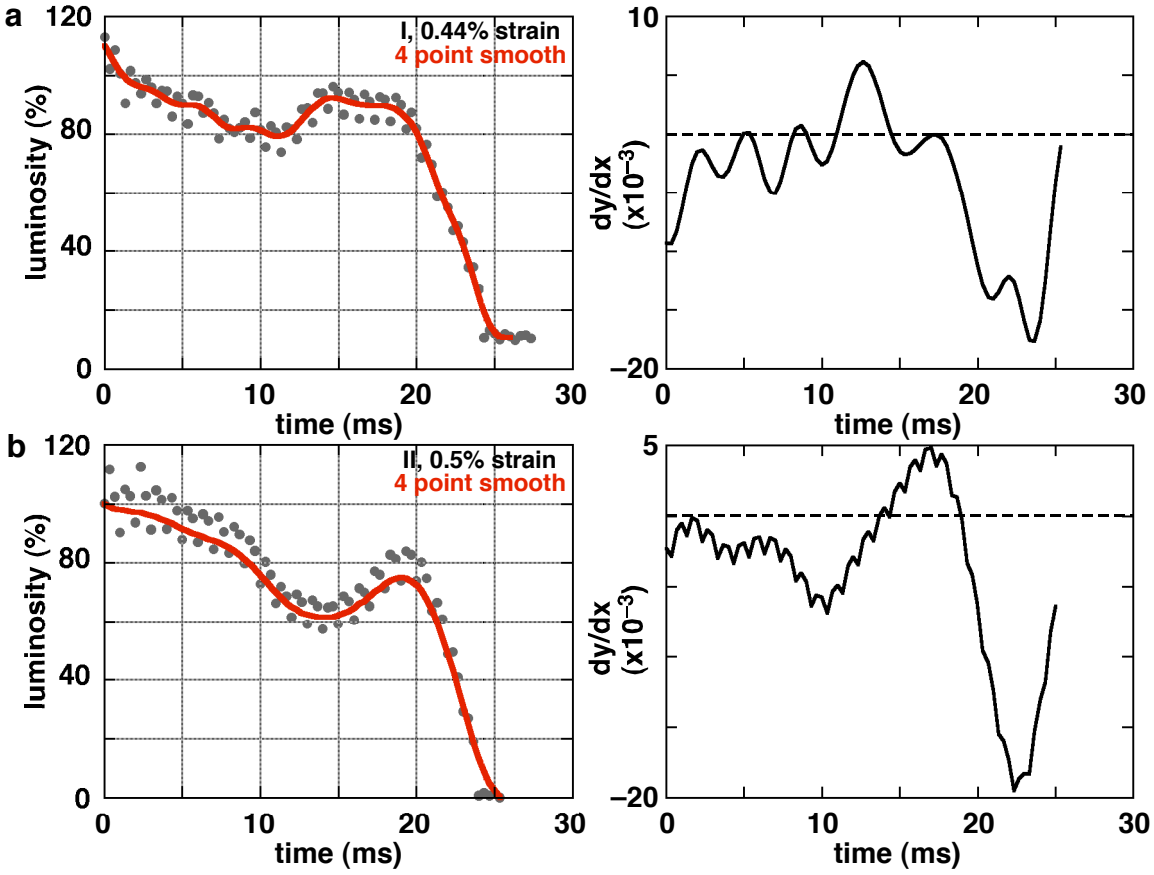
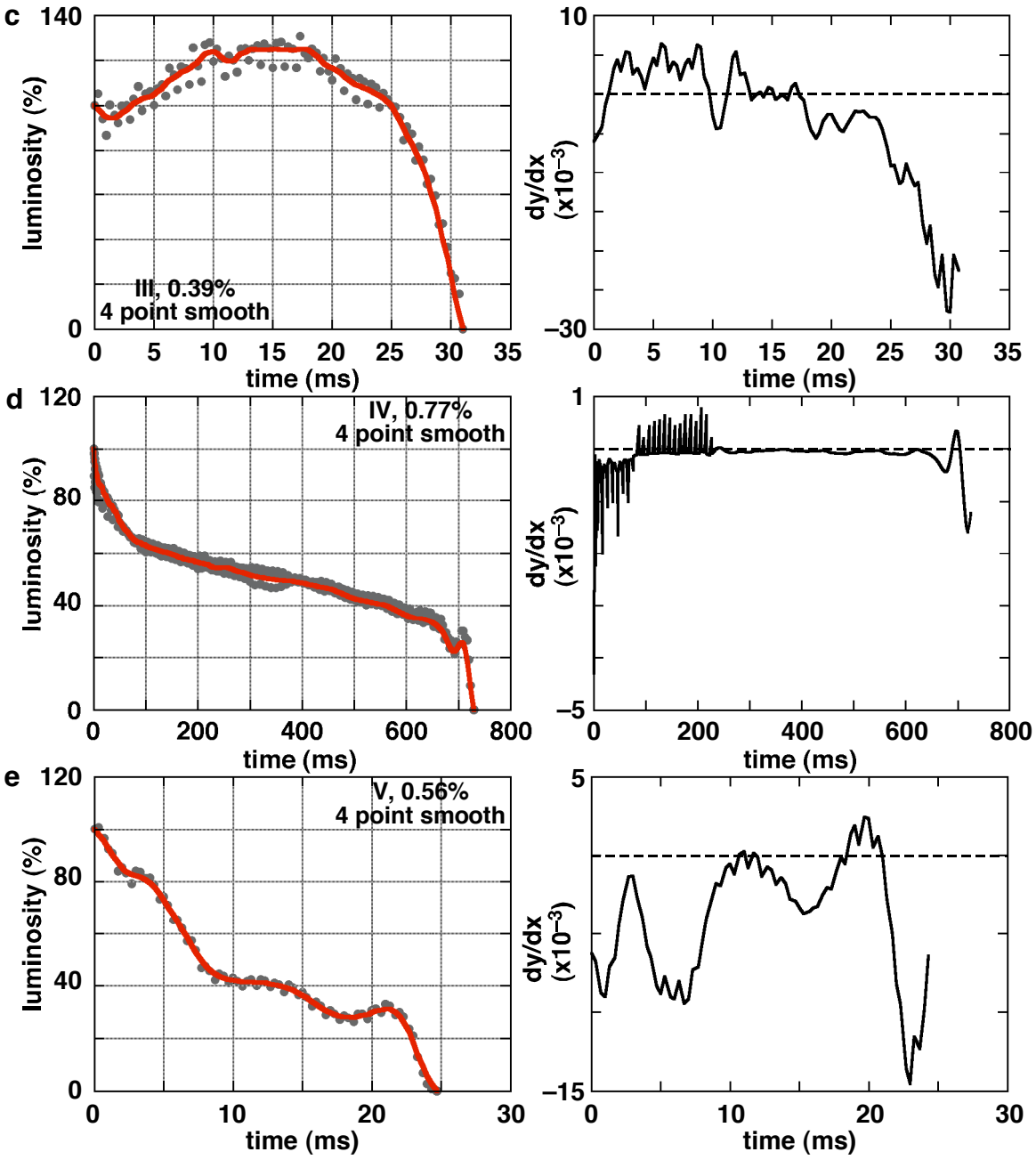
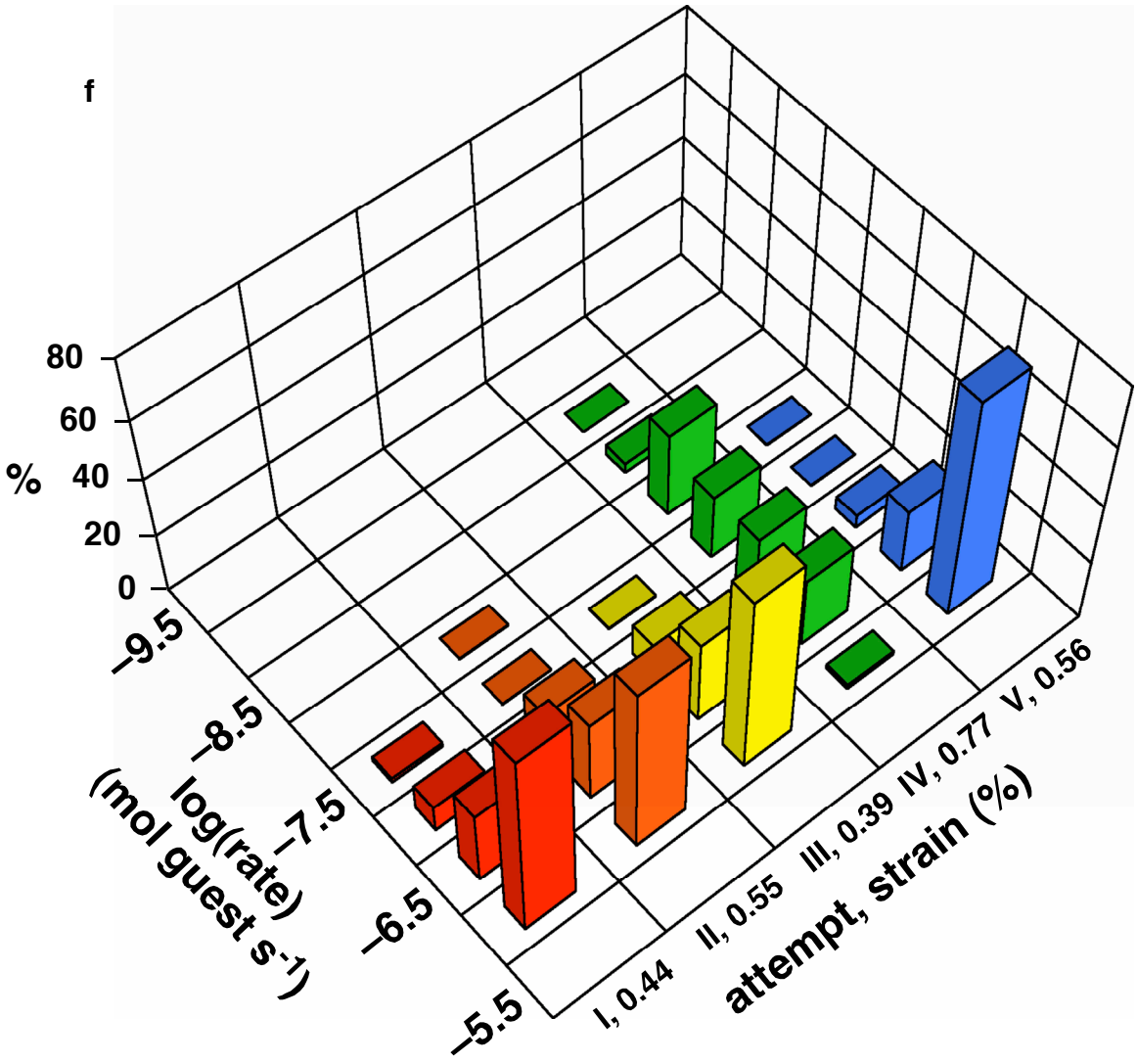



**Figure 4.33** Domain reversion kinetics for stress experiments described in Figures 4.28 through 4.32. The rates of reversion were measured during each of five cycles of stress and release for the same crystal containing 11.5 % 2-undecanone. **(a–e)** Plots of the percentage of daughter (calculated from the initial amount measured prior to stress release) vs. time, for stress attempts I through V, respectively. For these plots, luminosity (as a percentage of the initial value) is plotted using dark circles. As discussed in the text, a Fourier smoothing routine was used to eliminate time-dependent variations in the luminosity data. Here, smoothed luminosity data are plotted in red. In addition, first derivative plots of the smoothed data are provided (see Section 4.4.1.2). For each stress attempt, the maximum strain (in %) and the number of data points used in the smoothing procedure are provided. **(f)** A histogram plot of instantaneous reversion rates measured for each strain attempt. Here, the percentage of daughter that reverts within a given range of rates (spanning half log units) is plotted along the vertical axis. The percentages (of total) for half-log bins are provided in table **g**.


c
luminosity (%)
III, 0.39%
4 point smooth
time (ms)
dy/dx (x10$^{-3}$)
time (ms)
d
luminosity (%)
IV, 0.77%
4 point smooth
time (ms)
dy/dx (x10$^{-3}$)
time (ms)
e
luminosity (%)
V, 0.56%
4 point smooth
time (ms)
dy/dx (x10$^{-3}$)
time (ms)

f




g

**Percentage of daughter, sorted by log(rate)**

| log(rate) | I | II | III | IV | V |
|---|---|---|---|---|---|
| **–9.5** | – | – | – | – | – |
| **–9.0** | – | – | – | 0.09 | – |
| **–8.5** | – | – | – | 3.33 | – |
| **–8.0** | – | 0.21 | – | 28.29 | 0.41 |
| **–7.5** | 1.41 | 0.16 | 0.21 | 21.58 | 0.15 |
| **–7.0** | 8.85 | 13.92 | 10.78 | 22.14 | 4.29 |
| **–6.5** | 24.82 | 28.03 | 28.14 | 23.29 | 21.39 |
| **–6.0** | 64.92 | 57.69 | 60.88 | 1.29 | 74.14 |
| **–5.5** | – | – | – | – | – |

be complete in approximately 0.55 ms, long before the anomalous changes in luminosity observed here.) In every case, the principal contribution to the daughter population is from a thin stripe that spans the length of the sample area; smaller contributions come from other, smaller, domains including a {130}{130} daughter (see especially the fourth attempt, Figure 4.28p). In the image sequences, however, the decay of those additional regions did not appear to coincide with anomalous luminosity increases (see Figures 4.26f and 4.29 through 4.32). Based on the preceding discussion of optical effects in the crystals used for the reversion kinetics experiments, such variations do not appear to arise from retardation effects (since this crystal is 160 μm thick); currently, the cause of the anomalous increases in luminosity is not understood.

As with other stress experiments performed on other crystals, (Section 4.4.1), the kinetic plots (Figure 4.33a-e) exhibit regions of fast and slow reversion during each stress attempt. Overall, stress attempts I, II and V each reverted over approximately 25 ms; attempt III took a little longer (31.0 ms) to complete, while attempt IV reverted over 730.0 ms (see Figure 4.28). In addition to the measurements of differences in reversion duration, instantaneous rates provide valuable insight into the reversion process. (For all five attempts the time resolution is 3000 $s^{-1}$.) Due to anomalous increases in luminosity described above, some of the ultrafast frames may be unreliable. Since *increases* in luminosity oppose the effect of decreasing daughter size, the slowest rates measured using such frames become suspect. This is especially true for stress attempts I, II, III and V, where the slowest rates were observed during or near periods of anomalous changes in luminosity (Figure 4.33a-c, e). For this reason, data from several frames were excluded from the kinetic analysis; these frames are described in Figure 4.28.

As tabulated in Figure 4.28, the fastest instantaneous rates spanned a factor of 2.6 ($3.32 \times 10^{-7}$ to $8.48 \times 10^{-7}$ mol guest $s^{-1}$; attempts IV and V, respectively), while the entire range of rates varied by a factor of about 2400 ($3.56 \times 10^{-10}$ to $8.48 \times 10^{-7}$ mol guest $s^{-1}$; attempts IV and V, respectively). Histogram distributions (separated into half log bins) are presented in Figure 4.33f; values for each bin are tabulated in Figure 4.33g. In the histograms, one notes that although the fastest bin ($10^{-6}$ mol guest $s^{-1}$) is populated for each stress attempt, the slowest bin varies somewhat: stress attempts I and III exhibit the fastest *minimum* rates ($10^{-9}$ mol guest $s^{-1}$), while attempts II, IV and V revert over slower bins. As discussed below, population of the slowest rate bins may arise from changes in reversion behavior for daughters formed in different stress attempts.

For stress attempts I, II and III (to 0.44%, 0.55% and 0.39% strain, respectively), the distributions appear quite similar: a majority (58-65%) of domain reversion occurs within the fastest bin ($10^{-6}$ mol guest $s^{-1}$), and the population within each bin tails off at slower rates (see Figure 4.33g). During stress attempt IV (to 0.77% strain), this distribution shifts to slower rates, although the fastest rate bins ($10^{-6}$ mol guest $s^{-1}$) remains populated. In stress attempt V (to 0.56% strain), the rate distribution appears similar to the rate distribution for stress attempt III, although over 74% of this daughter reverts in the fastest bin ($10^{-6}$ mol guest $s^{-1}$).

These distributions suggest a possible link between reversion rate and the amount of strain applied. For each attempt, regardless of strain, the fastest bin is populated (although the populations vary widely) and the fastest instantaneous rates do not vary appreciably. However, a look the daughter domains formed in stress attempts I, II and III (see Figure 4.28 d, h, l) suggests the daughter was formed over the same region during

these initial attempts (see also Figure 4.34j-l); during reversion, the crystal exhibits a trend between *minimum* rate and applied strain. For attempts I and III (to 0.44% and 0.39% strain, respectively), the minimum rates ($1.94 \times 10^{-8}$ and $1.85 \times 10^{-8}$ mol guest $s^{-1}$, respectively) are approximately five times faster than the minimum rate ($4.42 \times 10^{-9}$ mol guest $s^{-1}$) observed for attempt II (to 0.55% strain). This trend is continued for attempt IV (to 0.77% strain); here, the daughter domain becomes appreciably larger than in attempts I-III (see Figures 4.28p and 4.34). For this attempt, the slowest rate ($3.56 \times 10^{-10}$ mol guest $s^{-1}$) is observed, and the reversion event takes a substantially longer time to complete. During the period of fastest decay (the first few milliseconds), Figure 4.34 illustrates that domain reversion is not readily observed in the ultrafast video sequence. Instead of domain switching along a well-defined domain wall, this daughter appears to fade in intensity; nevertheless, the slowest rates observed for this daughter conform to the trend linking strain and minimum reversion rate. Once a smaller stress is again applied (attempt V, 0.56%), the rates again increase to values more commensurate to those observed in the first three attempts.

If slower rates do not arise artificially from crystal motion (or other factors, discussed above), the correlation between strain and reversion rates may support the defect hypothesis described in Section 4.3.3. For instance, during stress attempt V (to 0.56% strain), the minimum rate ($8.04 \times 10^{-9}$ mol guest $s^{-1}$) has increased appreciably when compared to attempt IV (0.77% strain, 3.56 ¥ $10^{-10}$ mol guest $s^{-1}$); this rate lies between the slowest rates observed for entries I (or III) and II, and it fits the relationship between strain and minimum rate observed for attempts I-IV. However, it is interesting that the daughter formed in attempt V is much larger than the one formed in attempt II.

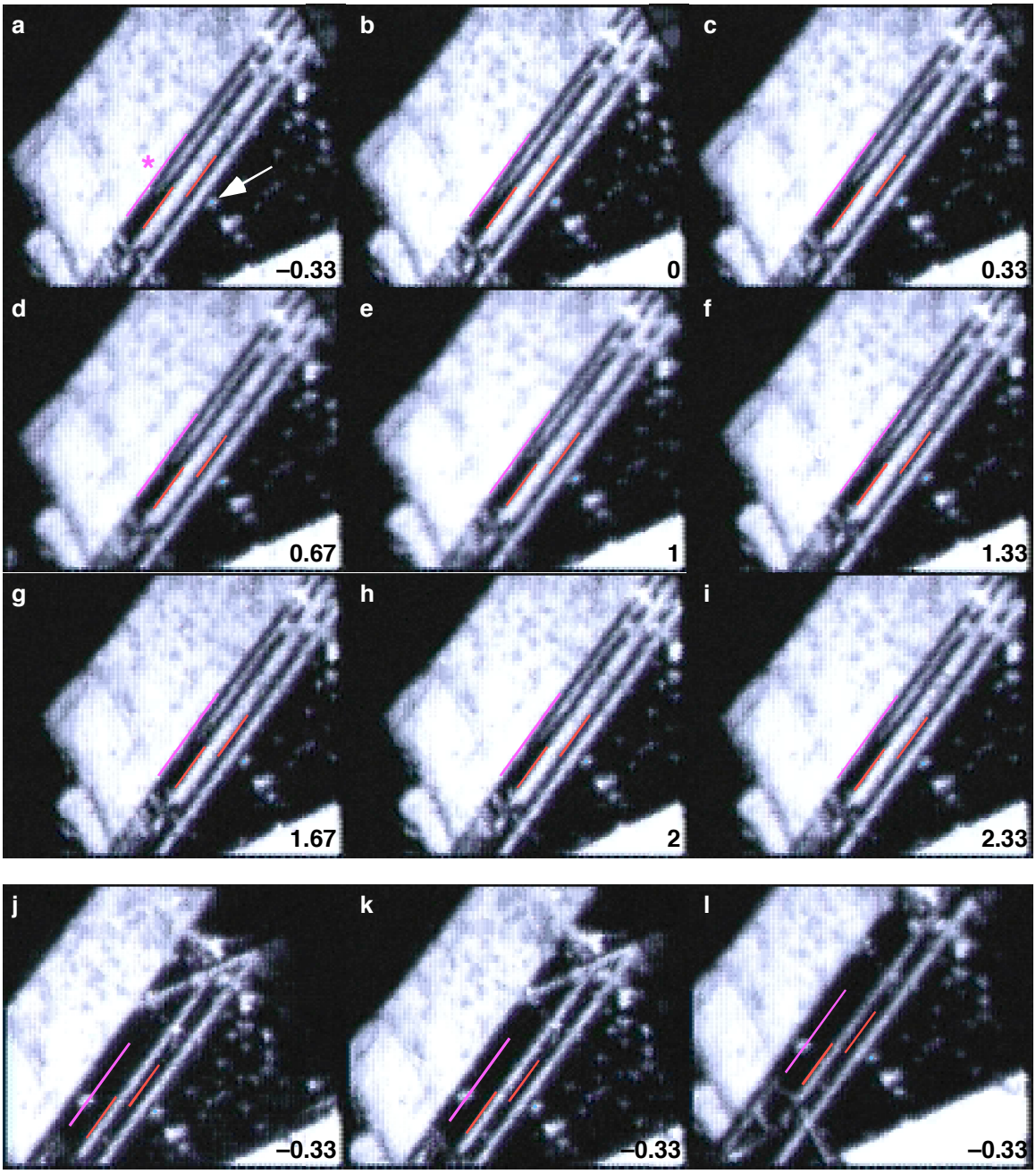



**Figure 4.34.** A comparison of daughter regions in stress attempts I through IV. **(a–i)** Stress attempt IV: ultrafast video images collected 0.33 ms prior to stress release (**a**), at stress release (**b**) and in 0.33 ms intervals to 2.33 ms following release. In each, the outer boundaries of the original daughter domain are denoted by the red lines. The violet line (see * in **a**) denotes the location of a daughter domain not analyzed. Crystal motion was compensated for using the small bright region at lower right (see blue dot and arrow). During this time span, no visible change in daughter size is observable. **(j–l)** Ultrafast video images, collected 0.33 ms prior to stress release for stress attempt I (**j**), II (**k**), and III (**l**). The daughter boundary lines used in **a**–**i** (attempt IV) have been superimposed on these images to illustrate differences in domain size between the experiments. See text for details.

(These daughters were grown from 0.55% and 0.56% strain, respectively.) The possibility of defects favoring and resisting domain reversion was described in Section 4.3.3; these same defects might be operative during domain switching from mother to daughter. Although it is tempting to ascribe the apparent correlation between crystal history, strain and minimum rates to the defect structure of the reverting crystal, this discussion will be deferred to Chapter 5, where additional information is available.

From the experiments described, domain reversion kinetics appear to be influenced by several factors including the magnitude of applied strain, the location of daughter and crystal history (e.g., prior stress attempts). For example, in stress IV, the maximum strain (0.77%) was applied, and the daughter grew to its largest size. Upon release, the rates were observably slower than in previous attempts. Since this daughter was larger than daughters formed in previous stress attempts, slower reversion rates could result from the defect structure of the newly switched region or from changes in domain structure within regions that formed daughter in previous stress attempts. From the return to "normal" reversion behavior observed in attempt V, which included switching over the larger crystal region, the first possibility appears quite reasonable: in this stress attempt, the enlarged daughter region reverted at rates comparable to those observed for smaller daughter domains formed in the initial stress attempts. Defect annealing (discussed in Section 4.2.4) provides one possible mechanism through which the number of defects can be altered. This possibility and its effect on domain wall motion will be discussed more fully in Chapter 5.

## 4.5 Discussion

The remarkable change in ferroelastic behavior for UICs crystals containing mostly 2,10-undecanedione and 13-14% 2-undecanone reveals a critical threshold for the effect of this relaxive impurity on ferroelastic properties. In abbreviated terms, the critical threshold is representative of an "all-or-nothing" phenomenon: either pseudoelastic reversion occurs or it does not. This sort of behavior makes ferroelasticity very sensitive to minor changes in composition near the critical concentration. In the current system, a small variation in impurity concentration near 13-14% yields a drastic change in the pseudoelastic response of the crystal to applied stress at strains close to 1%.

The observation of a critical concentration threshold for pseudoelastic behavior in urea inclusion compounds may be the first such observation for an organic ferroelastic. For these as well as other ferroelastic materials, local cooperativity that extends over large distances is thought to play a role in the observed ferroelastic behavior. Nominally, daughter and mother domains are degenerate; however, the observation of pseudoelasticity indicates a difference in stability. Below the critical threshold, incomplete domain reversion (or none at all) is observed following the release of stress. Such domains probably include channels for which spontaneous reversion is energetically preferable; however, the long-range connectivity between channels renders "local" reversion energetically unfavorable. The introduction of the relaxive impurity 2-undecanone permits pseudoelastic behavior, possibly by breaking up this cooperative network, which leads to a reduction in the kinetic barrier between mother and daughter. However, the same impurity can also increase the stability of the daughter domain by facilitating stressed defect repair, which (on its own) leads to an *increase* in the kinetic

barrier. Kinetics experiments reveal no obvious correlation between 2-undecanone content and reversion rate; instead, they suggest that this relaxive impurity reduces the tendency for defect sites (whatever their nature) to inhibit domain wall motion.

As discussed in Section 4.2.4, the recovery of strain epitaxy can drive domain reversion. It is envisioned that acoustomechanical vibration can reestablish strain epitaxy near defect sites, but it may also facilitate the reconstruction of host-guest hydrogen bonds in a stressed crystal. Whereas the first possibility increases stability within the daughter, the second increases the barrier to reversion. Both should give rise to reduced pseudoelastic behavior.

## References Cited


1. Wadhawan, V. K. *Introduction to Ferroic Materials*, (Gordon and Breach Science Publishers, Amsterdam, 2000), pp. 232-243 and 458.
2. Aizu, K. Possible species of "ferroelastic" crystals and of simultaneously ferroelectric and ferroelastic crystals. *J. Phys. Soc. Japan* **27**, 387-96 (1969).
3. Hollingsworth, M. D. & McBride, J. M. Specific long-range effects on relaxation of local stress during a solid-state reaction. *J. Am. Chem. Soc.* **107**, 1792-3 (1985).
4. McBride, J. M., Segmuller, B. E., Hollingsworth, M. D., Mills, D. E. & Weber, B. A. Mechanical stress and reactivity in organic solids. *Science (Washington, D. C.)* **234**, 830-5 (1986).
5. Hollingsworth, M. D. & McBride, J. M. Infrared studies of long-range stress in solid-state peroxide photoreactions. *Mol. Cryst. Liq. Cryst.* **161**, 25-41 (1988).
6. McBride, J. M. The role of local stress in solid-state radical reactions. *Acc. Chem. Res.* **16**, 304-312 (1983).
7. Hollingsworth, M. D. & McBride, J. M. Coupling of $CO_2$ asymmetric stretching in dimers photogenerated within long-chain diacyl peroxide single crystals. *Chem. Phys. Lett.* **130**, 259-64 (1986).
8. Hollingsworth, M. D. & McBride, J. M. Photochemical mechanism in single crystals: FTIR studies of diacyl peroxides. *Adv. Photochem.* **15**, 279-379. (1990). The concept of mechanical stress and its effect on reaction mechanism is discussed on pages 288-290 of this article.
9. Hollingsworth, M. D., Peterson, M. L., Pate, K. L., Dinkelmeyer, B. D. & Brown, M. E. Unanticipated guest motion during a phase transition in a ferroelastic inclusion compound. *J. Am. Chem. Soc.* **124**, 2094-2095 (2002).
10. Cohen, M. D. & Schmidt, G. M. Topochemistry I. A survey. *J. Chem. Soc.*, 1996-2000 (1964).
11. Cohen, M. D. The photochemistry of organic solids. *Angew. Chem. Int. Ed.* **14**, 386-393 (1975).
12. Megaw, H. D. *Ferroelectricity in Crystals*, (Methuen & Co Ltd., London, 1957) pp. 14–15.
13. Salje, E. *Phase Transitions in Ferroelastic and Co-elastic Crystals*, (Cambridge University Press, New York, 1990), pp. 1-8.
14. Salje, E. Phase transitions in ferroelastic and co-elastic crystals. *Ferroelectrics* **104**, 111-120 (1990).
15. Tsukamoto, T., Hatano, J. & Futama, H. Refraction and reflection of light at ferroelastic domain walls in Rochelle salt crystal. *J. Phys. Soc. Japan* **51**, 3948-3952 (1982).
16. Brown, M. E. & Hollingsworth, M. D. Stress-induced domain reorientation in urea inclusion compounds. *Nature (London)* **376**, 323-327 (1995).
17. Heaton, N. J., Vold, R. L. & Vold, R. R. Deuterium quadrupole echo study of urea motion in urea/n-alkane inclusion compounds. *J. Am. Chem. Soc.* **111**, 3211-3217 (1989).
18. Bell, J. D. & Richards, R. E. Nuclear spin relaxation studies on urea + hydrocarbon clathrates. *Trans. Faraday Soc.* **65**, 2529-2536 (1969).

19. Lines, M. E. & Glass, A. M. *Principles and Applications of Ferroelectrics and Related Materials*, (Clarendon Press, Oxford, 1977), p. 9.
20. Wadhawan, V. K. *Introduction to Ferroic Materials*, (Gordon and Breach Science Publishers, Amsterdam, 2000), pp. 7-8.
21. Hollingsworth, M. D., Peterson, M. L., Rush, J. R., Brown, M. E., Abel, M. J., Black, A. A., Dudley, M., Raghothamachar, B., Werner-Zwanziger, U., Still, E. J. & Vanecko, J. A. Memory and perfection in ferroelastic inclusion compounds. *Cryst. Growth Des.* **5**, 2100-2116 (2005).
22. Dec, J. Paraelastic-ferroelastic interfaces. *Phase Transit.* **45**, 35-58 (1993).
23. Sapriel, J. Domain-wall orientations in ferroelastics. *Phys. Rev. B* **12**, 5128-5140 (1975).
24. Wadhawan, V. K. Ferroelasticity: Introductory survey and present status. *Phase Transit.* **34**, 3-18 (1991).
25. Chung, H., Dudley, M., Brown, M. E. & Hollingsworth, M. D. Synchrotron white beam X-ray topography characterization of defect structures in 2,10-undecanedione/urea inclusion compounds. *Mol. Cryst. Liq. Cryst.* **276**, 203-212 (1996).
26. Yeates, T. O. Detecting and overcoming crystal twinning. *Methods Enzymol.* **276**, 344-358 (1997).
27. Cahn, R. W. Twinned crystals. *Adv. Phys.* **3**, 363-445 (1954).
28. Rush, J. R. Laboratory notebook entry jrr-d105. (2004).
29. Rush, J. R. Laboratory notebook entry jrr-f277-1. (2007).
30. Rush, J. R. The line profiles were recorded on laboratory notebook entry jrr-f025. Measurements of FWHM (in δ) and 75% change (in ϕ) are provided in fig 310 table.xls. (2005).
31. Hollingsworth, M. D. & Peterson, M. L. Twinning, epitaxy and domain switching in ferroelastic inclusion compounds. *NASA Conference Publication* **2003-212339**, 283-288 (2003).
32. Hollingsworth, M. D., Brown, M. E., Hillier, A. C., Santarsiero, B. D. & Chaney, J. D. Superstructure control in the crystal growth and ordering of urea inclusion compounds. *Science (Washington, D. C.)* **273**, 1355-1359 (1996).
33. Hollingsworth, M. D. Crystal engineering: from structure to function. *Science (Washington, DC, United States)* **295**, 2410-2413 (2002).
34. Hollingsworth, M. D. Personal communication to J. R. Rush (2005).
35. Rush, J. R. Laboratory notebook entry jrr-f274. (2007).
36. Otsuka, K. & Wayman, C. M. "Mechanism of shape memory effect and superelasticity" in *Shape Memory Materials*, (Cambridge University Press, New York, 1998) pp. 27-48 (see especially pp. 44-45).
37. Salje, E. *Phase Transitions in Ferroelastic and Co-elastic Crystals*, (Cambridge University Press, New York, 1990) p. 4.
38. Luty, T. & Eckhardt, C. J. General theoretical concepts for solid state reactions: Quantitative formulation of the reaction cavity, steric compression, and reaction-induced stress using an elastic multipole representation of chemical pressure. *J. Am. Chem. Soc.* **117**, 2441-52 (1995).

39. Luty, T. & Eckhardt, C. J. "Cooperative effects in solid-state reactions" in *Reactivity of Molecular Solids*, vol. 3 (eds. Boldyreva, E. & Boldyrev, V.) (John Wiley & Sons, Ltd., Chichester, 1999) pp. 51-87.
40. White, K. M., Dye, R. C. & Eckhardt, C. J. Molecular motions in organic crystals. *Mol. Cryst. Liq. Cryst.* **134**, 265-78 (1986).
41. Cahn, R. W. Metallic rubber bounces back. *Nature (London)* **374**, 120 (1995).
42. Otsuka, K. & Ren, X. Mechanism of martensite aging effect. *Scripta Mater.* **50**, 207-212 (2004).
43. Ren, X. & Otsuka, K. Origin of rubber-like behavior in metal alloys. *Nature (London)* **389**, 579-581 (1997).
44. Ren, X. & Otsuka, K. Universal symmetry property of point defects in crystals. *Phys. Rev. Lett.* **85**, 1016-1019 (2000).
45. Suzuki, T., Tonokawa, T. & Ohba, T. Role of short-range order in martensitic transformation. *J. Phys. IV* **5**, 1065-1070 (1995).
46. Marukawa, K. & Tsuchiya, K. Short-range ordering as the cause of the rubber-like behavior in alloy martensites. *Scripta Metall. Mater.* **32**, 77-82 (1995).

47. Abel, M. J., Rush, J. R. & Hollingsworth, M. D. Unpublished Observation. (2003).
48. Hollingsworth, M. D. Personal communication to J. R. Rush (2002).
49. Rush, J. R. Laboratory notebook entry jrr-f202. (2006).
50. Black, A. A. & Abel, M. J. Unpublished Observation. (2002).
51. Rush, J. R. Laboratory notebook entry jrr-c262-10. (2004).
52. Rush, J. R. Laboratory notebook entry jrr-f052. (2005).
53. Rush, J. R. Laboratory notebook entry jrr-f051. (2005).
54. Rush, J. R. Laboratory notebook entries jrr-f053 and jrr-f055. (2006).
55. Glazer, A. M., Lewis, J. G. & Kaminsky, W. An automatic optical imaging system for birefringent media. *Proceedings of the Royal Society of London, Section A* **452**, 2751-2765 (1996).
56. Johannsen, A. *Manual of Petrographic Methods*, (McGraw-Hill Book Company, New York, 1918), pp. 343-345.
57. Geday, M. A., Kaminsky, W., Lewis, J. G. & Glazer, A. M. Images of absolute retardance $L \bullet \Delta n$, using the rotating polariser method. *J. Microsc.* **198**, 1-9 (2000).

58. Stoiber, R. E. & Morse, S. A. *Crystal Identification with the Polarizing Microscope*, (Chapman & Hall, London, 1994) pp. 87-97.
59. EXFO. X-Cite 120 light source lamp power output. Accessed July 12, 2006, at http://www.exfo-lifesciences.com/products/X-cite/Xenon-X-Cite120-LampComparison.pdf.
60. Melles-Griot. Five Schott Glass Types. Accessed September 24, 2006, at http://www.mellesgriot.com/products/optics/mp_3_1.htm#BK7. (2002).
61. Siebrand, W. & Wildman, T. A. Dispersive kinetics: A structural approach to nonexponential processes in disordered media. *Acc. Chem. Res.* **19**, 238-243 (1986).

62. Hollingsworth, M. D. & McBride, J. M. Photochemical mechanism in single crystals: FTIR studies of diacyl peroxides. *Adv. Photochem.* **15**, 279-379. (1990). The concept of nonexponential kinetics in solid-phase reactions is discussed on pages 283-284 of this article.
63. Rush, J. R. Laboratory notebook entry jrr-f160. (2006).
64. Rush, J. R. Laboratory notebook entries jrr-f160 and jrr-f275. (2007).
65. Rush, J. R. Laboratory notebook entry jrr-f140. (2006).
66. Rush, J. R. Laboratory notebook entry jrr-f276. (2007).